

Vibration of Branched Circular Cylindrical Shells as Applied to Airway Walls

Pui Ming Au

A thesis
submitted to Auckland University of Technology
in fulfilment of the
requirement for the degree of
Doctor of Philosophy

Auckland
New Zealand

© Pui Ming Au
March 2005

Declarations

I hereby declare that this submission is my own work and that, to the best of my knowledge and belief, it contains no material previously published or written by another person nor material which to a substantial extent has been accepted for the award of any other degree or diploma of a university or other institution of higher learning, except where due acknowledgement is made in the acknowledgements.

I authorise the Auckland University of Technology to lend this thesis to other institutions or individuals for the purpose of scholarly research.

Signature

I further authorise the Auckland University of Technology to reproduce this thesis by photocopying or by other means, in total or in part, at the request of other institutions or individuals for the purpose of scholarly research.

Signature

Borrower's Page

The Auckland University of Technology requires the signatures of all persons using or photocopying this thesis. Please sign below, and give your address and date.

Acknowledgements

I would like to express my true and sincere thanks to my supervisor, Professor Ahmed Al-Jumaily, for his guidance, patience and support that made this thesis possible. Professor Al-Jumaily has continued his efforts in monitoring work progress through the weekly meetings, and would like to advise and resolve problems in all possible ways for student's success. As the Director of Diagnostics and Control Research Centre at Auckland University of Technology, Professor Al-Jumaily emphasises team-work in facilitate research outcome effectively and efficiently.

Special thanks are due to Keith Ufton and Heather Stonyer for their help in proof-reading my first assignment for the doctoral candidature, and Jennie Walters in managing resources, facilities and updates to my research need and environment. My thanks also goes to Associate Professor Elaine Rush, Karen Searancke, Dr. John Kolbe, Hong K. Chan, Hans Oberst, Dr. Maximiano Ramos, Dr. Simon Chan, Muhammad Sakhawat, Warren Ng, Tristan Bellingham, Alex Du, Robert Paxton, Prasika Manilal, Tung Vuong and especially to Vera Hermawan for her partial assistance in the acoustic pressure chamber measurements.

Last of all, but not least, the dearest people no-one should ever forget, family. I have to thank my wife and children for their patience and help, even if it may just be a hug just to brighten the day or the night, depending.

Abstract

This research focuses on investigating the vibration characteristics of branched circular cylindrical shells with applications to airway passages. Analytical modelling is carried out based on Donnell–Mushtari equations of thin elastic membrane type of shells while numerical validation is conducted using the Finite Element Method (COSMOS/Works). Further validation of the results is performed using experimental investigation of tracheobronchial tissues dissected from pigs. The analytical, numerical and experimental results are in acceptable agreement.

Further investigation of the vibration characteristics of the airways for cases which cannot be dealt with analytically is carried out using COSMOS/Works. Results show a strong trend relationship which suggests that the natural frequency of the trachea and the primary tracheobronchi is approximately 10 Hz. Radial resonances of lower bronchi are predictable through trends found in this work that the resonant frequency is a linear function in certain region of generations.

Table of Contents

Declarations.....	ii
Borrower's Page	iii
Acknowledgements.....	iv
Abstract	v
Table of Contents.....	vi
List of Figures.....	ix
List of Tables.....	xiv
Chapter 1 Introduction	1
1.1 Background.....	1
1.2 Human Respiratory System	3
1.3 Lung Morphology.....	6
1.4 Airway Dichotomy	7
1.5 Histological View of Airways.....	8
1.6 Airway Physiology	9
Chapter 2 Literature Review	13
2.1 Introduction.....	13
2.2 Airway Mechanics.....	14
2.2.1 Airway Fluid Mechanics Approach.....	15
2.2.2 Airway Narrowing Mechanisms	18
2.2.3 Dynamic Characteristics of Airway and Lung Tissues	20
2.2.4 Measurements of Dynamic Parameters	28
2.3 Objectives	33
Chapter 3 Analytical Models.....	35
3.1 Introduction.....	35
3.2 Governing Equations	36
3.3 Proposed Solutions	43
3.4 Boundary Conditions.....	45
3.5 Other Analytical Frequency Equations of Cylindrical Thin Shells.....	47

3.6 Application to Respiratory walls.....	50
3.7 Results	54
3.8 Application of Analytical Models to Airways	56
Chapter 4 Numerical Models	58
4.1 Introduction.....	58
4.2 Modelling with COSMOS/Works	59
4.3 Verification of COSMOS/Works	65
4.4 The Trachea.....	68
4.5 Individual Bronchus	75
4.6 Angular Branching	77
4.7 Tracheobronchial Models	78
4.8 Model of a Symmetric Airway Tree.....	80
4.9 Closure	85
Chapter 5 Experimental Validation	87
5.1 Introduction.....	87
5.2 Modal Analysis and Testing	89
5.3 Mechanical Excitation	90
5.4 Acoustic Excitation	95
5.5 Experimental Samples	95
5.6 Experimental Procedures	97
5.7 Mechanical Excitation Experimentation.....	99
5.8 Acoustic Excitation Experimentation.....	102
5.9 Mechanical Excitation Results.....	104
5.10 Acoustic Excitation Results	106
5.11 Closure	108
Chapter 6 Discussion	109
6.1 Introduction.....	109
6.2 Analytical Modelling.....	110
6.3 Numerical Modelling.....	115
6.3.1 Numerical Modelling and Analytical Modelling	116

6.3.2	Sensitivity of Boundary Conditions and Physical Properties	117
6.3.3	Numerical Modelling and Experimental Validation	125
6.4	Experimental Validation	126
6.5	Conclusions	134
6.6	Future Work	137
Appendices	138
Appendix A	Respiratory System and Tidal Breathing Cycle	139
Appendix B	Morphological and Physical Data of Lungs	140
Appendix C	Kraus’s Analytical Validation on Koval & Cranch’s Experiment Measurements of a Cylindrical Thin Shell	141
Appendix D	A Sample of Analytical Calculation with Mathcad	143
Appendix E	Frequency mode 1 to 100 of the Tracheobronchial Generation 0 to 16 by COSMOS/Works Analysis	144
Appendix F	Frequency mode 1 to 100 of the Tracheobronchial Generation 0 to 16 by COSMOS/Works Analysis (Half density and double wall thickness)	153
Appendix G	Experimental Data and Results	158
Appendix H	Analytical Results on Experimental Validation Sample A1	167
Appendix I	COSMOS/Works Validation	168
Appendix J	COSMOS/Works Resonant Characterisation on Geometric and Physical Parameters of the Trachea	171
Reference	173

List of Figures

Figure 1.1	Schematic comparison of airway wall, in cross-section between bronchus and peripheral bronchiolus where cartilage disappears. EP, epithelium; BM, basement membrane; SM, smooth muscle [43, 48]. ... 9
Figure 1.2	(a) Circumferential and longitudinal layers of smooth muscle of airways [51]. (b) Contrarily, components of the major blood vessels with inner longitudinal and outer circumferential muscles [34]. 11
Figure 2.1	Tissue composition of central airway walls. 19
Figure 2.2	Parameters considered for dynamic characteristics of airways. 21
Figure 2.3	Four-element lung mechanical model Avanzolini and Barbini [87]. ... 28
Figure 3.1	A cylindrical membrane element with normal and shear stresses [98]. 37
Figure 3.2	The graph of the square root of elasticity to density ratio versus the generation number z from the trachea to bronchus 16. 53
Figure 3.3	The ring frequency distribution in tracheobronchial generation. The curve behaves quite linearly over the range. 54
Figure 3.4	Comparison of the analytical frequency results from equations of the membrane f_m , approximate membrane f_{m-} , Kraus's lowest f_1 and the lowest radial frequency f_{r1} 56
Figure 4.1	Modelling bronchus 4 with SolidWorks by extruding a circular base. Two reference inclined planes are added for generating bronchi 5 in symmetric branching. Dimensions are in mm. 62
Figure 4.2	Illustration of the angular branching from bronchus 4 to bronchi 5 by extruding the base circles on the reference planes. 63
Figure 4.3	A regular tetrahedral is a perfect FEA solid which can be meshed as a linear element with 4 nodes, or a parabolic element with 6 extra mid-side nodes. A linear triangular element with 3 nodes or a parabolic triangular element with 6 nodes is meshed for shell structure analysis. 64
Figure 4.4	The angular branching of bronchus 4 and 5 is modelled as solid cylinders and then meshed into shells in analysis. 65

Figure 4.5	Verification of COSMOS/Works results: 663 Hz with coarse or default mesh of 0.52" and 551 Hz of user defined mesh of 0.25" versus analytical solution of lowest frequency of 552 Hz by Kraus on the experimental sample of Koval and Cranch [93, 105].	67
Figure 4.6	Mode 1 of the trachea with both twist and bending, (a) 2.4 Hz with default mesh; (b) 2.0 Hz with fine mesh.	71
Figure 4.7	The trachea radial frequency with default mesh: (a) 5.6 Hz, fundamental of pure radial mode, and (b) 11.2 Hz, the first harmonic with twist and radial modes.	73
Figure 4.8	The trachea radial frequency with fine mesh: (a) 5.6 Hz, fundamental of pure radial mode, and (b) 11.2 Hz, the first harmonic with twist and radial modes.	74
Figure 4.9	Comparison of COSMOS/Works mode 1 frequency, with default and fine mesh, versus generation number.	75
Figure 4.10	Comparison of membrane, approximate membrane, Kraus's lowest and lowest radial frequencies resulted analytically.	76
Figure 4.11	Frequency dependence on the angles between bronchus 4 and 5 of branching airway.	78
Figure 4.12	A deformation mode of the one-sided branching model from the trachea to the bronchus 4.	79
Figure 4.13	Frequencies of one-sided branching of trachea, trachea to Bronchus 1 (TB1), 2 (TB2), 3 (TB3) and 4 (TB4), together with the tracheobronchial tree (TB7).	80
Figure 4.14	A pseudo-symmetric model of airway tree, bronchus 3 to bronchus 9.	81
Figure 4.15	Mode shape 1 of the regional airway model from bronchus 3 to bronchus 9. Bronchus 4 is excited at the frequency 34 Hz.	82
Figure 4.16	Frequencies of airway tree from bronchus 3 to bronchus 9. The model is first analysed with the physical properties of bronchus 9 (Homogeneous B9), then with the updated properties of the respective	

	generations, and finally the updated properties with finer mesh of 0.6 mm.	83
Figure 4.17	Mode shape 191 of the regional airway model from bronchus 3 to bronchus 9. Bronchus 4 left is excited in the radial mode at the frequency 76.6 Hz.....	84
Figure 4.18	Mode shape 191 of the regional airway model from bronchus 3 to bronchus 9. Bronchus 4 right is excited in the radial mode at the frequency 76.8 Hz.....	84
Figure 5.1	A block diagram of the experimental set-up.	91
Figure 5.2	A photo of the experimental set-up.	93
Figure 5.3	Polytec OFV 505 sensor head.	93
Figure 5.4	Polytec OFV 5000 vibrometer.....	94
Figure 5.5	The Tektronix TDS1012 in Math FFT mode displays the frequency spectrum of signal input from the Polytec OFV 5000 vibrometer.	94
Figure 5.6	Mounting set-up of the pig trachea [126] adopted in natural frequency measurements.	99
Figure 5.7	Nails were used to provide simple supports around the carina.	100
Figure 5.8	A circular split clamp of 16.5 mm to support the pig trachea sample.	101
Figure 5.9	Fixture and mounting of the pig tracheobronchi for resonance measurements, with the laser beam focused at the mid position.....	102
Figure 5.10	Mounting of the trachea section of sample 1 in the acoustic pressure chamber, with pined supports on corks at the ends.	103
Figure 5.11	Mounted pig trachea with branched bronchi and simple supports at the carina and ends.	104
Figure 5.12	Trachea frequency spectrum of a sectioned pig trachea, sample 1, measured at the central position.	105
Figure 5.13	Logarithmic trachea frequency spectrum of the sectioned pig trachea, sample 1, measured at both the central and off-central positions (A1 for trachea of sample 1).	105

Figure 5.14	The acoustic (measured with the acoustic pressure chamber) frequency spectrum of the sectioned trachea of sample 1.....	107
Figure 6.1	Comparison of analytical frequencies of airway from trachea to bronchus 16, where f_1 , f_{r1} , f_m - and f_m are the lowest frequency, the lowest radial frequency and the membrane frequency of circular cylindrical thin shells.	113
Figure 6.2	Comparison of frequencies by analytical and numerical modelling. .	120
Figure 6.3	Comparison of frequencies by analytical and numerical modelling, with double shell thickness and half density.....	120
Figure 6.4	Frequency ratios of results from Table 6.2 and Table 6.3, the COSMOS/Work results of f and f_{r1} , and the analytical results of f_s ...	122
Figure 6.5	The tracheobronchial radial frequencies with linear curve fittings. ...	124
Figure 6.6	The tracheobronchial (of half density and double wall thickness) radial frequencies with linear curve fittings.....	124
Figure 6.7	Logarithmic frequency spectra of experiment A1, the sectioned trachea of pig sample 1.	127
Figure 6.8	Logarithmic frequency spectra of experiment A2, the sectioned trachea with bronchi of pig sample 2.....	128
Figure 6.9	Logarithmic frequency spectra of experiment A3, the trachea with bronchi of pig sample 3.....	128
Figure 6.10	Logarithmic acoustic frequency spectrum of experiment B1, the sectioned trachea of pig sample 1.....	129
Figure 6.11	Logarithmic acoustic frequency spectra of experiment B2, the trachea with bronchi of pig sample 3.....	129
Figure 6.12	Logarithmic acoustic frequency spectra of experiment B3, the trachea with bronchi of pig sample 3.....	130
Figure 6.13	Frequency spectra of experiment A3 with increasing shaker frequency for trial 1 and decreasing frequency for trial 2.	131
Figure A.1	An overview of the respiratory system organs and tidal breathing cycle [39].....	139

Figure C.1 Natural frequencies for a freely vibrating circular cylindrical shell with clamped ends (with referring equations) [93, 105]..... 142

List of Tables

Table 3.1	Geometric and physical data of airways from the trachea to the 16th bronchus, including the analytical ring frequency of each branch.	52
Table 3.2	Comparison of analytical frequencies of tracheobronchial generations.	55
Table 4.1	The lowest frequency comparison of experimental, analytical and COSMOS/Works results on the experimental steel cylinder [105].	66
Table 5.1	Comparison of the average geometric and physical parameters between pig's and human trachea.	95
Table 5.2	Dimensions on experiments with mechanical excitation.	98
Table 5.3	Dimensions on experiments with acoustic excitation.	98
Table 5.4	Resonant frequency (f_x in Hertz) summary of experiments with mechanical excitation.	106
Table 5.5	Resonant frequency (f_x in Hertz) summary on experiments with acoustic excitation.	107
Table 6.2	Comparison of COSMOS/Works and theoretical fundamental or lowest resonant frequencies (with the clamped frequencies for reference). ...	118
Table 6.3	Comparison of COSMOS/Works and theoretical fundamental or lowest resonant frequencies, with double shell thickness and half density (with the clamped frequencies for reference).	119
Table 6.4	Comparison of frequency ratios of results Table 6.2 to Table 6.3.	121
Table 6.5	Average ratios of radial to simply supported frequencies, and radial to membrane frequencies of Table 6.2 and Table 6.3.	123
Table 6.6	Resonant frequencies by COSMOS/Works on pig trachea samples with mode 1, f_1 and the first radial resonant frequency, f_{r1}	125
Table 6.7	Comparison of resonant frequencies of experimental pig trachea samples with numerical and analytical results.	132
Table B.1	The geometric [42, 48] and physical [84] properties are listed for the generation z from 0 (the trachea) to the 16 th bronchus.	140

Table C.1	Natural Frequencies (Hertz or cycles/second) of Clamped Steel Cylinders [93] (radius $a = 3$ inch, thickness $h = 0.01$ inch, and length $l = 12$ inch.).....	141
Table E.1	Results of COSMOS/Works of individual tracheobronchus from the trachea (T0) to the 16 th bronchus (B1-B16). Analyses include default mesh and fine mesh data of mode 1 to 100. The radial frequencies (in bold) are the same for each branch and independent of the mesh size of the analysis.	144
Table F.1	Results of COSMOS/Works of individual tracheobronchus from the trachea (T0) to the 16 th bronchus (B1-B16). Analyses include default mesh and fine mesh data of mode 1 to 100. The radial frequencies (in bold) are the same for each branch and independent of the mesh size of the analysis.	153

Chapter 1

Introduction

1.1 Background

Branched circular cylindrical shells have a wide range of engineering, physical and biological applications [1-18]. Water distribution networks are one of many which are found in every city or village in modern societies; not to mention the petroleum pipelines, sewage systems, etc which are essential components of our current life styles. In biological applications, the blood circulation and respiratory systems are two of many. The focus of this work is on a branched system made up of thin elastic shells with direct application to the human respiratory system. This work represents the foundation for the vibration resonance of the lungs which must be understood in an attempt to determine whether this response could be used to help relieve airway constrictions.

Asthma is defined as “A disorder characterised by the narrowing of airways which is reversible with time, either spontaneously or as a result of treatment.” [19]. Asthma, either intrinsic or extrinsic, affects one out of six New Zealanders [20]. The extrinsic

or atopic asthma is a type of allergic reaction to allergens, while the intrinsic or nonatopic asthma has an unknown cause and is believed to be a type of over-response of the immune system to triggers [21]. The Asthma and Respiratory Foundation of New Zealand reported in *The Burden of Asthma in New Zealand* (18 February 2002), “Asthma costs NZ over \$800 million a year” [22]. New Zealand has a high prevalence of asthma among developed countries such as Australia, the United Kingdom and the United States. Developing countries also have the up-trend records due to various factors, possibly the westernised living patterns, and better than ever health facilities and treatments to people on a whole. However, there are more issues to consider other than the financial stress [22-24].

Asthma is an allergic pulmonary disease and is not curable at this time [25]. Severe episodes can be fatal, the higher the morbidity the higher the mortality, unless proper treatments and management are observed carefully [26]. During attacks, subjects may suffer one, two, or all of three kinds of symptoms, such as airway constriction, inflammation of airway walls and mucus secretions. Consequently, airway passages are clogged with mucus and occluded by contraction and inflammation of smooth muscles to some extent, making conduction of air either difficult or impossible [19, 27-35].

To be free from inducers or triggers [19] of this allergic disease seems to be the best solution. Medication is the traditional care and treatment to relieve or prevent asthmatic attacks, and should be carried at all times for often and severe sufferers. Proper management keeps asthma under control quite well except that some side

effects are of concern recently [36-38]. Unfortunately, mortality of asthma is still a great concern. This leads one to ask the question:

Is it possible to relieve asthma by physical rather than medical means?

In physical aspects, airways are a series of branched tubing from the trachea down to the bronchioles, ending with the alveolar sacs where gas exchange takes place. Science conceives that the airway network should behave similar to any physical system and has its own natural frequencies of vibration at which it responds spontaneously once excited. Therefore, it is logical to perceive that identifying the natural frequency characteristics of the complex branching tree structure is crucial in such a novel thought of utilising the mechanical relaxation for relief of asthmatic contraction of airways.

This thesis is the first insight in a research to investigate the natural frequencies of free vibrations of the airway system with the conceptive applications of the dynamic property parameters for an alternate means of relief of asthma.

1.2 Human Respiratory System

The respiratory system, as one of the biological circuits in the human body, provides a unique function of breathing in air to live. This system is so critical to living cells and different from the other ten systems: the integumentary, the skeletal, the muscular, the nervous, the endocrine, the circulatory, the digestive, the urinary, the excretory and the reproductive systems, that its proper functioning is essential within minutes. The respiratory system intakes, transports and diffuses oxygen to human

tissues for metabolism of all living cells for growth, maintenance and development, while disposing of the waste out of the body. Cells, tissues and organs live on oxygen and may permanently starve to death so fast that recovery is not possible. Therefore asthmatic subjects can be in fatal conditions because constrictions and occlusions tend to occur in numerous and tiny peripheral airways during an asthmatic attack. Both internal and external respirations are not sufficient or ceased by the increasing flow resistance of airways.

The overall anatomy or structure of the human respiratory system has the airway passages as the main frame which looks like an inverted tree. Air is breathed in and out through the nasal cavity, pharynx, larynx, and then to the subglottal respiratory system of the trachea, the primary, secondary and tertiary bronchi, the bronchioles and the acinus of alveoli (Appendix A). Such rhythmic ventilation occurs when the dome-shaped diaphragm beneath the lungs is pulled downward by the spontaneously cyclic muscle contraction. Physically, a vacuum is created as the lung volume expands following the contraction of the thoracic muscles and muscles controlling the diaphragm. Air is drawn into and fills the lungs for ventilation. When muscles relax, the elastic lungs return to their shape at rest and the gas content is expelled out of the lungs. During the inspiration and expiration process, a tidal volume of 0.5 litre flows in and out of the total lung capacity of 6 litres of an adult. Maximum voluntary effort can drive extra 3.1 litres for the inspiratory reserve volume and 1.2 litres for the expiratory reserve volume. That means that 1.2 litres of the residual volume remains inside the lungs all the times [28, 39].

Air transports through the conducting zone of the cartilaginous trachea and subsegmental bronchi, and the noncartilaginous bronchioles or terminal bronchioles to the respiratory zone of the respiratory bronchioles, alveolar ducts and alveolar sacs with over 300 million sites contributing to the diffusion surface equivalent to a tennis court with an area of 70 to 80 square metres [28, 32, 40]. To fulfil the metabolism of life, gases are diffused and exchanged through these invisible but incredible surfaces next to numerous capillaries where blood circulates throughout the whole body and tissue cells for the supply of nutrients and disposal of wastes [32, 33, 41].

The trachea bifurcates its main windpipe into the left and right primary bronchi at the carina and such branching continues with tapering radii down to twenty-three generations. The bronchial ducts are termed bronchioles before they run into the alveolar sacs where gases diffuse across the cell membrane walls of the sacs and the capillaries of blood. Geometrically, all branches are similar in shape except for the physical dimensions. Structurally, they vary slightly from one generation to the next. As the main stem of the respiratory tree, the trachea is much stiffer than others with 16 to 20 C-shaped cartilaginous rings spaced along the 12 cm longitudinal dimension [28, 32, 40]. It ends with the carina where the trachea branches into two principal bronchi. The cartilage support gradually vanishes when the bifurcation comes to the bronchiole levels. These are the dominant regions where constrictions occur during an asthmatic attack.

Asthma places a physiological challenge on the respiratory system, and disturbs and even prohibits the conduction of air in and out of the airways. Gas exchange is a transport process in series in numerous branches similar to a complex electrical series and parallel circuit. Any open circuit in the path stops part of branches or the whole system from functioning. Inter-diffusion of gases across membranes between alveoli and capillaries is deficient when expired gases are trapped in airways and cannot exchange with fresh air in the environment.

Although monitored biologically, the prescribed function of lungs and airways are physical in nature and should be able to be modelled mechanically for investigation. To do so, the geometric description and restraints on the system should be assumed in order to proceed.

1.3 Lung Morphology

Weibel [42-44] had done a tremendous amount of work on lung morphology and measurements as investigated in “Morphometry of the Human Lung” [42]. In this book, Weibel started his first sentence with “The present monograph deals with a systematic approach to a quantitative morphologic analysis of the architecture of the human lung.” This implies that he realised the role of morphology in lung studies and was one of the first pioneers who studied the morphology of the lung.

Weibel [42] modelled lungs to have air, blood and tissue as their basic components with the first two mobilizing to exchange gases through the localized tissues or membranes. The inspired air enters the nose, the upper respiratory tract, and then the

conductive zone starting from the trachea to the sixteenth bronchus, the transitory zone and the respiratory zone where external respiration occurs when oxygen and carbon dioxide are exchanged between alveoli and bloodstreams. Finally, gas diffusion between bloodstreams and body tissue cells is referred to as internal respiration. Weibel summarised the architecture of the human airway system in two models, the regular and the irregular dichotomy branching patterns.

1.4 Airway Dichotomy

Weibel's [42] regular or symmetric dichotomy pattern of the lung is termed Model "A", which is a simplified version as opposed to the irregular dichotomy, Model "B", which is more realistic to human lungs. Model "A" bifurcates the parent into two daughter branches at equal angles, equal radius and equal length while Model "B" has unequal branching parameter values. The symmetric model is beneficial to most research work because of its regularity in geometry which makes modelling easier and gives the first insight of results when such an assumption can lead to a fairly good approximation. This is particularly true in human airways where a precise response of individual tracheobronchial branches is critical when considering the overall lumped system of lungs.

Horsfield and Cumming [45] term the asymmetric airway branching as orders of a count-up system instead of generations of a count-down system by Weibel. The Horsfield order starts with the alveolar sacs and counts up to the trachea with the order of thirty-one [45, 46] and is practical and more applicable to the asymmetric airways in reality with the advantage that paths of the same Horsfield order can be

assumed to have the same physical dimensions, or the path length [47]. Fredberg and Moore adopted the Horsfield order in the self-consistent branching model of the airways of the human lung in simulating the distributed response of complex branching duct networks [4].

1.5 Histological View of Airways

Airways of the tracheobronchial tree are responsible for clear passages of air ventilation of the respiratory system. The continuous branching tracheobronchial tree varies not only in the geometric dimensions, but also in the physical properties down from the trachea to the bronchioles and the alveoli.

In the histological aspect as seen in Figure 1.1, airways are covered with the epithelium over the inner surface as the first defence from the external intruders, similar to the lumens of other human organs. This lining of pseudostratified ciliated columnar cells sits on top of a basement membrane which separates smooth muscles of the lamina propria layer. The outermost cartilaginous layer diminishes progressively and finally disappears in bronchioles of 1 mm in diameters or less.

On top of the cilia is a sol layer and a gel layer which form the mucous blanket for trapping debris from further invasion into the alveoli where diffusion occurs. The wavelike movement of cilia vibrates about at 1500 times per minute and drives the sol layer to escalate the more viscous gel layer along with foreign particles, at roughly 2 cm per minute, up to the larynx for cleaning purposes. This mucociliary transport mechanism may not function properly due to various factors.

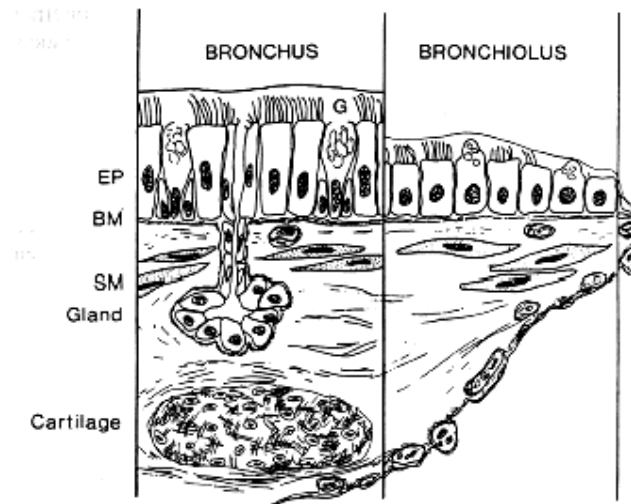


Figure 1.1 Schematic comparison of airway wall, in cross-section between bronchus and peripheral bronchiolus where cartilage disappears. EP, epithelium; BM, basement membrane; SM, smooth muscle [43, 48].

The mechanism of asthma is irrespective of the cause, whether due to inducers or triggers, and is more or less the same. Mast cells are considered to be the releasers of mediators such as histamine and leukotrienes upon initiation of asthma. These mediators act on cells of receptors on the airway smooth muscles and bronchoconstriction occurs. The current view of asthma is more concerned with the inflammation caused by such cells that initiate the mechanism rather than the contraction of airway smooth muscles [19, 31, 49, 50].

1.6 Airway Physiology

Human airways are passages for gas transport in the lungs. The lumen areas should be free from dirt and debris for smooth flow of gases during breathing cycles. A segmental cross-sectional view depicts the layers of the epithelial lining of the airway wall. The goblet cells and the submucosal glands secrete the mucous blanket

of the gel and the sol layers. The viscous gel layer traps foreign particles while the sol layer is escalated by the cilia so that the mucous blanket moves up to the larynx as sputum at approximate 2 cm per minute. A basement membrane separates the epithelium and the lamina propria. Goblet cells are distributed intermittently among basal cells in the epithelial layer. In the lamina propria, an inner circular and an outer longitudinal thin layer of smooth muscle as in Figure 1.2 [34, 51] lie right next to the basement membrane and parasympathetic nerves immersed in the rest of space. Finally it comes to the cartilaginous layer which is the stiffest part of the epithelial lining of the airways. The stiffness of the airway wall therefore depends greatly on the proportion of the cartilaginous layer which diminishes as fast as the generation branches grow.

Air is first cleaned and moistened at the nostrils of the respiratory system similar to the function of the carburettor of an automobile. The ciliated epithelium with secreted mucus filters the inspired air, which is also warmed and moistened by the heat generated around the nasal cavity wall to ensure that the incoming air is close to the body temperature. The cleaning process is then maintained by the escalating beating process of the epithelial cilia to bring any debris up for removal. All these should occur in the passages of the trachea and the upper bronchi as bronchioles are physically too small and too far down to provide any cleaning job.

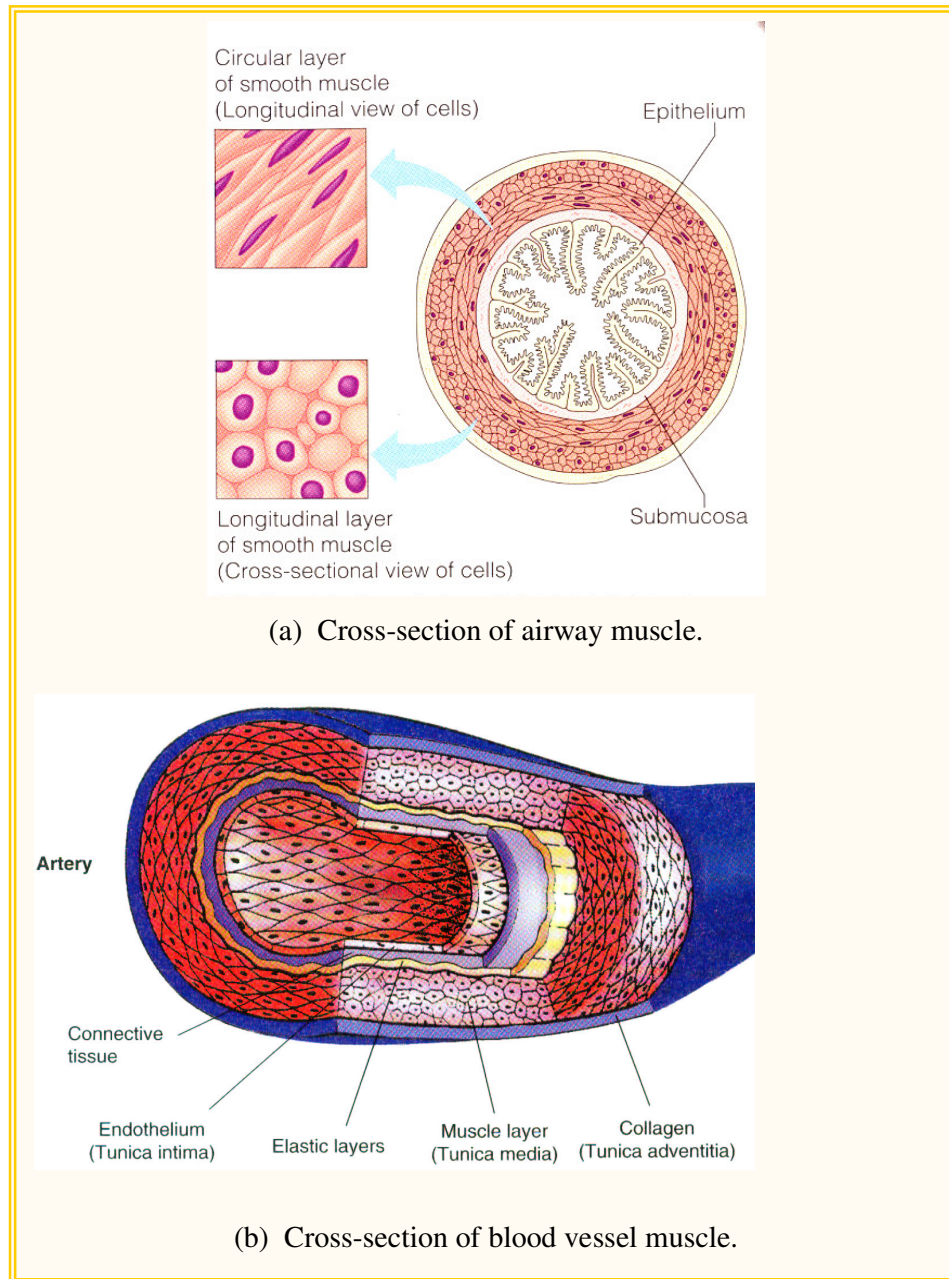


Figure 1.2 (a) Circumferential and longitudinal layers of smooth muscle of airways [51]. (b) Contrarily, components of the major blood vessels with inner longitudinal and outer circumferential muscles [34].

Once air comes to the alveolar sacs, ventilation takes place by diffusing gases across the membrane boundary between the lungs and the vascular capillaries. The exchange of oxygen with carbon dioxide oxygenates the blood with haemoglobins. The heart pumps the body's blood in and out of its atria and ventricles in circulation for the supply of oxygen and disposal of waste, mainly carbon dioxide. Physiologically, carbon dioxide concentration in blood monitors the rhythm of breathing. The central nervous system will initiate to speed up the breathing rate once it senses a high level of carbon dioxide concentration.

This chapter has described the general background of respiratory system related to this work. Chapter 2 is a literature review on work of the respiratory system related to the title. The theoretical analysis of the circular cylindrical thin shell is presented in Chapter 3, resulting in the resonant frequencies of such a shell as membrane. This serves as the fundamental unit in the expanded modelling of the complex airway network. Further numerical investigation using Finite Element Analysis (FEA) COSMOS/Works, a computing software integrating the modelling and analysis features is presented in Chapter 4. Chapter 5 gives the experimental validation for the resonant frequencies obtained from pigs' tracheobronchial system. Chapter 6 discusses the analytical modelling, numerical modelling, experimental validation, the overall view of this thesis, and finally recommendations for future work.

Chapter 2

Literature Review

2.1 Introduction

Branched circular cylindrical shells have many physical, biological and engineering applications. To cite a few, the human body blood circulation, and respiratory systems, water distribution networks, petroleum distribution networks... etc. Most of these systems have been dealt with from fluid flow, load analysis, acoustics and elasticity modelling [5, 7, 10, 11, 14-17, 52-62]. No work has been found which deals with the vibration of branched circular cylindrical shells. This problem entitles the complexity of the boundary conditions and the discontinuity of the branches and the junctions. This work represents one of the first to deal with the vibration of branched circular cylindrical shells with specific application to the respiratory branching structure.

Study of lungs arises in the response to lung disorders in human beings. Medical and clinical study of lungs focuses on the biological and cellular level. Anatomy, a study

of human structure, is the basic knowledge required beyond the general understanding of chemistry and biology. The next or concurrent course with anatomy is physiology which is more concerned about the functioning of human and animal organs.

Lung functioning is critical to life. However, the physiological study of the lung may come before the anatomy [42, 63] and physics is definitely a related subject other than chemistry and biology in medical study. The physical study of lungs includes the movement of air in and out of the body, the physical properties of tissues and muscles and such geometric dimensions as factors of the respiratory functioning. All such related studies can be termed as airway mechanics.

2.2 Airway Mechanics

Airway mechanics is a broad subject in applying physical laws in lungs and airways.

The available literature on this subject may be classified into four main categories:

1. Airway fluid mechanics approach
2. Airway narrowing mechanisms
3. Dynamic characteristics of airways and lung tissues
4. Measurements of dynamic parameters

In the following sections, a brief description is presented on each one of the categories [46].

2.2.1 Airway Fluid Mechanics Approach

Airway pressure drop is proportional to the momentary flow rate and the regional resistance of the airway, which is inversely proportional to the cross-sectional area. In the lower generations of the bronchial tree, numerous bronchi are shunted together to equivalent to a huge cross-sectional area as seen by the pressure head; therefore the drop is practically negligible. Contribution to pressure drop is less than 10% [64] for generations beyond 10, or diameters less than 0.5 mm. Therefore, the dead space volume exists at the alveolar ending because of slow flow in this region. The electrical analogy provides an alternative form of analysis of the airway mechanics.

Historical development of airway mechanics applied to the respiratory system can be traced back to 1915 when Rohrer [63] first proposed the Rohrer's equation: airway pressure drop is a function of the instantaneous flow rate. Rohrer assumed that the pressure drop in the respiratory system from the mouth down to the alveoli is contributed by a linear and a quadratic function of the flow and can be expressed as follows:

$$\Delta P = K_1 \dot{V} + K_2 \dot{V}^2 \quad (2.2.1)$$

where ΔP is the airway pressure drop,

\dot{V} is the flow rate,

K_1 and K_2 are empirical constants.

Consequently, the airway resistance R as a ratio of pressure drop to flow rate is expressed as:

$$R = K_1 + K_2 \dot{V} \quad (2.2.2)$$

Therefore, the airway resistance is not 'ohmic' as indicated. Twelve years later, von Neergaard and Wirz [65], designed the so-called Interrupter Method for experimental or clinical measurements of airway resistance [66, 67]. The pressure drop is defined as the pressure difference between the airway opening pressure and the mean alveolar pressure which comes with no direct method of measuring. The Interrupter Method overcame this difficulty by assuming that the sudden occlusion or interruption of flow in the airway causes no variation of the alveolar pressure which is equated to be the instant pressure at the airway opening after the closure of the shutter. The experimental airway resistance can therefore be determined by the ratio of the pressure drop due to the interruption and the airway flow rate prior to such an occlusion [66-68]. This technique was superseded by the Body Plethysmography Technique [69] in the late 1950's, but became common again due to its non-invasiveness of patients and its incorporation with the forced and high frequency techniques thereby expanding the scope of applications [70-74].

Rohrer's assumption of low and high-speed flow contributions lacked theoretical support. Pedley et al. [64] investigated the pressure drop and its relation with the lower airway resistance in another manner. He claimed that the airway flow, somewhat in a laminar way, should be considered to be in turbulent mode and that

the Poiseuille flow was not applicable even in smaller airways [75]. The derived equation for the pressure drop with respect to the Weibel's model is:

$$\Delta P = K (\rho\mu)^{1/2} \dot{V}^{3/2} \quad (2.2.3)$$

where K is a constant depending only on lung anatomy, ρ and μ are the density and dynamic viscosity of air respectively, and \dot{V} is the volumetric flow rate.

An additional factor Z , based on the Poiseuille equation, accounts for the turbulent disruption at bifurcations and is expressed as:

$$Z = \frac{C}{4\sqrt{2}} \left\{ Re \frac{d}{l} \right\}^{\frac{1}{2}} \quad (2.2.4)$$

where C is an experimental constant estimated to be 1.85 in the developed model, Re is the Reynolds number, d is airway diameter, and l is the airway length.

However this factor, a ratio of the real resistance to the Poiseuille resistance, can be used to multiply the pressure drop estimated in the laminar flow only when $Z > 1$.

A correlation has been made on the pressure-flow data with normalisation on the family of curves obtained from an extension of Rohrer's development to a wide range of conditions by Jaffrin and Kesic [59]. Conclusively, the airway resistance at any given lung volume is proportional to the high flow rate or the flow of heavy gases; otherwise is independent for the opposite extremes. With concern of turbulence at bifurcations, Jaffrin and Kesic's model in estimation of the pulmonary resistance can be summarised as follows:

$$\frac{\Delta P}{\frac{1}{2}\rho u^2} = f(Re) \quad \text{Pressure drop in straight tubes} \quad (2.2.5)$$

$$\frac{P_n - P_{n+1}}{\frac{1}{2}\rho u_n^2} \cong 2\left(\frac{u_{n+1}}{u_n}\right)^2 - 2\left(\frac{u_{n+1}}{u_n}\right)\cos\psi_n \quad \text{Pressure drop across bifurcation} \quad (2.2.6)$$

$$G = \frac{1}{R} = a(V - b) \quad \text{Low conductance (resistance) and lung volume} \quad (2.2.7)$$

where ΔP and $P_n - P_{n+1}$ are pressure drops in straight airways and across n th and $n+1$ th generations,

u_n and u_{n+1} are velocity of gas in n th and $n+1$ th generations,

G is the conductance (the reciprocal of resistance R) and V is the lung volume,

ψ_n is the angle of branching at n th generation, and

a and b are constants.

2.2.2 Airway Narrowing Mechanisms

Airway obstruction can be caused either by inflammation or airway smooth muscle (ASM) contraction as far as asthma is concerned. Inflammation is due to irritation resulting in epithelium thickening, mucous production and the non-specific defence of the immunity response. ASM contraction is mainly due to the airway hyper-responsiveness of the asthmatics. Emotions are no longer believed to be factors for such episodes; instead they contribute to the effects of the cause. Physiologically, the airway wall (cross-sectional) area can be approximated to a circular ring with mainly the inner mucosa, airway smooth muscle and the outer adventitia, Figure 2.1

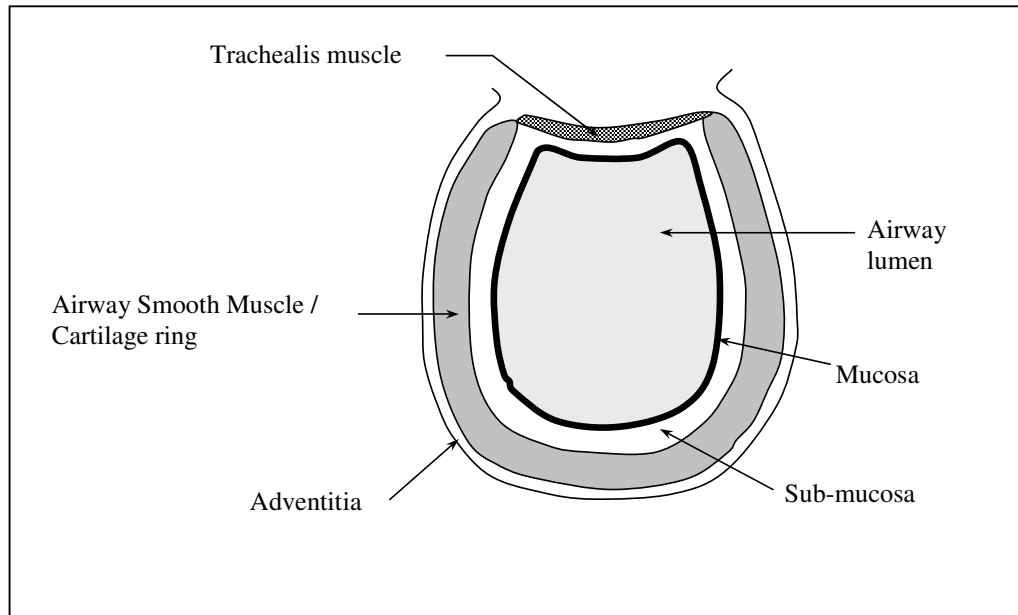


Figure 2.1 Tissue composition of central airway walls.

Human muscles are classified into three types, smooth muscle, cardiac muscle and skeletal muscle. Smooth muscle is the most dominant type in the airway walls or the respiratory system, and gradually replaces the supportive cartilage rings in the lowering, branching and narrowing bronchi. An airway smooth muscle is composed of two layers orthogonal to each other. The inner layer is circumferential while the outer is axial to the airway geometry. To preserve the muscle volume, contraction in either direction results in thickening of the airway wall (cross-section) area, that is, narrowing of the airway lumen. Airway smooth muscle shortening has less effect on lumen occlusion for normal subjects than the asthmatic ones [76] because of the nervous control of self-regulation.

Fredberg [77] studied the molecular basis of mechanical friction by measuring the rates of mechanical energy dissipation and actomyosin adenosine triphosphate (ATP) utilisation in canine airway smooth muscle and found its dependence on the rate of cross-bridge cycling, instead of the classic viscosity. The force maintenance or latch in the low-friction contractile state might be responsible for the irreversibility of the asthmatic subjects to spontaneous airway obstruction with a deep inspiration. Away from the internal control of the smooth muscle mechanism, a simulation [50] was made on the airway narrowing by applying works from Weibel's symmetrical dichotomous branching tracheobronchial tree, Pedley et al. [64] fluid dynamic equations and Lambert et al. [78, 79] airway pressure-area curves. It linked the physical parameters of the airway smooth muscle shortening, airway wall thickness and pulmonary resistance through simulating the control of the S-shaped dose-response. The resulting pulmonary resistance versus dose-response curves could be a potential tool to investigate obstructive diseases if such behaviour was realistic.

2.2.3 Dynamic Characteristics of Airway and Lung Tissues

A dynamic system has its statics as the building blocks for real-time investigation. Energy is the driving source for all dynamic operations. The energy dissipating factors depend on the modelling of the system. The pressure energy of fluid flow in a simple channel can be utilised in three ways:

1. to overcome viscous forces exerted by the channel wall
2. to accelerate the fluid or to overcome the inertial effect - inertance
3. to expand the channel wall if it is elastic or non-rigid

It is quite possible to extend the channel flow idea to the complicated airway breathing system including other effective factors or parameters. A stimulated frequency response [71], later in higher frequency [80], can probe into the system to reveal the dynamic characteristics, as breathing is an unsteady cyclic process with continually varying pressure, flow rate and volume due to inspiration and expiration. The inter-dependence among the mechanical, physical properties of the airway wall and tissues, and the acoustical properties of the air should also be observed. Critical parameters in the dynamic analysis of the tracheobronchial tree are: airway wall compliance (reciprocal of elastance); lung tissue resistance (damping) and elastance; acoustical properties such as bulk modulus and the density of air. Propagation of acoustic waves is limited to one dimension in the longitudinal direction while the transverse mode is negligible for the small radial dimension compared to the applied wavelength. Figure 2.2 depicts the overview.

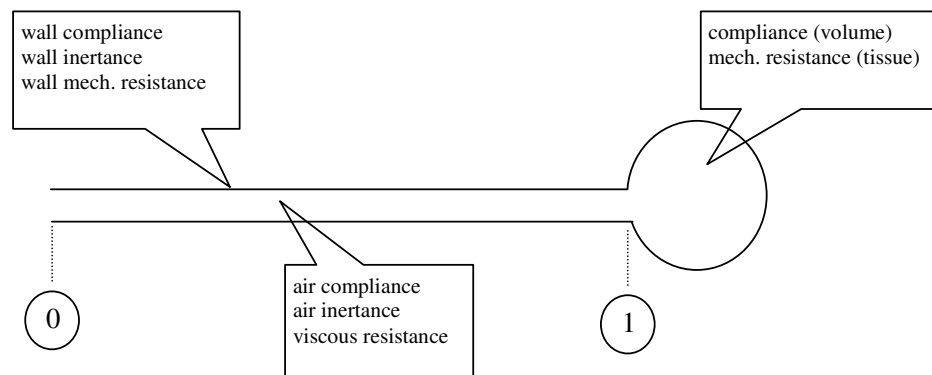


Figure 2.2 Parameters considered for dynamic characteristics of airways.

The impedance [16, 81] of such a non-conducting tube could be given as a function of perturbation frequency along with the physical and mechanical properties of the system as follows:

$$Z_0 = \left(\frac{\rho_0 c}{S} \right) \left[\frac{Z_L + j \left(\frac{\rho_0 c}{S} \right) \tan(kL)}{\left(\frac{\rho_0 c}{S} \right) + j Z_L \tan(kL)} \right] \quad (2.2.8)$$

where ρ_0 is the mean air density,
 L and S are the length and cross-section area of the tube (airway) respectively,
 k is the wave number, i.e. ratio of frequency (ω) to sonic speed (c),
 Z_0 and Z_L are impedances at section '0' and '1' respectively, and
 $j = \sqrt{-1}$.

The impedance Z_L is however governed by the boundary conditions at section 1, in Fig 2.2 which depends on the mechanical response of the alveoli. Modification and improvement [15] can be made on this simple model to a rigid symmetric Nth order branching network as the tracheobronchial tree.

Schmid-Schoenbein and Fung [82] developed a distributed model (multi-degree of freedom) treating the respiratory system as a continuous elastic body. The lung dynamic characteristics were simulated using a lumped mass-damper-spring model. The model consisted of the dynamics of the airways, lung parenchyma, chest wall, diaphragm and abdomen. The non-linear governing partial differential equations were linearised for small perturbations and solved subject to boundary conditions

with a number of simplifying assumptions. They used the method of series expansion and collocation to solve the governing equations of the abdomen, lung parenchyma and the chest wall. They concluded from their study that by using a continuum model that more realistic dynamic characteristics of the respiratory system could be obtained to interpret various pulmonary diseases.

Fredberg and coworkers [4, 5, 83, 84] investigated the dynamic characteristics of branching networks including the tracheobronchial tree under various conditions. Simulations were carried out with a view of modal analysis of asymmetrically branching networks. Two structures were analysed: a bushlike structure consisting of a trunk that divides into N siblings of variable lengths and cross-sections; and an asymmetric structure of the tracheobronchial tree. For the bushlike structure, the undamped system eigenvalues and the normalised input impedance of the damped system were given by:

$$S_0 \cot(k_0 L_0) - \sum_{n=1}^N S_n \tan(k_n L_n) = 0 \quad (2.2.9)$$

$$\frac{Z_{i,n}}{Z_0} = -j \frac{\cot(\hat{k}_0 L_0) - \sum_{n=1}^N \left(\frac{S_n}{S_0}\right) \tan(\hat{k}_n L_n)}{1 + \cot(\hat{k}_0 L_0) \sum_{n=1}^N \left(\frac{S_n}{S_0}\right) \tan(\hat{k}_n L_n)} \quad (2.2.10)$$

where k_0 , S_0 and L_0 are complex wave number, the cross-sectional area and length of the main trunk,

S_n and L_n are the cross-sectional area and length of siblings,

\hat{k}_n is the complex wave number,

Z_0 is $\rho_0 c_0 / S_0$, and

$Z_{i,n}$ are the input impedance of main trunk and branches respectively.

Fredberg and Moore [4] presented a mathematical model to simulate the distributed response of asymmetric branching networks. Simulations were carried out on the human lung to investigate the response of pressure with frequency, path and position. The model included mechanical inhomogeneities from origin to terminations as well as parallel ways. The impedance matrix of a link was given by:

$$\begin{bmatrix} P_0 \\ P_L \end{bmatrix} = \begin{bmatrix} \alpha_{11} & -\alpha_{21} \\ \alpha_{21} & -\alpha_{11} \end{bmatrix} \begin{bmatrix} V_0 \\ V_L \end{bmatrix} \quad (2.2.11)$$

where P_0 , P_L and V_0 , V_L are the pressure and the volume rate at the ends of the link and α 's are given by:

$$\alpha_{11} = \frac{Z_a}{\tanh(j k_a L)} \quad : \quad \alpha_{21} = \frac{Z_a}{\sinh(j k_a L)} \quad (2.2.12)$$

where Z_a is the complex characteristics of the tree link and k_a is the complex wave number. They used recursive matrix formulation to determine the impedance at successive nodes along the principal path. From the simulation results they concluded that the effects of tree asymmetry are significant above 100 Hz in the air-filled lung.

Fredberg and Hoenig [84] presented an efficient method for computing the input impedance of complex asymmetrically branching duct networks. The proposed method incorporated the concept of a 'self consistent' network to deal with the

complex non-symmetric structures. Self-consistency of a branching network implies that the impedance boundary conditions in all terminal links are identical. Governing equations of the model comprised the description of the dynamic characteristics of conducting airways, alveolar ducts and airway terminals. Conducting airways were represented with resistance, inertance and compliance components for both gas and airway walls. An additional factor was also introduced for the conducting airways to account for the thermal resistance of the air. For alveolar ducts, the resistance, inertance, compliance and thermal resistance of air were considered. The terminals of the airways were described by using a six-component model to account for resistance, inertance and compliance of both the lung tissue and thorax wall. The model was simulated to obtain the dynamic response of the lungs of normal adult humans in the frequency range exceeding 10,000 Hz. They concluded that the response of comparable symmetric and asymmetric networks differ at high frequency (> 2 kHz.) and the airway wall response is an important factor in determining system resonance and damping.

Al-Jumaily and Al-Saffar [85] have extended the model developed by Fredberg [4] above by including the effect of the wall inertia to study the dynamic response of the respiratory system. Further Al-Jumaily and Mithraratne [54] developed a theoretical acoustical model of the respiratory system based on the Weibel's symmetric dichotomy and simulated the dynamic response of rigid as well as compliant airway walls with rigid and compliant terminations. Occlusions, if any, may be revealed and analysed systematically by the normalised curves of the input impedance versus

the stimulating frequency, at each generation from alveolar sacs up to the distal end of the primary bronchi.

Margolis and Tabrizi [14] presented a method to investigate the dynamics of the lung using 'bond graphs'. The model included the distributed dynamics of the proximal airways (trachea and main bronchi), with the distal generations represented in lumped resistance and compliance. The model was capable of simulating system dynamic characteristics of frequencies as high as 8500 Hz. With appropriate modifications the model claimed to predict the input-output relation between the mouth and any desired lung segment location.

A technique was developed by Raphael [15] to determine explicit resonance conditions at the open end of a rigid, symmetrical, branching structure with an arbitrary number N of successive bifurcations resulting in $2N$ terminal closed branches. In general, recursive matrix techniques are used to obtain the impedances at the nodes in a branching network and Raphael manipulated the equations [71] to express explicitly the overall resonance condition of the entire network related to the branch lengths, areas, the angular frequency and the integral harmonic number.

Raphael and Epstein [16] also extended the technique of branching networks [4, 15, 83] to estimate the volume of symmetrically branching structures using the resonance mode analysis in two approaches, using fundamental frequency and equivalent length. The volume estimation using the former method for a 3rd order bifurcation network is given by:

$$V \approx \frac{S_1 c}{4 f_1} \quad (2.2.13)$$

where V is the total volume,
 S_1 is the cross-section of the 1st (main) branch,
 c is the acoustic velocity, and
 f_1 is the fundamental frequency.

They considered two special cases with the Weibel model under the fundamental frequency method.

1. Equivalent area where the total cross-sectional area of each generation remains the same.
2. The successively fractional diameter decreasing case where the diameter of each lower generation is a fraction of its parent link.

The studies conducted on the respiratory system using the acoustical approach attempted mainly to determine the lung structure using non-invasive methods. It is clear from scrutiny of the literature pertinent to the subject concerned that some models have incorporated the airway dynamic characteristics (inclusion of mechanical properties) into the acoustics of the system while others have simply treated the airways as rigid walls. None of the dynamic analysis studies reported in the literature has considered the dynamic characteristics of the airways (walls). This basically involves mode shapes and the natural frequencies of the airways. Identifying these parameters will give a better understanding of the ways of expanding airways that have been contracted due to respiratory disorders. Furthermore, investigation of these parameters may have a clinical relevance.

2.2.4 Measurements of Dynamic Parameters

Dynamic parameters of the lung are clues in the diagnosis of the respiratory system. The measuring techniques integrate the background knowledge of physiology and fundamental concepts on airway mechanics with dynamic frequency response as the probing tools, also the narrowing mechanism incorporated for relief of occlusion. Investigations so far are mainly on experimental measurements of pressure, volume and volume flow rate, under a variety of conditions depending on the model designed, to reflect indirectly the diagnostic parameters such as pulmonary resistance, lung dynamic elastance. Clinical practice and research share similar equipment [40, 86] in functioning whilst focusing on respective purposes. In general, the latter searches for a methodology for the former to apply.

With the four-element lung mechanical model, Figure 2.3, Avanzolini and Barbini [87] presented and evaluated three proposed recursive algorithms: (i) equation error (ii) two-stage-least-square and (iii) output error.

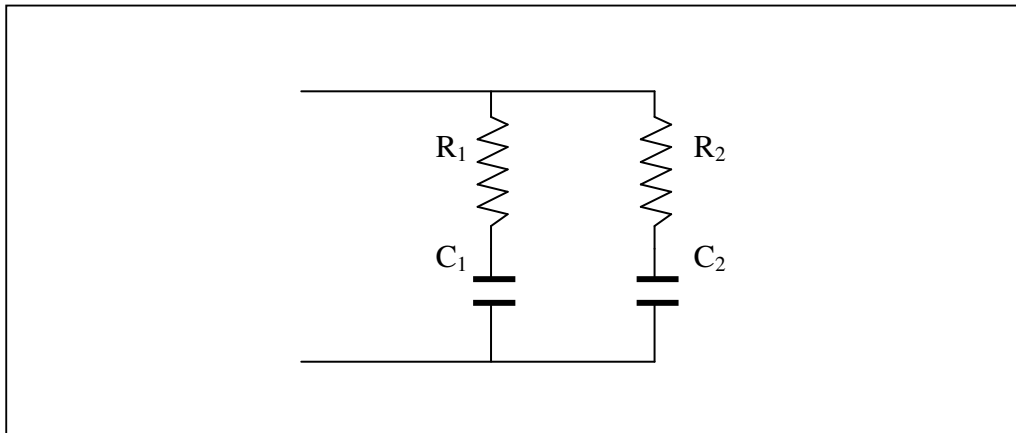


Figure 2.3 Four-element lung mechanical model Avanzolini and Barbini [87].

The four-element biquadratic impedance arrangement represented the respiratory mechanics of the patients undergoing artificial ventilation. The general input–output identification model for discrete time was given by:

$$y = \frac{B(z^{-1})}{A(z^{-1})} u + v \quad (2.2.14)$$

where y is the output, u is the input, v is the disturbance (noise), A and B are functions of z transforms of discrete time functions.

The signals used for identification were the airflow at the mouth and the pressure difference between the trachea and the pleurae. They have reported that the output error algorithm, in general, gives a better disturbance screening or rejection effect than the equation error method and it is attractive for practical applications since it needs less computational effort.

Hantos et al. [8] studied the regional input impedance of airways and lung tissues using the measurements by a modified wave-tube technique. Small-amplitude computer generated pseudorandom forced oscillations between 0.1 and 48 Hz were applied through catheters placed in 2mm diameter bronchi in dogs' lungs. The impedance was evaluated using simple models that were considered adequate to describe the gross mechanical behaviour of the lung periphery. The models for data fitting consisted of the resistance, inertance of segmental airways, the resistance of the collateral channels, and the damping and elastance of the tissues. The separated elastance and damping was claimed for better impedance results to the single tissue

compliance. The model parameters were estimated by means of a global optimisation procedure minimising the fitting error.

Pedersen et al. [61] investigated experimentally the peak expiratory flow using the wave-speed flow-limiting mechanism. Peak expiratory flow (PEF) is defined as the highest flow achieved at the mouth during a maximum forced vital capacity (FVC) manoeuvre starting at full inspiration. That the volumetric flow rate through an airway segment approaches maximum when the convective velocity reaches the sonic speed, the maximum flow \dot{V}_{\max} may be given by:

$$\dot{V}_{\max} = A \left[\frac{A}{\rho C} \right]^{0.5} \quad (2.2.15)$$

where A is the airway cross-sectional area,

ρ is the air density, and

C is the airway compliance.

Therefore, if PEF is limited by the sonic speed, then the peak flow should occur when the velocity of the accelerating flow reaches sonic speed at some point in the

airway and at that point the speed index $\left(SI = \frac{\dot{V}}{\dot{V}_{\max}} \right)$ is equal to one. From the

experimental measurements made on healthy and asthmatic subjects they concluded that SI , when the PEF reached, is close to unity for healthy subjects but is less than 1 for most asthmatic subjects.

Officer et al. [88] measured with a volume-displacement plethysmograph [28] the pulmonary resistance and lung elastance in normal subjects and in subjects with emphysema and asthma, then compared, through least square data fitting, the response by the four models as follows:

1. a single resistance and elastance
2. separate resistances and elastances for each half breath
3. separate inspiratory and expiratory resistance with a single elastance
4. separate inspiratory and expiratory resistance, an expiratory interaction term and a single elastance

They concluded that all the models gave comparable responses with the exception of models 1 and 3 overestimating the dynamic elastance and inspiration resistance. It has also been found that model 4 appears to give a good measure of inspiratory resistance and dynamic elastance. Further they concluded that the expiratory resistance is larger than the inspiratory resistance in normal and asthmatic subjects and that inspiratory resistance is higher than the expiratory resistance in subjects who experience severe broncho-constriction.

Kaczka et al. [89] proposed a method to partition the total lung resistance (R_L) into two components, the airway resistance (R_{aw}) (viscous dissipation) and the lung tissue resistance (R_{ti}) (mechanical resistance). With this approach they compared the resistive components in asthmatic and healthy subjects. Another parameter that was used in the study for comparison purposes was the lung elastance. By measuring the lung impedance at different frequencies around the breathing rate, they were able to partition R_{aw} and R_{ti} since these two components have distinct frequency–response

characteristics. From the comparative studies they proposed four models to cover experimental data obtained from asthmatic subjects:

- (a) A homogeneous airway model consisting of a rigid-walled airway channel with parameters for airway resistance (R_{aw}) and inertia (I_{aw}) followed by a visco-elastic tissue compartment with parameters for tissue damping (G) and tissue elastance (E).
- (b) An airway shunt model consisting of an additional parameter for airway compliance (C_{aw}).
- (c) An inhomogeneous airway model consisting of two separate airway pathways both leading to identical visco-elastic tissue compartments.
- (d) An Inter-regional flow model with an additional collateral resistance in parallel with the tissues.

The study investigated the relative contribution of the two partitioned factors, airway resistance and tissue resistance, to the overall lung resistance in asthmatics before and after albuterol inhalation, compared to previous results with healthy subjects during methacholine-induced bronchoconstriction. They found that the contribution ratio was relatively the same and independent of the constriction of the smooth muscle. However, asthmatics had a greater airway to peripheral resistance ratio.

The human respiratory system, as part of the circulatory system, provides a unique function, breathing of air to live. This system is so critical and different from the others, the integumentary, the skeletal, the muscular, the nervous, the endocrine, the circulatory, the digestive, the urinary, the excretory and the reproductive systems. It delivers and provides oxygen for metabolism of all living cells for growth, repair and

development. Cells may be starved of oxygen to death within minutes. For that asthmatic subjects can be in fatal condition because constriction and occlusion tend to occur in peripheral airways during attacks.

2.3 Objectives

Since no previous research was found to focus on investigating the vibration characteristics of branched circular cylindrical shells, the main objectives of this research are summarised as follows:

1. Investigate the possibility of modelling such a branched circular cylindrical thin shell analytically. In this respect it is expected to use an appropriate thin shell theory and suitable boundary conditions to reflect that of the respiratory branching structure.
2. Since no values for validation are available, a finite element code will be used to determine the natural frequencies and mode shapes of a branched structure.
3. The results of step 2 above will be used for validation as well as for studying other cases which cannot be dealt with analytically.
4. Since obtaining an experimental natural frequency and mode shape of human airways for validation purpose is very cumbersome if not impossible, and requires equipment which are not available at AUT, the natural frequency of a trachea and a tracheobronchial system will be determined with pig samples

through the modal analysis and testing techniques for the dynamics response in terms of the radial resonance and mode shape.

5. Utilise the results so that a thorough understanding of the dynamics of the lungs as a network of circular cylindrical thin shells so that there may be radial relaxation of constriction and occlusion with pulmonary disorders.

Chapter 3

Analytical Models

3.1 Introduction

Airways are the transport passages of air to and fro between the alveoli and the environment. The luminal diameters of the trachea and bronchi determine how easy the gases can pass through in the breathing rhythm. The trachea, or windpipe and each bronchus have a pipe shape with thin walls slightly tapering as it progresses.

To model airways for the natural frequencies, both geometric and physical parameters of the concerned system are the critical factors of the outcome. The extreme thinness of these layers relative to the longitudinal dimensions of the conducting passages suggests a circular cylindrical shell structure when ignoring the small tapering of branching. In the same token, it is quite legitimate to approximate the respiratory branching tree as homogeneous with isotropic wall properties. As the vibration response of this system is modelled for the first time, it is felt that such assumptions will generate reasonable results which may not be accurate, but definitely will show the trend of variation. The continuum can then be analysed by considering an isolated element of the airway wall which is membrane-like and

sustains a very small bending moment which may be neglected in comparison with axial forces. Due to the fact that the airway passages undergo mainly radial deformations, the in plane deformation is relatively small in comparison with the radial ones, and may be neglected in the present investigation.

The base unit of the airway tree is a narrowing tube which can be modelled as a circular cylindrical thin shell, assuming that the slight tapering contribute no significant deviation from the expected results. Such a concept can then be extended to all branching components of the overall structure.

3.2 Governing Equations

Soedel [90] praises Galileo Galilei (1564-1642) as the pioneer in vibration analysis in his study of the frequency dependence on the length of a simple pendulum. Since then, development phases continue from continuous systems by Robert Hooke (1635-1703), longitudinal vibrations of rods by Chladni and Biot, transverse vibration of flexible thin beams by Daniel Bernoulli and Euler, and torsional vibrations by Coulomb, Cauchy, Poisson, and Saint-Venant. Further vibration work on membranes, plates and shells are studied by Euler, Bernoulli, Lagrange, Kirchhoff, Love and Rayleigh, while Sophie Germain (1776-1831) is the first who investigated shell vibrations before 1821. The basic classical theory of shells was formulated by Love based on the vibrations of thin plates by Kirchhoff.

A thin circular cylindrical shell [90-95] is now considered as the fundamental structure of the overall airways. In fact, the airway walls are so thin relative to the

lumen radius and the branch length [42, 48, 96, 97] that they are actually considered as membranes with no resistance to both loads and bending. Consider an element of the airway walls as a shell element exposed to planer forces N_x , N_θ and $N_{x\theta}$ only. Bending is assumed insignificant as compared to other loadings in this analysis. Consider a cylindrical membrane element of radius a , Figure 3.1, with axial force per unit length N_x , circumferential force per unit length, N_θ and shear force $N_{x\theta}$ per unit length.

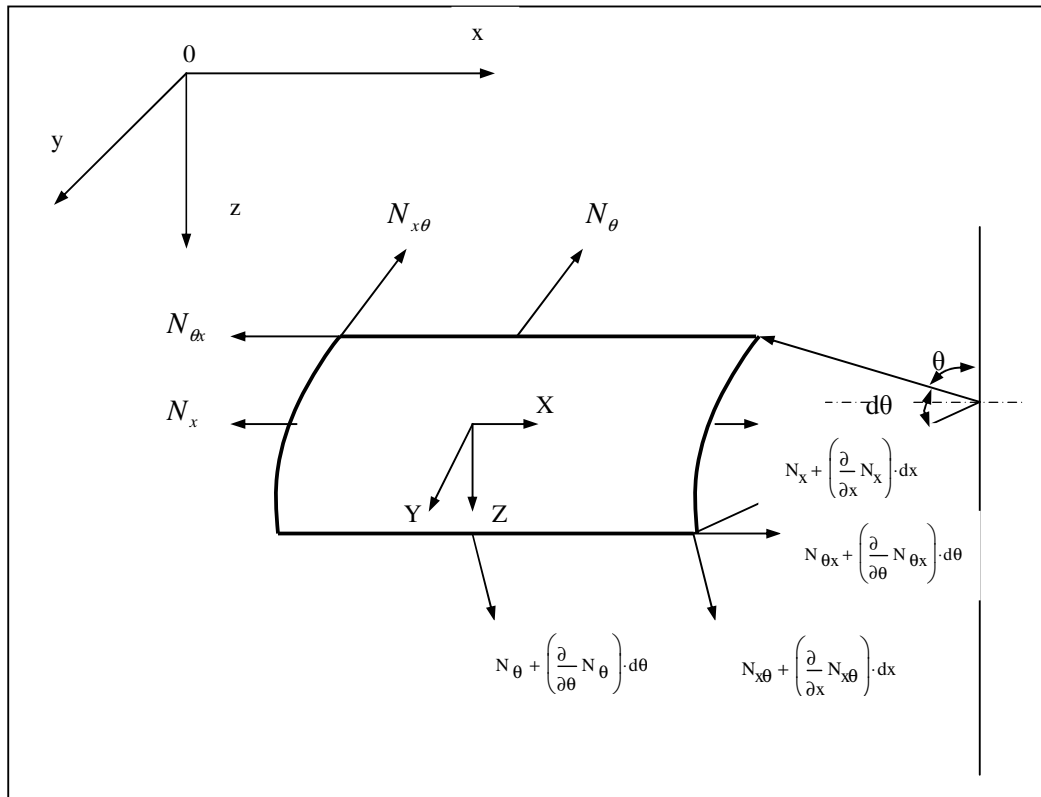


Figure 3.1 A cylindrical membrane element with normal and shear stresses [98].

Applying Newton's second law and the first equilibrium condition in the axial direction x leads to

$$\left(N_x + \frac{\partial N_x}{\partial x} dx \right) a d\theta - N_x R d\theta + \left(N_{\theta x} + \frac{\partial N_{\theta x}}{\partial \theta} d\theta \right) dx - N_{\theta x} dx + X a d\theta dx = 0 \quad (3.2.1)$$

This can be simplified to:

$$\frac{\partial N_x}{\partial x} + \frac{\partial N_{\theta x}}{a \partial \theta} + X = 0 \quad (3.2.2)$$

where the N 's are the normal stresses (with single subscripts) and the shear stresses (with double subscripts) in the captioned direction x .

Similarly, applying Newton's second law in the θ -direction with some simplification leads to the resulting forces in the y direction

$$\frac{\partial N_{x\theta}}{\partial x} + \frac{\partial N_\theta}{a \partial \theta} + Y = 0 \quad (3.2.3)$$

To satisfy the condition of equilibrium of moment about the z axis implies that

$$N_{x\theta} = N_{\theta x} \quad (3.2.4)$$

Then equation (3.2.3) can be re-written as

$$\frac{\partial N_{\theta x}}{\partial x} + \frac{\partial N_\theta}{a \partial \theta} + Y = 0 \quad (3.2.5)$$

Similarly, summing forces in the z -direction can lead to

$$N_\theta dx \frac{d\theta}{2} + \frac{\partial N_\theta}{\partial \theta} dx \frac{(d\theta)^2}{2} + N_{\theta x} dx \frac{d\theta}{2} + Z a d\theta dx = 0 \quad (3.2.6)$$

Neglecting the second order term of $d\theta$ gives

$$\frac{N_{\theta}}{a} + Z = 0 \quad (3.2.7)$$

Since the aim is to determine the natural frequencies of the cylindrical membrane element, the only external loads are the inertial components. Based on d'Alembert's principle, the dynamic equations (3.2.2), (3.2.5) and (3.2.7) reduce to

$$\begin{aligned} \frac{\partial N_x}{\partial x} + \frac{\partial N_{\theta x}}{a \partial \theta} &= \rho h \frac{\partial^2 u}{\partial t^2} \\ \frac{\partial N_{\theta x}}{\partial x} + \frac{\partial N_{\theta}}{a \partial \theta} &= \rho h \frac{\partial^2 v}{\partial t^2} \\ \frac{N_{\theta}}{a} &= \rho h \frac{\partial^2 w}{\partial t^2} \end{aligned} \quad (3.2.8)$$

where ρ is the density, h is the thickness of the membrane and t is the time.

Obviously, stresses are not the practical parameters of measurements that can be transformed into the axial, circumferential and radial displacement u , v and w respectively, stress-strain relationships, along with the physical parameters of the Young's modulus of elasticity E and Poisson's ratio ν , can be written as [92, 94, 98-100]

$$\begin{aligned} N_x &= \frac{Eh}{1-\nu^2} \left[\frac{\partial u}{\partial x} + \nu \left(\frac{\partial v}{a \partial \theta} - \frac{w}{a} \right) \right] \\ N_{\theta} &= \frac{Eh}{1-\nu^2} \left[\frac{\partial v}{a \partial \theta} - \frac{w}{a} + \nu \frac{\partial u}{\partial x} \right] \\ N_{x\theta} &= \frac{Eh}{2(1-\nu)} \left(\frac{\partial u}{a \partial \theta} + \frac{\partial v}{\partial x} \right) \end{aligned} \quad (3.2.9)$$

Substituting equation (3.2.9) into equation (3.2.8) one obtains

$$\begin{aligned}
\frac{\partial^2 u}{\partial x^2} + \frac{1-v}{2a^2} \frac{\partial^2 u}{\partial \theta^2} + \frac{1+v}{2a} \frac{\partial^2 v}{\partial x \partial \theta} + \frac{v}{a} \frac{\partial w}{\partial x} - \frac{1-v^2}{E} \rho \frac{\partial^2 u}{\partial t^2} &= 0 \\
\frac{1+v}{2a} \frac{\partial^2 u}{\partial x \partial \theta} + \frac{1-v}{2} \frac{\partial^2 v}{\partial x^2} + \frac{1}{a^2} \frac{\partial^2 v}{\partial \theta^2} + \frac{1}{a^2} \frac{\partial w}{\partial \theta} - \frac{1-v^2}{E} \rho \frac{\partial^2 v}{\partial t^2} &= 0 \quad (3.2.10) \\
\frac{v}{a} \frac{\partial u}{\partial x} + \frac{1}{a^2} \frac{\partial v}{\partial \theta} + \frac{w}{a^2} + \frac{1-v^2}{E} \rho \frac{\partial^2 w}{\partial t^2} &= 0
\end{aligned}$$

The terms double underlined are the inertial forces in the longitudinal and circumferential directions, which are suppressed, as more interest is on the radial deformation of the airways, in addition to the fact they are much smaller than the radial inertias. Equation (3.2.10) is rewritten as

$$\begin{aligned}
\frac{\partial^2 u}{\partial x^2} + \frac{1-v}{2a^2} \frac{\partial^2 u}{\partial \theta^2} + \frac{1+v}{2a} \frac{\partial^2 v}{\partial x \partial \theta} + \frac{v}{a} \frac{\partial w}{\partial x} &= 0 \\
\frac{1+v}{2a} \frac{\partial^2 u}{\partial x \partial \theta} + \frac{1-v}{2} \frac{\partial^2 v}{\partial x^2} + \frac{1}{a^2} \frac{\partial^2 v}{\partial \theta^2} + \frac{1}{a^2} \frac{\partial w}{\partial \theta} &= 0 \quad (3.2.11) \\
\frac{v}{a} \frac{\partial u}{\partial x} + \frac{1}{a^2} \frac{\partial v}{\partial \theta} &= -\frac{w}{a^2} - \frac{1-v^2}{E} \rho \frac{\partial^2 w}{\partial t^2}
\end{aligned}$$

Among the three displacement variables, u , v and w , the focus of this work is on the radial deformation. Therefore, it is necessary to eliminate the first two in order to observe the behaviour of the third, w . Although the algebraic process is tedious, the approach is no more than solving three simultaneous equations of three unknowns.

Apply the following operations, $\frac{\partial^2}{\partial x^2}$ and $\frac{1}{a^2} \frac{\partial^2}{\partial \theta^2}$ on the first expression in equations (3.2.11) [91, 93]. This gives:

$$\frac{\partial^4 u}{\partial x^4} + \frac{1-v}{2a^2} \frac{\partial^4 u}{\partial x^2 \partial \theta^2} + \frac{1+v}{2a} \frac{\partial^4 v}{\partial x^3 \partial \theta} + \frac{v}{a} \frac{\partial^3 w}{\partial x^3} = 0 \quad (3.2.12)$$

$$\frac{1}{a^2} \frac{\partial^4 u}{\partial x^2 \partial \theta^2} + \frac{1-v}{2a^4} \frac{\partial^4 u}{\partial \theta^4} + \frac{1+v}{2a^3} \frac{\partial v}{\partial x \partial \theta^3} + \frac{v}{a^3} \frac{\partial^3 w}{\partial x \partial \theta^2} = 0 \quad (3.2.13)$$

Now apply $\frac{\partial^2}{\partial x \partial \theta}$ on the second expression of the equation (3.2.11) and we have

$$\frac{1+v}{2a} \frac{\partial^4 u}{\partial x^2 \partial \theta^2} + \frac{1-v}{2} \frac{\partial^4 v}{\partial x^3 \partial \theta} + \frac{1}{a^2} \frac{\partial^4 v}{\partial x \partial \theta^3} + \frac{1}{a^2} \frac{\partial^3 w}{\partial x \partial \theta^2} = 0 \quad (3.2.14)$$

Substitute the v terms in equation (3.2.12) and (3.2.13) into equation (3.2.14) and simplify to

$$\frac{a(1-v)}{(1+v)} \frac{\partial^4 u}{\partial x^4} + \frac{2a(1-v)}{(1+v)} \frac{\partial^4 u}{a^2 \partial x^2 \partial \theta^2} + \frac{a(1-v)}{(1+v)} \frac{\partial^4 u}{a^4 \partial \theta^4} + \frac{v(1-v)}{1+v} \frac{\partial^3 w}{\partial x^3} - \frac{1-v}{a^2(1+v)} \frac{\partial^3 w}{\partial x \partial \theta^2} = 0 \quad (3.2.15)$$

Since

$$\nabla^4 = \nabla^2(\nabla^2) \Rightarrow \frac{a(1-v)}{(1+v)} \nabla^4 u + \frac{v(1-v)}{1+v} \frac{\partial^3 w}{\partial x^3} - \frac{1-v}{a^2(1+v)} \frac{\partial^3 w}{\partial x \partial \theta^2} = 0 \quad (3.2.16)$$

$$\nabla^4 u + \frac{v}{a} \frac{\partial^3 w}{\partial x^3} - \frac{1}{a^3} \frac{\partial^3 w}{\partial x \partial \theta^2} = 0 \quad (3.2.17)$$

Another similar expression to equation (3.2.17), but in terms of v, by applying $\frac{\partial^2}{\partial x^2}$

and $\frac{\partial^2}{\partial \theta^2}$ on the second expression in equations (3.2.11), then substituting the u

terms into the first expression in equation (3.2.11) had resulted after the operation

of $\frac{\partial^2}{\partial x \partial \theta}$, and is expressed as

$$\nabla^4 v + \frac{2+v}{a^2} \frac{\partial^3 w}{\partial x^2 \partial \theta} + \frac{\partial^3 w}{a^4 \partial \theta^3} = 0 \quad (3.2.18)$$

To eliminate u and v , $\frac{v}{a} \frac{\partial}{\partial x}$ on equation (3.2.17), and $\frac{1}{a^2} \frac{\partial}{\partial \theta}$ on equation (3.2.18)

were applied and added up to result

$$\left(\frac{v}{a} \frac{\partial}{\partial x} \nabla^4 u + \frac{v^2}{a^2} \frac{\partial^4 w}{\partial x^4} - \frac{v}{a^4} \frac{\partial^4 w}{\partial x^2 \partial \theta^2} \right) + \left(\frac{1}{a^2} \frac{\partial}{\partial \theta} \nabla^4 v + \frac{1}{a^6} \frac{\partial^4 w}{\partial \theta^4} + \frac{2+v}{a^4} \frac{\partial^4 w}{\partial x^2 \partial \theta^2} \right) = 0 \quad (3.2.19)$$

Grouping the underlined terms and simplifying the double-underlined terms leads equation (3.2.19) to be

$$\nabla^4 \left(\frac{v}{a} \frac{\partial u}{\partial x} + \frac{1}{a^2} \frac{\partial v}{\partial \theta} \right) + \frac{v^2}{a^2} \frac{\partial^4 w}{\partial x^4} + \frac{2}{a^4} \frac{\partial^4 w}{\partial x^2 \partial \theta^2} + \frac{1}{a^6} \frac{\partial^4 w}{\partial \theta^4} = 0 \quad (3.2.20)$$

Note that the bracketed terms are exactly the same as the left handed side of equation (3.2.11) and can be replaced by the right handed side equivalent. This gives

$$\begin{aligned}
\nabla^4 \left(-\frac{w}{a^2} - \frac{1-v^2}{E} \rho \frac{\partial^2 w}{\partial t^2} \right) + \frac{v^2}{a^2} \frac{\partial^4 w}{\partial x^4} + \frac{2}{a^4} \frac{\partial^4 w}{\partial x^2 \partial \theta^2} + \frac{1}{a^6} \frac{\partial^4 w}{\partial \theta^4} &= 0 \\
\frac{v^2}{a^2} \frac{\partial^4 w}{\partial x^4} + \frac{2}{a^4} \frac{\partial^4 w}{\partial x^2 \partial \theta^2} + \frac{1}{a^6} \frac{\partial^4 w}{\partial \theta^4} &= \frac{1}{a^2} \nabla^4 w + \frac{1-v^2}{E} \rho \frac{\partial^2}{\partial t^2} (\nabla^4 w) \\
\frac{v^2}{a^2} \frac{\partial^4 w}{\partial x^4} + \left(-\frac{1}{a^2} \frac{\partial^4 w}{\partial x^4} + \frac{1}{a^2} \frac{\partial^4 w}{\partial x^4} \right) + \frac{2}{a^4} \frac{\partial^4 w}{\partial x^2 \partial \theta^2} + \frac{1}{a^6} \frac{\partial^4 w}{\partial \theta^4} &= \frac{1}{a^2} \nabla^4 w + \frac{1-v^2}{E} \rho \frac{\partial^2}{\partial t^2} (\nabla^4 w) \\
\frac{v^2}{a^2} \frac{\partial^4 w}{\partial x^4} - \frac{1}{a^2} \frac{\partial^4 w}{\partial x^4} + \frac{1}{a^2} \frac{\partial^4 w}{\partial x^4} + \frac{2}{a^4} \frac{\partial^4 w}{\partial x^2 \partial \theta^2} + \frac{1}{a^6} \frac{\partial^4 w}{\partial \theta^4} &= \frac{1}{a^2} \nabla^4 w + \frac{1-v^2}{E} \rho \frac{\partial^2}{\partial t^2} (\nabla^4 w) \\
\frac{v^2-1}{a^2} \frac{\partial^4 w}{\partial x^4} + \frac{1}{a^2} \nabla^4 w &= \frac{1}{a^2} \nabla^4 w + \frac{1-v^2}{E} \rho \frac{\partial^2}{\partial t^2} (\nabla^4 w) \\
\frac{v^2-1}{a^2} \frac{\partial^4 w}{\partial x^4} &= -\frac{v^2-1}{E} \rho \frac{\partial^2}{\partial t^2} (\nabla^4 w)
\end{aligned}$$

$$\text{or} \quad \frac{\partial^4 w}{\partial x^4} + \frac{a^2}{E} \rho \frac{\partial^2}{\partial t^2} (\nabla^4 w) = 0$$

(3.2.21)

3.3 Proposed Solutions

Equation (3.2.21) is a fourth order partial differential equation with a biharmonic term. The assumed solution is expected to involve four constant coefficients C_i and can be expressed as,

$$w = \sum_{i=1}^4 W(x, y) \cos \omega t$$

with $W(x, y) = C_i e^{\frac{\lambda_i x}{l}} \cos n\theta$, giving

$$w = \sum_{i=1}^4 C_i e^{\frac{\lambda_i x}{l}} \cos n\theta \cos \omega t \quad (3.3.1)$$

where the radial deformation w is a function of the longitudinal displacement u , the circumferential displacement v , and the time t with their relevant controlling parameters λ_i , n , the longitudinal length l and the angular frequency, ω

Substitute this expression into the last expression of equation (3.2.21) and take only the time derivative of it. This gives [101]

$$\frac{\partial^4 w}{\partial x^4} - \frac{a^2}{E} \rho \omega^2 \nabla^4 w = 0 \quad (3.3.2)$$

where w is reduced to be a function of the longitudinal displacement x and the circumferential folding number n only. Equations (3.2.21) and (3.3.2) result in .

$$\left(\frac{\lambda_i}{l}\right)^4 C_i e^{\frac{\lambda_i x}{l}} \cos n\theta - \Delta \left[\left(\frac{\lambda_i}{l}\right)^4 C_i e^{\frac{\lambda_i x}{l}} \cos n\theta + \left(\frac{\lambda_i}{l}\right)^2 \frac{(-n^2)}{a^2} C_i e^{\frac{\lambda_i x}{l}} \cos n\theta + \left(\frac{n^4}{a^4}\right) C_i e^{\frac{\lambda_i x}{l}} \cos n\theta \right] = 0$$

which, with $\Delta = \rho a^2 (1 - \nu^2) \frac{\omega^2}{E}$, could be further simplified to get

$$\left(\frac{\lambda_i}{l}\right)^4 - \Delta \left[\left(\frac{\lambda_i}{l}\right)^4 - \left(\frac{\lambda_i}{l}\right)^2 \left(\frac{n^2}{a^2}\right) + \frac{n^4}{a^4} \right] = 0$$

This can be solved to get

$$\begin{aligned} \left(\frac{\lambda_i a}{nl}\right)^4 &\approx \Delta (-1)^2 \\ \lambda_i &= \frac{nl}{a} \sqrt[4]{\Delta} \end{aligned} \quad (3.3.3)$$

Therefore λ can be expressed in terms of a real parameter K as

$$\begin{aligned}
\lambda_1 &= K \\
\lambda_2 &= -K \\
\lambda_3 &= jK \\
\lambda_4 &= -jK
\end{aligned}
\tag{3.3.4}$$

where j is the imaginary part $\sqrt{-1}$ of a complex number.

3.4 Boundary Conditions

The respiratory system is embedded in a complicated spongy moist environment with tedious boundary conditions for each of the branches. If embedded elastic elements are assumed, it will complicate the system and make it impossible to generate an analytical solution. Since the main goal of this investigation is to determine the trend of variation of the natural frequencies, a simply support boundary condition will suffice the need for the undergoing research.

Consider the simply supported boundary conditions where displacements and moments at both ends of the cylindrical shell are zero ($u=0$, $v=0$, $N=0$ and $M=0$). Four simultaneous equations of the four coefficients resulted. For non-trivial solutions, the determinant of these coefficients requires that matrix be zero, implying the following values for the longitudinal mode parameter λ .

$$\begin{aligned}
\lambda_1 &= m\pi \\
\lambda_2 &= -m\pi \\
\lambda_3 &= jm\pi \\
\lambda_4 &= -jm\pi
\end{aligned}
\tag{3.4.1}$$

where $j = \sqrt{-1}$, and $m = 1, 2, 3, 4, \dots$ for simply supported boundary ends.

Equation (3.2.8) also leads to the membrane radial frequency (or membrane frequency for short) equation for the circular cylindrical shell membrane.

$$f_m = \frac{1}{2\pi a} \sqrt{\frac{E}{\rho}} \left(\frac{a^2 \lambda_i^2}{l^2 n^2} \right) \left(\frac{a^2 \lambda_i^2}{l^2 n^2} - 1 \right)^{-1} \quad (3.4.2)$$

This cylindrical membrane radial frequency equation may be considered as a product of three factors, namely, the frequency of a ring

$$f_{ring} = \frac{1}{2\pi a} \sqrt{\frac{E}{\rho}} \quad (3.4.3)$$

a membrane factor

$$\left(\frac{a^2 \lambda_i^2}{l^2 n^2} \right) \quad (3.4.4)$$

and a limiting factor

$$\left(\frac{a^2 \lambda_i^2}{l^2 n^2} - 1 \right)^{-1} \quad (3.4.5)$$

To confirm the positive value in frequency, the product of the last two factors needs to be positive, with the relevant value(s) of λ_i as given in equation (3.4.1). For both options of λ_3 and λ_4 , equation (3.4.2) becomes

$$f_m = \frac{1}{2\pi a} \sqrt{\frac{E}{\rho}} \left(\frac{a^2 (-m^2 \pi^2)}{l^2 n^2} \right) \left(\frac{a^2 (-m^2 \pi^2)}{l^2 n^2} - 1 \right)^{-1} \quad (3.4.6)$$

$$f_m = \frac{1}{2\pi a} \sqrt{\frac{E}{\rho}} \left(\pi^2 \frac{m^2 a^2}{n^2 l^2} \right) \left(\pi^2 \frac{m^2 a^2}{n^2 l^2} + 1 \right)^{-1} \quad (3.4.7)$$

Applying Yu's approximation to long cylinders with many circumferential waves

that $\pi^2 \frac{m^2 a^2}{n^2 l^2} \ll 1$, equation (3.4.7) is reduced to

$$f_{m-} = \frac{1}{2\pi a} \sqrt{\frac{E}{\rho}} \left(\pi^2 \frac{m^2 a^2}{n^2 l^2} \right) \quad (3.4.8)$$

Therefore, equation (3.4.7) is the analytical expression which is most applicable in determining the natural frequencies of the tracheobronchi for each branch considered as a simple circular cylindrical thin shell. The lowest frequency occurs when the axial integer $m = 1$. The circumferential integer n , however, should be equal to 1 for radial deformation.

In the case of $\pi^2 \frac{m^2 a^2}{n^2 l^2} \gg 1$, the resonant frequency will approach to the limit of the frequency of a ring.

3.5 Other Analytical Frequency Equations of Cylindrical Thin Shells

Yu [91] made an overview on vibrations of cylindrical thin shells and a justified approximation for solutions to Donnell's equations [90-94, 102-104] for the bending and buckling of cylindrical shells, by reducing the eighth order of the differential equation to the fourth. The characteristic equations of the resonant frequency of cylindrical shells with different boundary conditions, i.e. edges freely supported,

edges clamped, and one edge freely supported and other edge clamped, have the similar patterns as those of the lateral vibration of beams. The resulting frequency equation involves the frequency parameter to the power of three, implying that there are three resonant frequencies for each set of longitudinal and circumferential modal numbers.

Kraus [93] further investigated the free vibration of cylindrical shells with edges with clamped boundary conditions with Yu's approximation in the variational, and "exact" or analytical solutions. Kraus then compared results against the experimental data and results of clamped steel cylinders by Koval and Cranch [105].

Neglecting the higher frequency terms, an approximation to the lowest natural frequencies f_1 , the lowest natural frequencies for the radial character f_{r1} , without the longitudinal and circumferential inertia, and the simplified solutions of Rayleigh's approach [93, 100] $f_{\text{ray } 1}$ were found as the following equations respectively.

$$\Delta_1 = \frac{(n^8 / \xi) + (1 - \nu^2)(Ka/l)^4}{n^2(n^2 + 1) + (3 - \nu^2)n^6 / \xi(1 - \nu)} \quad (3.5.1)$$

$$\text{or } f_1 = \frac{1}{2\pi a} \sqrt{\frac{E \Delta_1}{\rho(1 - \nu^2)}}$$

$$\Delta_{r1} = \left[\frac{n^8}{\xi} + (1 - \nu^2) \left(\frac{Ka}{l} \right)^4 \right] \frac{1}{n^4} \quad (3.5.2)$$

$$\text{or } f_{r1} = \frac{1}{2\pi a} \sqrt{\frac{E \Delta_{r1}}{\rho(1 - \nu^2)}}$$

$$\Delta_{Rayl} = \frac{1}{\xi} \frac{n^2(n^2-1)^2}{n^2+1} \quad (3.5.3)$$

$$\text{or } f_{Rayl} = \frac{1}{2\pi a} \sqrt{\frac{E\Delta_{Rayl}}{\rho(1-\nu^2)}}$$

where $\frac{1}{\xi} = \frac{h^2}{12a^2}$ and $\Delta = \rho a^2(1-\nu^2)\frac{\omega^2}{E}$. Therefore, the frequency expression is

$$f = \frac{1}{2\pi a} \sqrt{\frac{\Delta E}{\rho(1-\nu^2)}} \quad (3.5.4)$$

Ventsel [94] determines the natural frequency for axisymmetric free flexural vibrations of cylindrical shells with simple supports to be

$$\omega^2 = \frac{E}{\rho a^2} (1 + \mu \lambda^4) \quad (3.5.5)$$

$$\text{or } f = \frac{1}{2\pi a} \sqrt{\frac{E(1 + \mu \lambda^4)}{\rho}}$$

$$\text{where } \mu = \frac{h^2}{12 a^2(1-\nu)^2}, \text{ and } \lambda = \frac{n\pi a}{l}.$$

In the case of fixed shell edges and application of Yu's approximation, the natural frequency and its second harmonic expressions are respectively

$$\omega_1^2 = \frac{E}{\rho a^2} \left[1 + \mu \left(4.73 \frac{a}{l} \right)^4 \right]$$

$$\text{or } f = \frac{1}{2\pi a} \sqrt{\frac{E}{\rho} \left[1 + \mu \left(4.73 \frac{a}{l} \right)^4 \right]}$$
(3.5.6)

and

$$\omega_2^2 = \frac{E}{\rho a^2} \left[1 + \mu \left(7.83 \frac{a}{l} \right)^4 \right]$$

$$\text{or } f = \frac{1}{2\pi a} \sqrt{\frac{E}{\rho} \left[1 + \mu \left(7.83 \frac{a}{l} \right)^4 \right]}$$
(3.5.7)

In the case of free asymmetric flexural vibrations of circular cylindrical shells, Ventsel [94] determines the natural frequency by differentiating the frequency parameter Δ expression for the minimum and the corresponding flexural number m values.

3.6 Application to Respiratory walls

Analytical solutions of the vibration of branched systems involve extreme complexity in matching the boundary conditions between generations and therefore are not found in the current literature. This work makes no attempt to strive for such solutions simply because the nature of the boundary conditions in the respiratory system is not clearly defined. Instead, a numerical approach is adopted for such an investigation and results are analysed and related to those from individual branches with simply supported and branched angles.

Although analytical solutions for branched systems are not possible at this stage, the concept of a circular cylindrical membrane or shell may be applicable to the

individual respiratory bronchus. Table 3.1 tabulates the physical properties, elasticity (of the numerical values of elastance) and density, from Fredberg [84], the airway wall thickness to radius ratios from Kamm [48], in addition to the geometric dimensions of tracheobronchial lengths and radii from Weibel [42]. The wall thickness of each branch can then be determined with the corresponding radius of the airway.

The elastance by Fredberg [84] is one order of magnitude greater than the Young's modulus from other literatures [106-108]. This work assumes only the numerical values of Fredberg's elastances and the orders of magnitudes and units of elasticity from Hill et al. [108], and Halpern and Grotberg [106-107] for the Young's moduli of the tracheobronchial generations.

Table 3.1 Geometric and physical data of airways from the trachea to the 16th bronchus, including the analytical ring frequency of each branch.

Generation	No. of Tubes	Radius	Length	Thickness /Radius	Wall thickness	Elasticity	Density	frequency of ring
z	2^n	a, mm	l, cm	t/a	t, mm	E, kN/m ²	ρ , kg/m ³	f, Hz
0	1	9.000	12.000	0.043	0.387	7.3	1351	41
1	2	6.100	4.760	0.044	0.268	5.7	1959	45
2	4	4.150	1.900	0.044	0.183	4.7	3103	47
3	8	2.800	0.760	0.045	0.126	4.7	1324	107
4	16	2.250	1.270	0.046	0.104	4.7	1069	148
5	32	1.750	1.070	0.047	0.082	3.9	1188	165
6	64	1.400	0.900	0.049	0.069	3.9	1132	211
7	128	1.150	0.760	0.050	0.058	3.9	1221	247
8	256	0.930	0.640	0.052	0.048	3.2	1035	301
9	512	0.770	0.540	0.054	0.042	3.2	1162	343
10	1024	0.650	0.460	0.056	0.036	3.2	1178	404
11	2048	0.545	0.390	0.059	0.032	3.2	1059	508
12	4096	0.475	0.330	0.063	0.030	2.1	966	494
13	8192	0.410	0.270	0.065	0.027	2.1	1256	502
14	16384	0.370	0.230	0.068	0.025	2.1	976	631
15	32768	0.330	0.200	0.071	0.023	2.1	835	765
16	65536	0.300	0.165	0.075	0.023	2.1	955	787

Resonant frequencies at the ring limits are calculated for the trachea and bronchi up to the 16th generation. The increasing frequency of the generations agrees with the ratio variation among the contributed geometric and physical parameters, and ranges from 41 Hz for the trachea to 787 Hz for bronchus 16. Figure 3.2 shows the variation of the square root values of the Young's modulus to the tracheobronchial density in an approximate 'linear' decreasing curve on the airway generations, with few exceptive points.

Such trend is applicable at generation 3 and onward to generation 16, particularly between generations 5 and 10. A graph of ring frequencies versus generations is plotted in Figure 3.3. The ring frequencies show a good linear trend between generation 2 and 16 and could be extrapolated to lower generations and the predicted frequencies can in turn be used in estimating the physical parameter like the Young's modulus if such a hypothesis holds true.

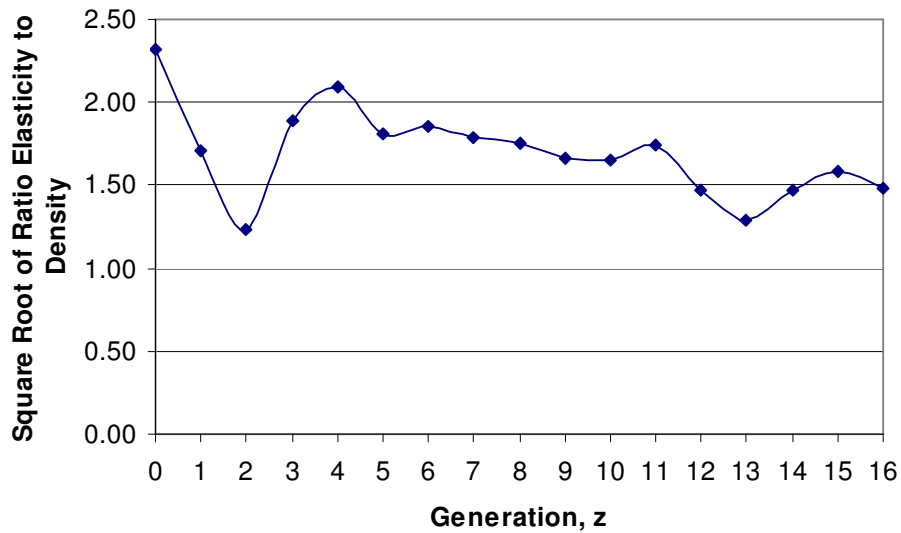


Figure 3.2 The graph of the square root of elasticity to density ratio versus the generation number z from the trachea to bronchus 16.

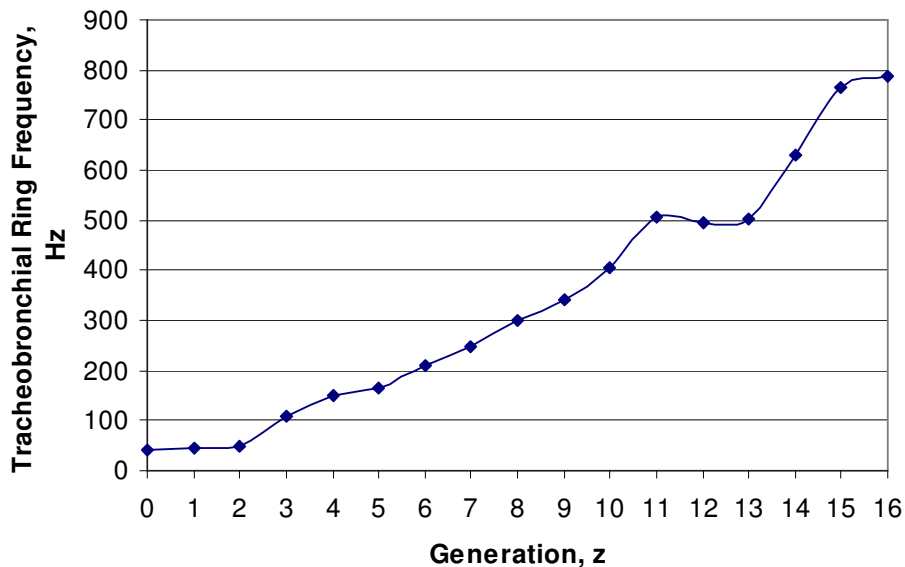


Figure 3.3 The ring frequency distribution in tracheobronchial generation. The curve behaves quite linearly over the range.

3.7 Results

The conceptive idea of this work is to link the circular cylindrical thin shell as the fundamental unit to the resonant frequencies of the complex airway structure. Therefore, it is worth investigating the trend related between the single simple unit and the overall airways with numerous branching. The derived membrane frequency equation for the fundamental shell has simple supports as contrast to the clamped restrains at the end boundaries in Kraus's investigation. Yu shows that the type of boundary conditions corresponds to different values of the characteristic constant or the longitudinal mode number m 's previously, which are whole integers for simply supported boundaries and are 1.506, 2.500, 3.500, 4.500, and so on, instead of clamped conditions. Comparison of analytical frequency is shown in Table 3.2.

Table 3.2 Comparison of analytical frequencies of tracheobronchial generations.

Generation	Ring frequency f_{ring}	Lowest frequency f_1	Radial mode 1 f_{r1}	Membrane frequency f_m	Membrane Approx. f_{m-}
z	Hz	Hz	Hz	Hz	Hz
0	41.11	1.67	2.36	2.16	2.28
1	44.50	5.12	7.24	6.21	7.21
2	47.20	15.72	22.23	15.11	22.22
3	107.11	101.45	143.50	61.33	143.49
4	148.33	32.52	46.00	35.08	45.95
5	164.76	30.80	43.57	34.41	43.50
6	210.98	35.70	50.50	40.67	50.39
7	247.34	39.62	56.04	45.59	55.89
8	300.95	44.49	62.93	51.90	62.72
9	343.05	48.86	69.12	57.34	68.84
10	403.59	56.47	79.88	66.44	79.53
11	507.73	69.53	98.36	82.05	97.86
12	494.00	71.77	101.54	83.87	101.02
13	502.03	81.11	114.76	93.07	114.25
14	631.11	114.37	161.82	128.40	161.20
15	764.89	145.81	206.31	162.00	205.53
16	786.90	181.96	257.48	193.58	256.74

There is a reason why the ratio of the approximate membrane (radial) frequency f_{m-} to the membrane (radial) frequency f_m ranges from 1.06 (the trachea) to 2.34 (bronchus 3) in the tracheobronchi. As the radius to length ratio of the shell increases, the deviation also increases as in bronchus 3. The other two frequencies f_l and f_{r1} are the approximate lowest frequency and the lowest radial frequency of thin shells. It is interesting to find that f_{m-} is almost the same as f_{r1} . And the membrane

frequency f_m is higher than the approximate lowest frequency f_l no more than 20% except for the trachea and bronchus 3 as shown in Figure 3.4.

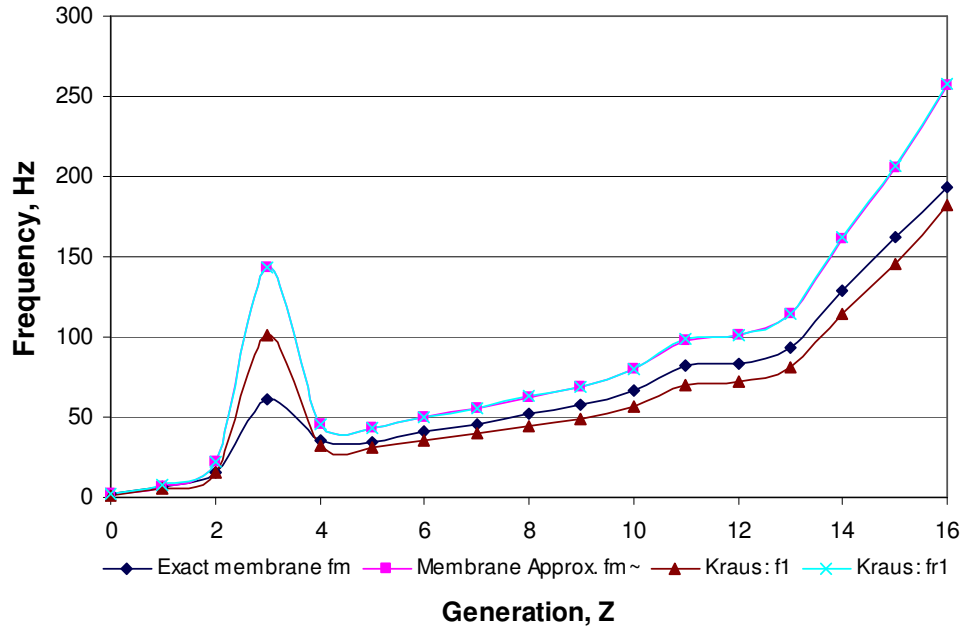


Figure 3.4 Comparison of the analytical frequency results from equations of the membrane f_m , approximate membrane $f_m \sim$, Kraus's lowest f_1 and the lowest radial frequency f_{r1} .

3.8 Application of Analytical Models to Airways

The analytical solution of a circular cylindrical shell serves as the preliminary investigation and a basis to the natural frequencies of airways in the absence of an analytical model for such an angular branching network. Morphology by Weibel and Horsfield [42, 45, 47, 109] is quite consolidated and applicable for research work although geometric dimensions vary among individuals. Physical properties and boundary conditions of the numerous branching structures of lungs are not that

clearly understood and defined in the literature. Modelling is a powerful technique in probing unknowns with simulation.

The analytical modelling of airways is not to search for the exact solutions as the boundary conditions between generations still remain as an un-attackable issue. Instead, the investigation is to search for the trend and behaviour of an individual shell unit in relation to the whole structure. Simple support is considered to be the suitable end or joint conditions in airways as it is not too loose as free and not too tight as clamped boundaries.

With numerical modelling with finite element analysis, the complexity of boundary conditions can be resolved by inter-connected elements of defined shape and structural analysis that lead to approximate solutions to some accuracy in return of the time and resource of the computing process. The following chapter is to model airways numerically for result comparison and trend of airway behaviour.

Chapter 4

Numerical Models

4.1 Introduction

Nowadays numerical modelling plays an important role in research and development. In this work numerical modelling is utilised to investigate the natural frequencies of the airways as analytical approaches are generally limited to simple geometry and ideal physical constraints; for instance, a single circular cylindrical shell with clamped or simply supported ends. Chapter 3 has modelled each tracheobronchial generation individually. Therefore, numerical models are needed for result comparison with the analytical models, and then extend the numerical investigation to models of the branched circular cylindrical shells as the complexity of human airways.

In 1943, Courant [110] elaborated the Ritz method in modelling the effect of torsion on cylindrical structures and initiated the foundation of the Finite Element Analysis (FEA), with variational calculus to vibration systems in structural engineering. The

Ritz method is an approximate solution to simple geometric shapes while the FEA utilises such concepts and extends that to complex structures by discretising the geometry into simple finite elements which can be solved numerically with given boundary conditions. Therefore, it is obvious that FEA is just an alternative approximation of the analytical models of thin shell theory which also involves applications of variational methods and principles, and there should be a good agreement between the analytical and numerical results on a simple thin shell as shown in the verification of COSMOS/Works in the later section.

Furthermore, FEA has the flexibility to by-pass or overcome the difficulty due to the boundary conditions of various geometric structures. Since analytical solutions are not feasible for many of the shell problems, in particular branched shells, FEA seems to be an excellent vehicle to numerically investigate the continuously branched airway tree structure, and overcome the difficulties due to branched angles and boundary conditions between generations. COSMOS/Works, which is the integration of the modelling software SolidWorks and FEA software COSMOS/Works, is adopted in this study. This program has proved excellent compatibility with SolidWorks which is normally used to generate almost any three dimensional drawing no matter how complex it is.

4.2 Modelling with COSMOS/Works

SolidWorks is one of the most popular modelling software in engineering. It is particularly well suited for three dimensional perspective structures. COSMOS/Works is adopted as the modelling tool in this work as it integrates the

mechanical design automation software, SolidWorks, and the FEA software COSMOS. SolidWorks implements the graphical user interface approach in design and creation of models which can then be analysed numerically by COSMOS in finite element methods. COSMOS/Works version 7.0 is used in this work.

The following steps outline the general procedure in model analysis, using COSMOS/Works:

1. Create a geometric model from SolidWorks.
2. Create a COSMOS/Works study name, analysis type of frequency and mesh type of either solid or shell using surface.
3. For shell analysis, define thickness to selected surface.
4. Define loads and boundary conditions.
5. Mesh the model.
6. Run the analysis.
7. Visualise results.

The branched geometric airways are modelled as a connected network with units of circular cylindrical thin shells. Investigation is first focused on individual airway branches or generations with simple supports at both ends as assumed in the analytical models. In this simple structure, each model could be built as a cylindrical thin shell to a specific length, radius and wall thickness with SolidWorks. With the add-in features of COSMOS/Works, the material properties of density, Young's modulus and Poisson ratio are inputted to the model which is then meshed for FEA. The mesh element size can be varied from the optimal value generated by the system.

Many problems arise when it comes to modelling branched structure with added generations. Constructing branched cylindrical thin shells becomes more difficult with two generations and tends to be impossible with further generations. It is good to find that COSMOS/Works has the solution which is to mesh selected surfaces as thin shells. Although models are built as solids, they can be meshed as thin shells with specific thickness to the selected surfaces. Models can then be edited with appropriate material properties for respective shell elements meshed as thin shells, and progress to FEA. The shell using the surfaces option in the mesh type of COSMOS/Works study is particularly useful in the airway tree models which are first created as solid angular branched tubes. This process reduces a great deal of difficulty when compared to modelling the shell structure to start and has solved the impossible task of constructing models of continuous branching airways of shells.

The following steps illustrate the modelling procedure of symmetric branched airways between generation 4 and 5.

1. A circle is first drawn to the diameter of bronchus 4, 4.5 mm Figure 4.1 (a).
2. The circle is then extruded to its length, 12.7 mm, to form a cylinder Figure 4.1 (b).
3. Two reference planes are created for the daughter generations of bronchus 5 which has a diameter of 3.5 mm and length 10.7 mm Figure 4.1 (c) and (d).
4. These two branched cylinders are built by extruding the two bronchial circles on the reference plane to their length Figure 4.2.

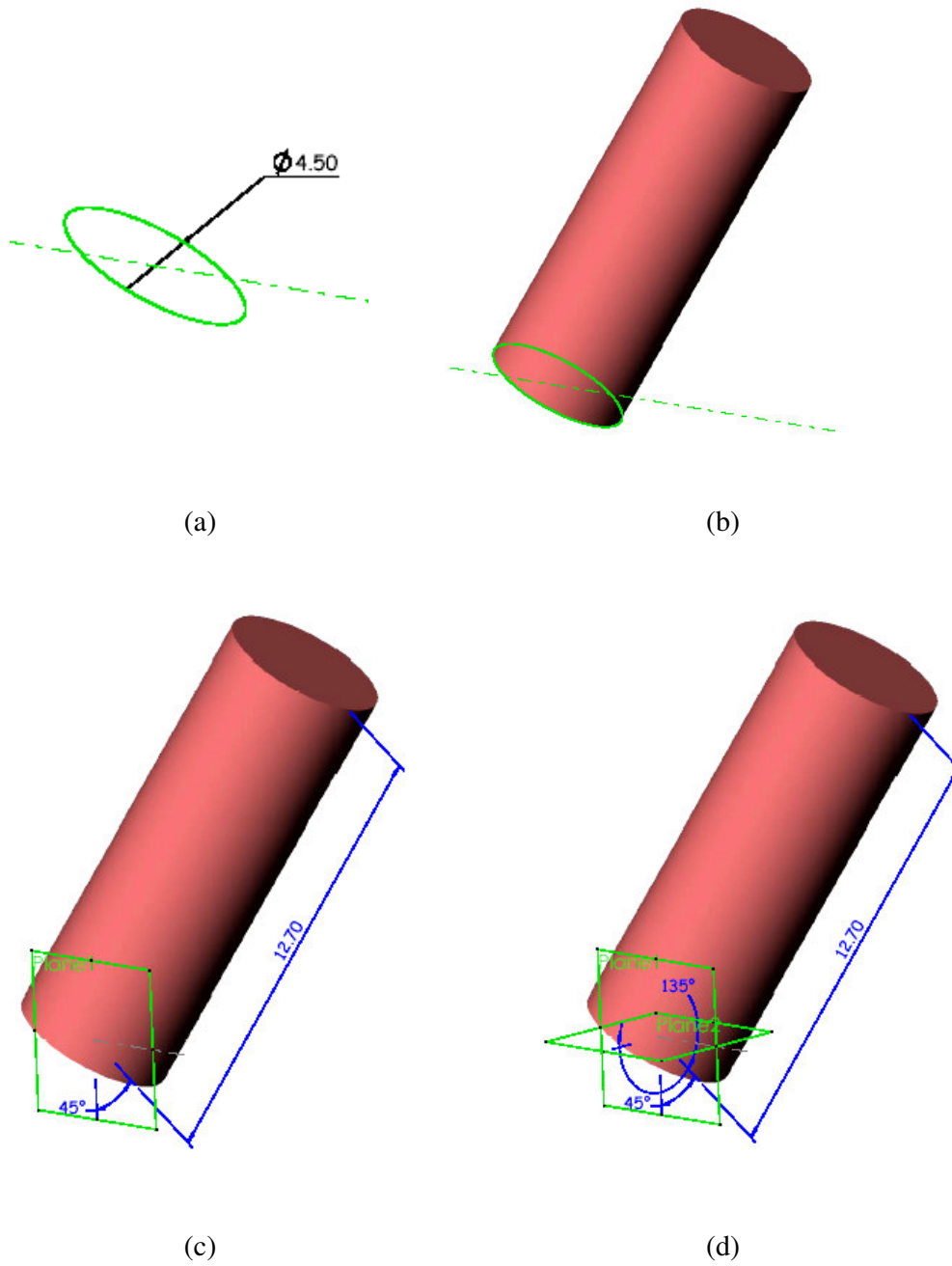


Figure 4.1 Modelling bronchus 4 with SolidWorks by extruding a circular base. Two reference inclined planes are added for generating bronchi 5 in symmetric branching. Dimensions are in mm.

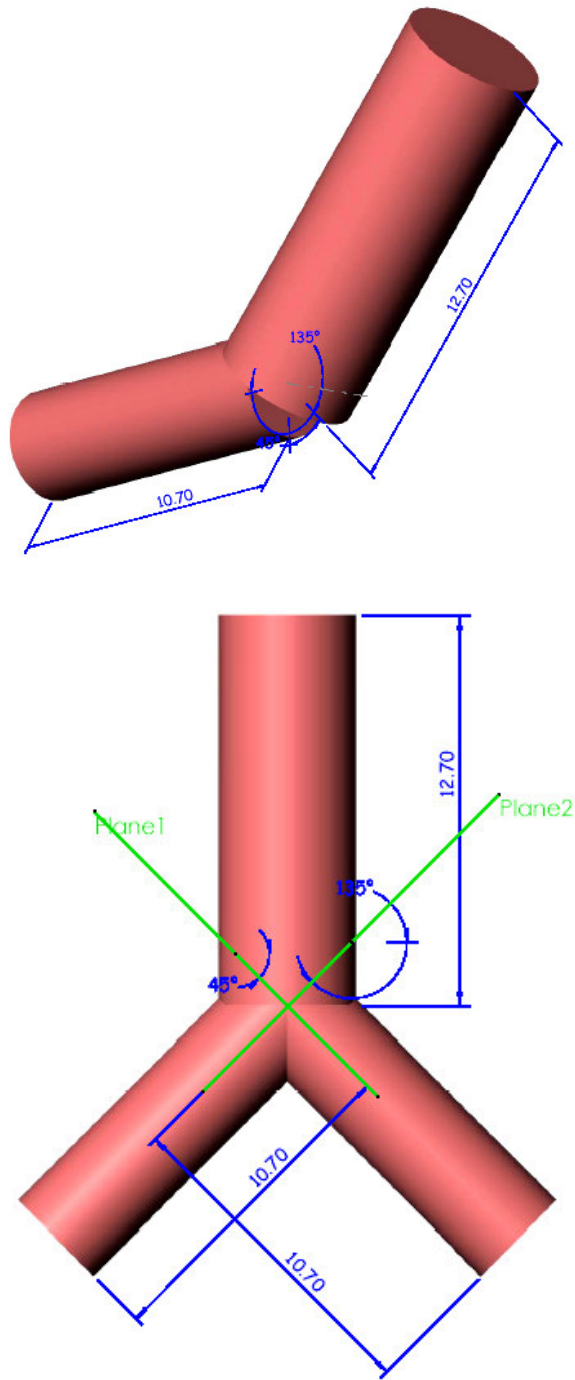


Figure 4.2 Illustration of the angular branching from bronchus 4 to bronchi 5 by extruding the base circles on the reference planes.

COSMOS/Works comes with two mesh checks, aspect ratio and Jacobian ratio, to measure the element quality. Numerical accuracy is based on the tetrahedral element with an aspect ratio of 1.0, i.e. the meshed element is a uniform perfect tetrahedral whose edges are equal in length, Figure 4.3 and Figure 4.4. A high quality element is a parabolic tetrahedral with 4 corner nodes as in a linear tetrahedral, plus 6 mid-side nodes to form a second order element, Figure 4.3. A shell mesh is either a linear triangular shell element defined by 3 corner nodes connected by 3 straight edges, or a parabolic triangular element with a mid-side node on each edge, with defined thickness of the geometry of the model. For a shell mesh, a triangular element of either linear or parabolic geometry is used instead of the tetrahedral. The Jacobian ratio is a measure of the element distortion with respect to the set Gaussian points in the mesh preference. The analysis program will stop with a negative Jacobian element.

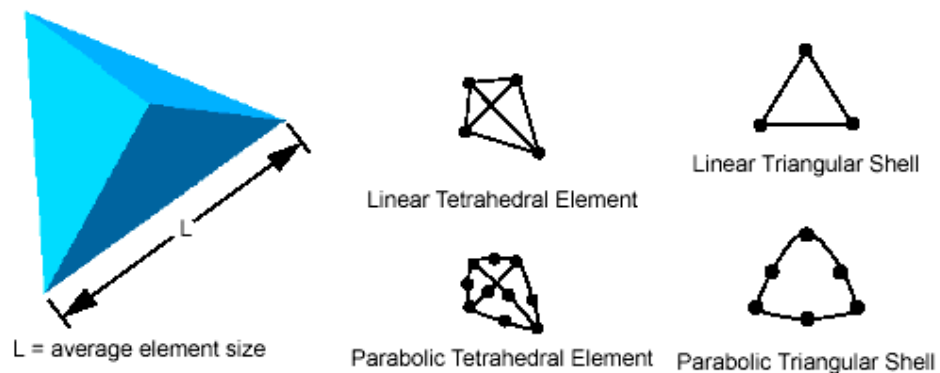


Figure 4.3 A regular tetrahedral is a perfect FEA solid which can be meshed as a linear element with 4 nodes, or a parabolic element with 6 extra mid-side nodes. A linear triangular element with 3 nodes or a parabolic triangular element with 6 nodes is meshed for shell structure analysis.

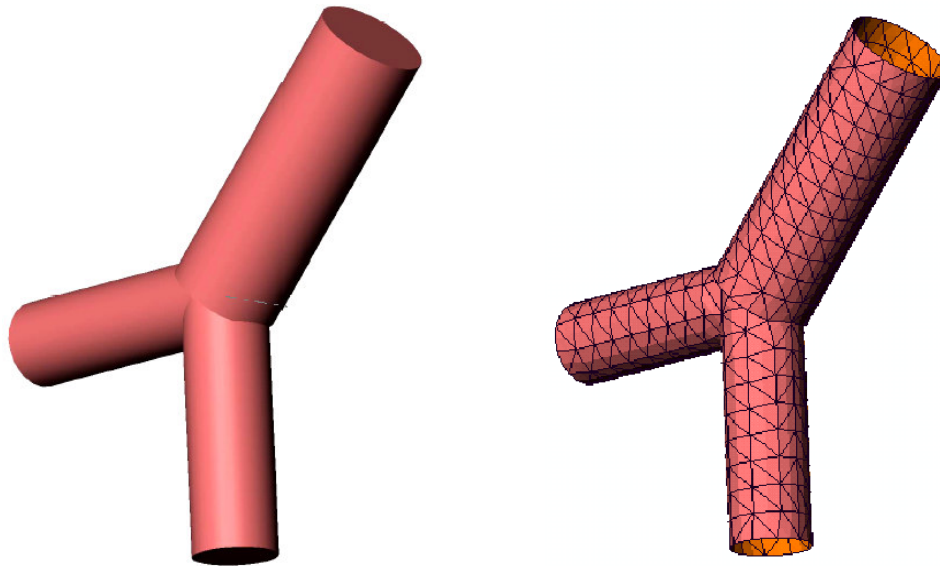


Figure 4.4 The angular branching of bronchus 4 and 5 is modelled as solid cylinders and then meshed into shells in analysis.

4.3 Verification of COSMOS/Works

To confirm the applicability of COSMOS/Works before proceeding to use it for further analysis, comparison is conducted with available literature. Koval and Cranch [105] reported an experimental investigation of a clamped-clamped circular cylindrical thin shell. Kraus [93] has determined the natural frequencies of the same shell using an “exact” analytical solution as well as an approximate analytical solution using the method of variation. In this work the same shell (radius $a = 3 \text{ in.}$, thickness $h = 0.01 \text{ in.}$, length $l = 12 \text{ in.}$, Young’s modulus of elasticity $E = 30 \times 10^6 \text{ psi}$, density $\gamma = 0.282 \text{ lb/in}^3$, and Poisson ratio $\nu = 0.3$) is used to determine the natural frequencies using COSMOS/Works. Two types of meshes were used, coarse mesh 0.52 inch and user mesh 0.25 inch. The experimental values, the analytical results as well as COSMOS/Works results are summarised in Table 4.1. It is clearly

indicated that the COSMOS/Works result with user mesh 0.25 inch falls in between the approximate analytical and experimental values (Refer to Appendix A for comparison of analytical and experimental results, and Appendix A for a sample of exact solution in Mathcad, a computing software). Figure 4.5 shows the appropriate mode shapes of such a shell using COSMOS/Works.

However, later analyses show that variation of mesh size has little effect on the natural radial frequencies of the current modelling of circular cylindrical thin shells with the applied dimension and physical property values.

Table 4.1 The lowest frequency comparison of experimental, analytical and COSMOS/Works results on the experimental steel cylinder [105].

	Koval & Cranch experimental results	Kraus's variational solution	COSMOS/Works	
			coarse mesh 0.52 inch	User mesh 0.25 inch
Lowest frequency	~530 Hz	552 Hz	663 Hz	551 Hz

The greatest advantage of the finite element analysis is that the investigation is not limited to a single circular cylindrical thin shell as it can overcome the difficulty of the boundary conditions of the numerous continuous branching airways. On the other hand, numerical modelling provides only approximate results which rely greatly on approximation and modelling techniques, and resources of computational capability. Therefore, the results of the numerical models are to serve the

verification of the analytical models which are not solvable in the branching network like airways.

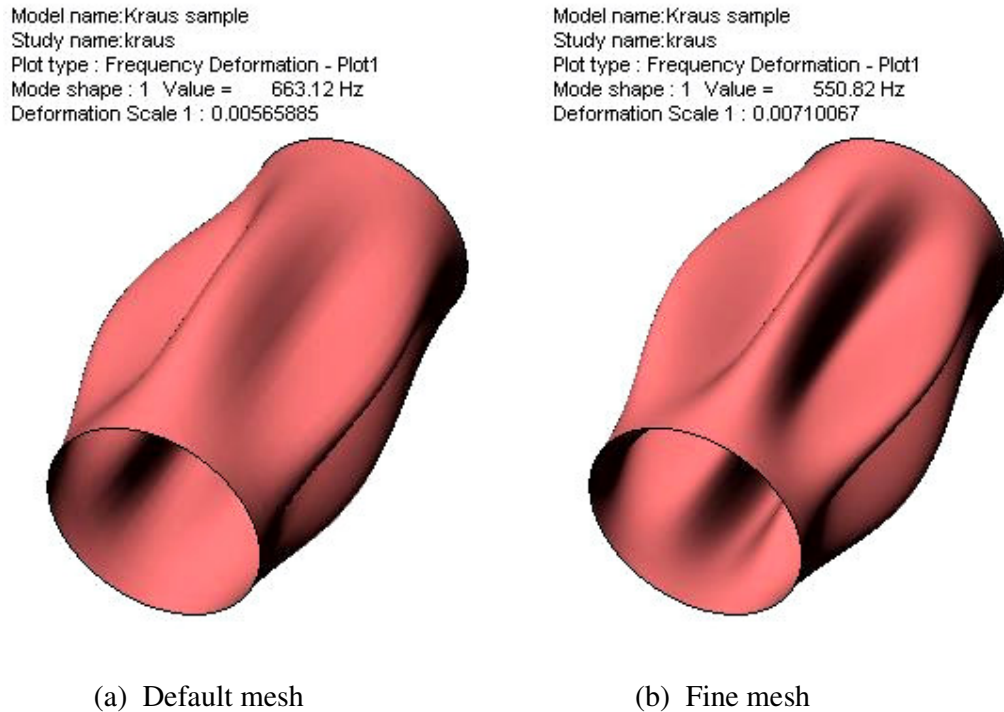


Figure 4.5 Verification of COSMOS/Works results: 663 Hz with coarse or default mesh of 0.52” and 551 Hz of user defined mesh of 0.25” versus analytical solution of lowest frequency of 552 Hz by Kraus on the experimental sample of Koval and Cranch [93, 105].

This has given the necessary confirmation to use the software for further investigation.

After the use of COSMOS/Works has been verified, it will be used for further investigations, in particular those which do not have analytical solutions. Particular attention will be made to mode shapes of the trachea and their corresponding frequencies, individual branch frequencies at different generations, the effect of the

branching (bifurcation) angle on the free vibration characteristics and the trache-bronchia combined model mode shapes.

In the following sections, the free vibration characteristics of each element of the respiratory system structure from the trachea to the sixteenth generation are thoroughly investigated.

4.4 The Trachea

The trachea is embedded in the thoracic muscle with layers of various properties in terms of thickness, stiffness and mass density. All these contribute to factors of the natural frequencies once the trachea is excited. The following assumptions are made in investigating the models of the trachea and the bronchi as well. The following assumptions should be kept in mind:

The classical or “the first approximation” theory of thin shells are assumed in this work. The thickness, strains and displacement are small compared with the other dimensions. The transverse normal stress is negligible, and normal to the middle surface which is not subject to deformation remain unchanged.

The physical properties are homogeneous and isotropic for simplicity and that the embedded muscle is much denser and stiffer than in the dimension of the wall thickness.

Boundary conditions at ends or joints between generations are simply supported to ensure that the whole airway is not too tight, but loose enough to move

longitudinally during the breathing cycles. A Poisson ratio of 0.49 is used as the volume is conserved.

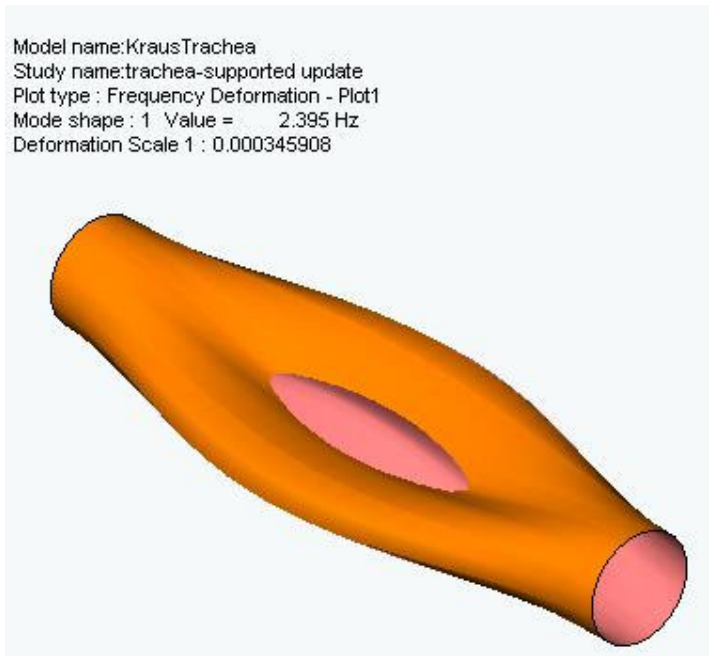
The trachea is modelled with SolidWorks as a cylinder of 18 mm diameter and 120 mm of length. With the COSMOS/Works added-in feature, a frequency study was created and the mesh type as shell mesh using surfaces was created. Then the material properties of Young's elastic modulus, density and Poisson ratio and simply support as the restraints at both ends were inputted. The model was meshed with the default size and then fine meshed for analysis and comparison. The number of modes is set as 100 in the study property in order to identify higher radial frequencies.

The geometric dimensions of airways are based on Weibel's measurements in the "Morphometry of Human Lung [42]". Mass densities of generations are adopted from Fredberg's [84] work in the "Mechanical Response of the Lungs at High Frequencies", and the magnitudes of the elastance as the Young's moduli because they seem to be too high for the airway walls. Halpern and Grotberg [106] have taken the bronchiole elasticity as 6×10^4 dynes/cm² (about 6 kPa) in their analysis. This work assumes the values of Fredberg's elastance as the elasticity of the airway walls so that they are in the right order of magnitude as in Halpern and Grotberg's work. For conserved volume, the Poisson ratio is 0.5 theoretically and 0.49 numerically in FEA. Appendix B summarises the geometric and physical data taken for numerical analysis in this chapter.

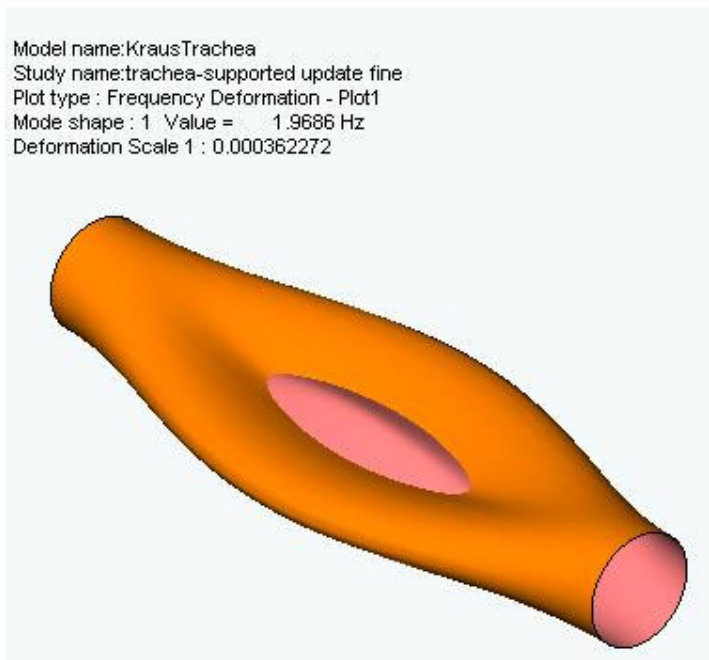
The airway wall is really a thin layer and the embedded environment has different physical properties in terms of stiffness and density. A simplified model is assumed as in most branched networks of airways [4, 5, 11, 15, 16, 58, 84]. Therefore, a non-embedded structure is assumed in the current modelling, which is a stand alone circular cylindrical shell or branching network. As the first investigation of this kind, the interest is focused on the dynamic trend of the natural frequencies of the overall airway structure.

Before running any analysis on the tracheobronchial models from the trachea to bronchus 16, an analytical characterisation of results by COSMOS/Works has been made on a trachea like model. The frequency modes are then plotted against the geometric dimensions, length, radius and thickness, and the physical parameters, the elasticity and density of the model for an overview. Results as shown in Appendix A behave in the trends as expected in theory, confirm the depending factors of the resonance frequencies and validate the applicability of COSMOS/Works for investigation in this work.

For the trachea, the lowest frequency is 2.4 Hz for the default mesh and 2.0 Hz for the fine mesh with a bending mode along the longitudinal direction as shown in Figure 4.6.



(a) Default mesh



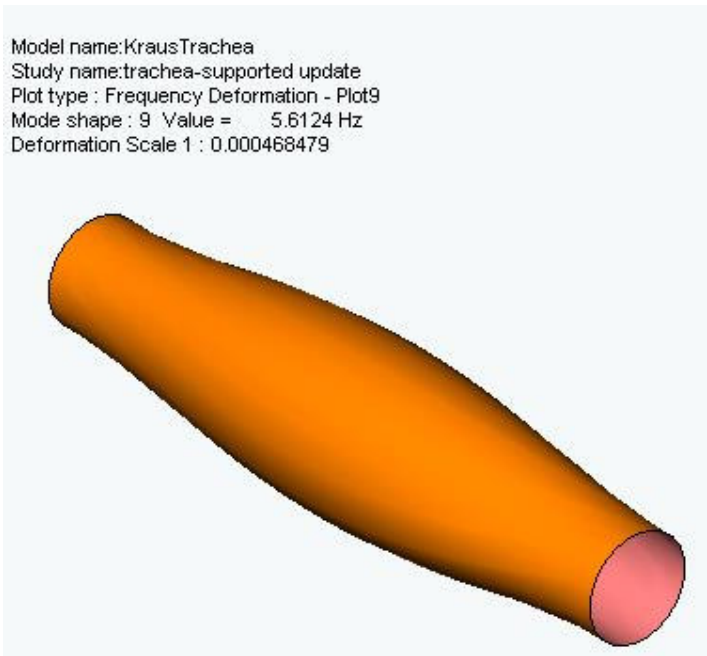
(b) Fine mesh

Figure 4.6 Mode 1 of the trachea with both twist and bending, (a) 2.4 Hz with default mesh; (b) 2.0 Hz with fine mesh.

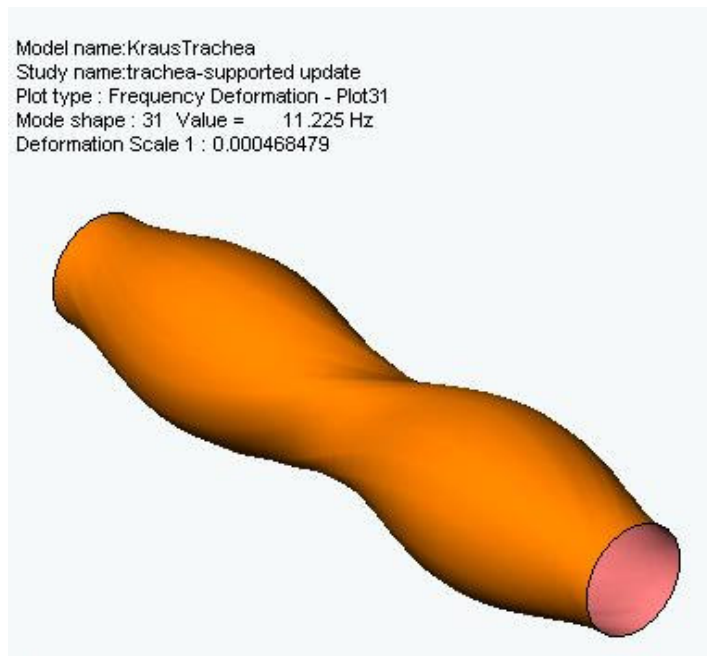
The trachea has the longest length in all tracheobronchi. The large ratio between the length and the radius of the shell tends to make the longitudinal mode excite first. Circumferential and radial modes generally occur in later modes at higher frequencies.

However, there are distinct radial modes of frequency 5.6, 11.2 and 16.84 Hz of the first, second and third harmonics respectively as listed in bold in Appendix E. Figure 4.7 shows the first two radial mode shapes of the trachea with default mesh. The first radial mode at 5.6 Hz is clearly a pure radial type while the second radial mode at 11.2 Hz can be considered as a mixture of radial and twisting modes (see Figure 4.7) although the former is the dominant. Figure 4.8 also shows the first two radial mode shapes of the same trachea, but with fine mesh. In numerical analysis, the mesh size varies, the resonance varies. The type of mesh, whether default or fine meshes, has some effect on most of the frequency modes, however not on the radial modes which have the same values regardless of the mesh size, as the mode shapes shown in Figure 4.7 and Figure 4.8, and the resonant frequencies listed in Appendix E, and Appendix F which has half of the densities and double the thickness.

Fisher et al. [72] measured the resonant frequency to be between 5 and 8 Hz, and Lee et al. [111] found that "... there is improved volume delivery at resonance frequency.", which was determined to range from 12 to 23 Hz.

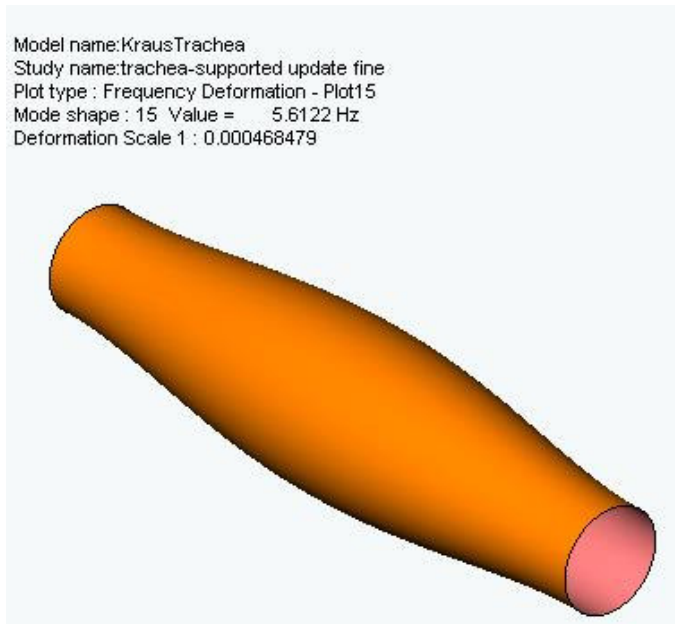


(a) Default mesh

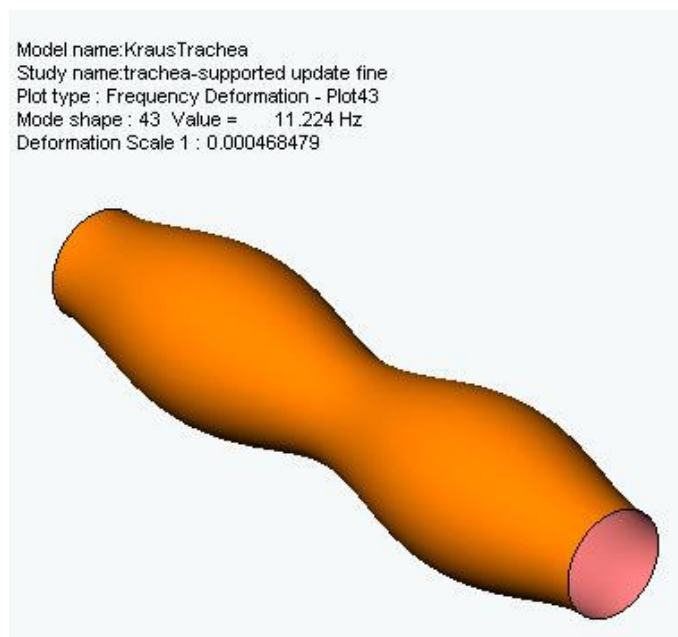


(b) Default mesh

Figure 4.7 The trachea radial frequency with default mesh: (a) 5.6 Hz, fundamental of pure radial mode, and (b) 11.2 Hz, the first harmonic with twist and radial modes.



(a) Fine mesh



(b) Fine mesh

Figure 4.8 The trachea radial frequency with fine mesh: (a) 5.6 Hz, fundamental of pure radial mode, and (b) 11.2 Hz, the first harmonic with twist and radial modes.

4.5 Individual Bronchus

Analyses similar to the trachea are conducted for the bronchi of generations one to sixteen for 100 modes. With smaller length to radius ratios, bronchial shells did not have their bending modes first; instead, it is a mix of circumferential and radial modes. Bronchus 1 has mode 1 at a frequency of 3.66 Hz with default mesh and 3.46 Hz with fine mesh, while, bronchus 16 has mode 1 at a frequency of 107 Hz with default mesh and at 106 Hz with fine mesh. Figure 4.9 shows the variation of the first mode frequency for various generations starting from the trachea to generation 16.

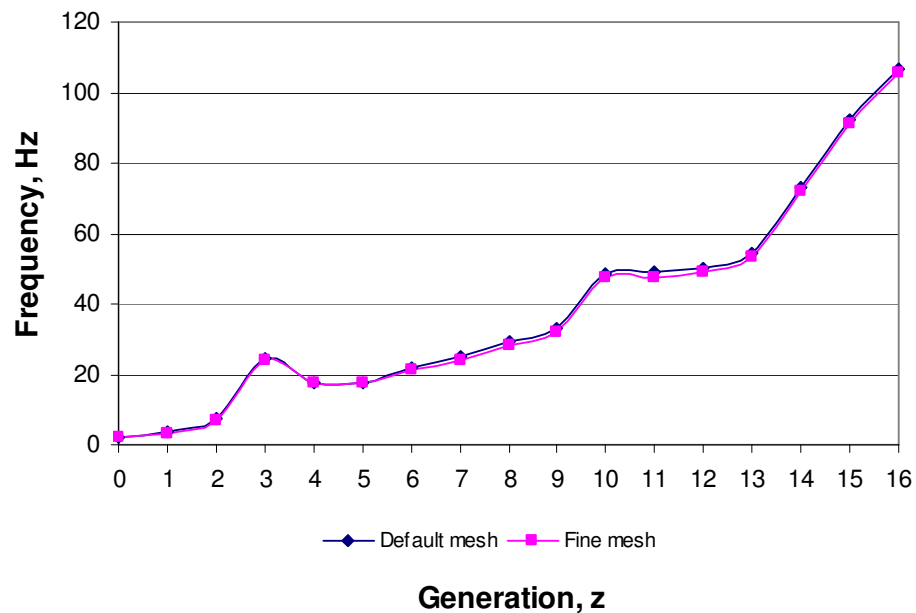


Figure 4.9 Comparison of COSMOS/Works mode 1 frequency, with default and fine mesh, versus generation number.

At mode 100, bronchus 1 frequency ranges from 34.8 Hz with default mesh and 31.8 Hz with fine mesh, while bronchus 16 frequency ranges from 890 Hz with default mesh to 865 Hz with fine mesh (Appendix E). Figure 4.10 shows plots of the membrane f_m , approximate membrane $f_{m\sim}$, Kraus's lowest frequency f_l , and lowest radial frequency f_{r1} versus tracheobronchial generations. Frequency f_l is relatively the lowest except for bronchus 3 where f_l is greater than the membrane frequency f_m , but is below the approximate membrane frequency $f_{m\sim}$ as well as the lowest radial frequency f_{r1} which are numerically the same within acceptable tolerance. This variation is obviously attributed to the dimensions of the branches.

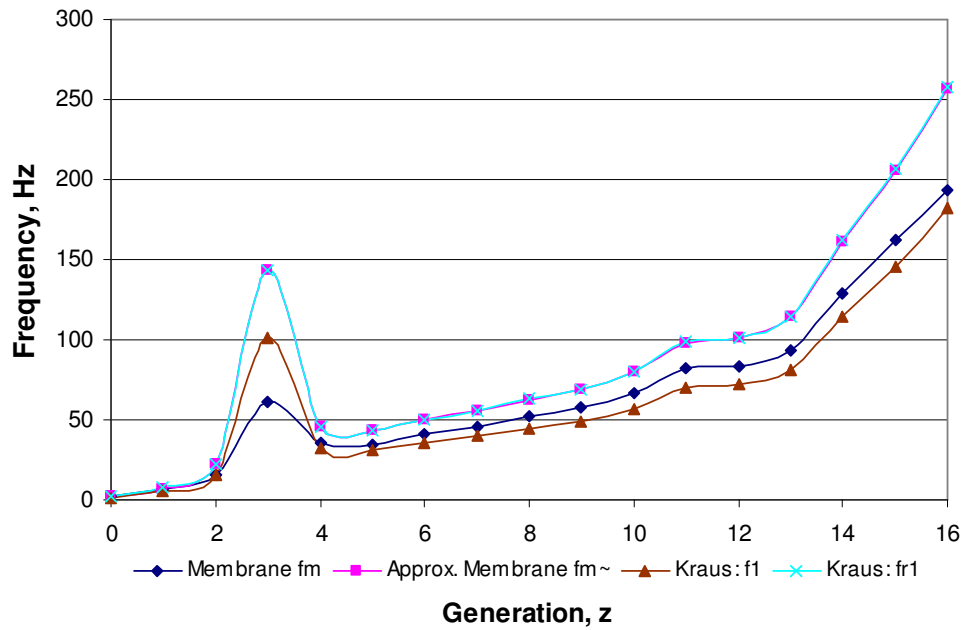


Figure 4.10 Comparison of membrane, approximate membrane, Kraus's lowest and lowest radial frequencies resulted analytically

4.6 Angular Branching

The tracheobronchial airway is an up-side-down tree pattern of numerically branching networks of cylindrical shells at various angles from one generation to another. To expand the investigation from individual branches to the airway network as a whole, it is necessary to observe the dependence of resonance on the angles of branching and the add-on generations. At this moment, the trachea section is not considered because of its comparatively longer length than others. A section of airway between generation 4 and 7 is modelled with various branching angles in the longitudinal direction while holding other parameters constant. The frequencies of the first five modes are plotted against the angle of branching between zero to 90° in steps of 5° as shown in Figure 4.11. All modes follow the same trend of variation in frequency. The deviation between the maximum and minimum frequency is about 5 Hz, except at the angle of 5° to the longitudinal bronchus 4. Therefore, it is quite appropriate to neglect the effect due to branching angles between generations as the probability of the end extreme angles in such a random structure like the airways are. This provides a good approximation of the natural frequencies of airways as the function of the generation number and the physical parameters of that generation, but independent of the angular branching to the next generation.

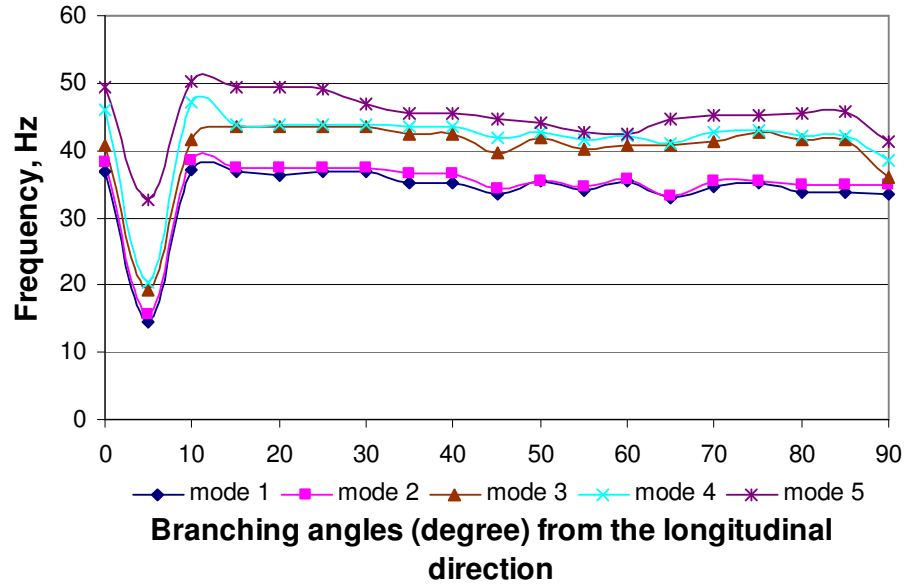


Figure 4.11 Frequency dependence on the angles between bronchus 4 and 5 of branching airway.

4.7 Tracheobronchial Models

The tracheobronchial tree has more than twenty generations starting from the trachea to the alveoli and has over eight million branches in the twenty-third generation according to Weibel's model. The tree grows in a simple algorithm but becomes tedious and complex in analysis due to the huge number of branching structure and the gradual variation of the physical properties. Pioneers such as Rohrer, [63] von Neergaard and Witz [65], Weibel [42-44], Horsfield [9, 45, 47, 109, 112-114], and Dubois [69, 71, 115-117] have done tremendously great foundation work for the continuity of research in lungs and airway mechanics.

A one-sided branching model is built on the fundamental unit of the airway tree, the trachea. Five cases are considered for investigation, the trachea alone, trachea to bronchus 1 (TB1), trachea to bronchus 2 (TB2), trachea to bronchus 3 (TB3), and trachea to bronchus 4 (TB4).

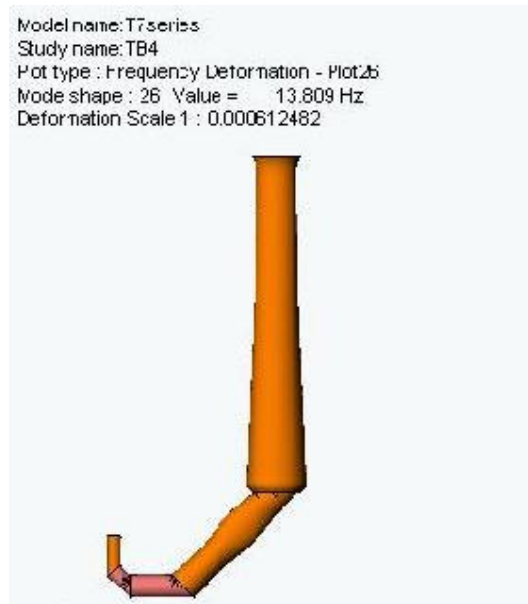


Figure 4.12 A deformation mode of the one-sided branching model from the trachea to the bronchus 4.

Results of these five-case, and trachea to bronchus 7 (TB7) are shown in Figure 4.13. The lowest frequency mode 1 is almost the same in all cases. As the mode number increases, the frequency tends to merge together for TB2, TB3 and TB4. However, the trachea and TB7 spread out to the upper and lower bounds respectively. Comparably, the trachea is much longer in length than the bronchi and therefore has a relatively higher frequency of vibration corresponding to a longer longitudinal half wavelength. The spreading space between TB4 and TB7 is due to the missing data

for TB5 and TB6. It may be concluded that the one-side branching model follows the trends that resonant frequencies occur approximately in response to the vibrations of individual branch of mode shapes.

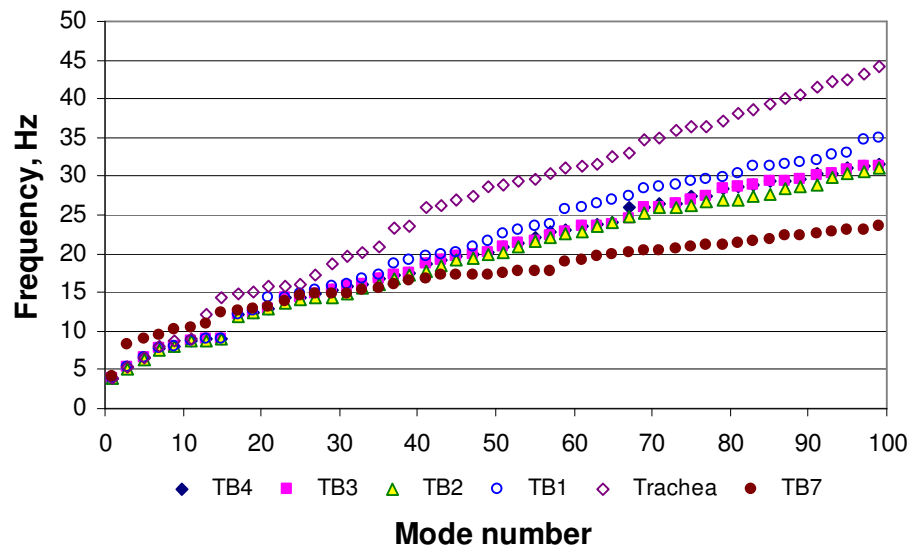


Figure 4.13 Frequencies of one-sided branching of trachea, trachea to Bronchus 1 (TB1), 2 (TB2), 3 (TB3) and 4 (TB4), together with the tracheobronchial tree (TB7).

4.8 Model of a Symmetric Airway Tree

A regional symmetric model of the airway tree is modelled for investigation and analysis, instead of the whole lung structure which involves a great deal of time and computing resources. The model starts from bronchus 3 to bronchus 9 in a pseudo-symmetric pattern as shown in the Figure 4.14. The main reason for excluding the trachea is to avoid its lower frequency mode shapes and stiffer physical properties when compared to the bronchi. Bronchus 3 is particularly shorter in length than its

parent and daughters. Therefore this region of the airway tree should present an optimal overview of the airway wall structure as the trachea is relatively too long and dominates the low frequency modes of vibration. On the other hand, the lower bronchi are too fine and improper in the preliminary investigation computing resource for finite element analysis. Figure 4.14 and Figure 4.16 show the SolidWorks model and the graph of the COSMOS/Works fundamental frequency versus the mode number, respectively.

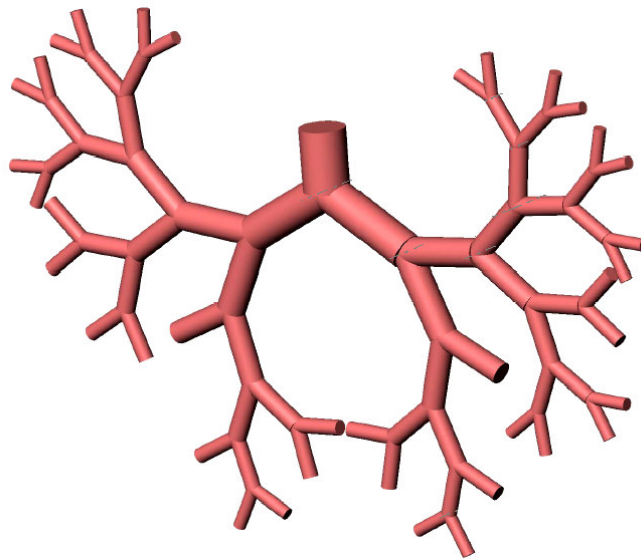


Figure 4.14 A pseudo-symmetric model of airway tree, bronchus 3 to bronchus 9.

First, the whole model was assumed to be of homogeneous in physical parameters of bronchus 9, then properties were updated to half of the densities and double the thickness according to the respective bronchial data in Table 3.1, so that the radial resonance could be observed in the earlier modes (Refer to Appendix E and Appendix F) and computing resources could be optimised. It has been verified that

the numerical resonances in COSMOS/Works agree quite well with the theoretical expectations in term of parameters of elasticity and density (Appendix A). Finally, the model was meshed to finer elements of 0.6 mm for analysis. Frequencies shifted vertically and remained in the similar trend. Figure 4.15 shows the mode shape 1 at the frequency 34.098 Hz and the major excitation is circumferential dominantly with bronchus 4 which has a longer longitudinal length than bronchus 3. Bronchus 5 had a minor deformation in the radial direction and the phenomenon was more obvious in the COSMOS/Works animation.

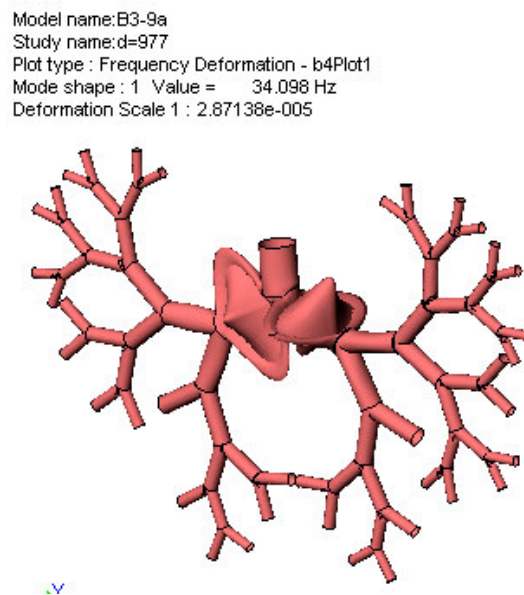


Figure 4.15 Mode shape 1 of the regional airway model from bronchus 3 to bronchus 9. Bronchus 4 is excited at the frequency 34 Hz.

The homogeneous curve behaved continuous as compared to the curves with updated properties of respective bronchi, and finer meshes as shown in Figure 4.16. The finer mesh curve was split into levels of frequency clusters. The analysis mesh size

magnified the quantum gap of the clusters between the frequency levels or mode shapes. Below mode 16, the frequency levels had the same mode span, which tended to be shorter with the increase in frequency levels.

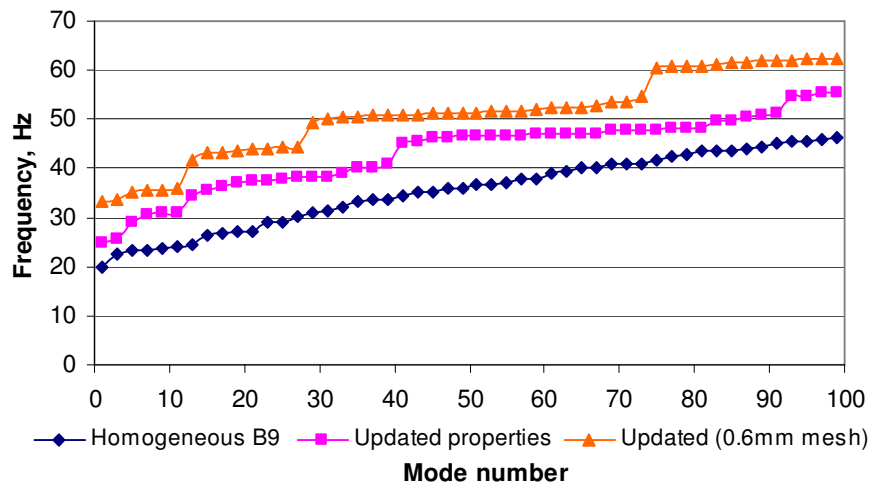


Figure 4.16 Frequencies of airway tree from bronchus 3 to bronchus 9. The model is first analysed with the physical properties of bronchus 9 (Homogeneous B9), then with the updated properties of the respective generations, and finally the updated properties with finer mesh of 0.6 mm.

Figure 4.17 and Figure 4.18 show the radial deformation pair of the bronchus 4 at 76.6 Hz and 76.8 Hz respectively. This resonant frequency is quite unique as deformations of other branches are not obvious or observable except of bronchus 3 which has a mixed mode of deformation. Referring to Appendix F, bronchus 4 has its first radial resonance at 68.5 Hz which is about 8 Hz below its resonance in this regional airway tree from bronchus 3 to 9. No additional radial mode of the same bronchus or others was observed in this model within the current computing resources.

Model name: B3-9a
Study name: d=977
Plot type : Frequency Deformation - b4radPlot191
Mode shape : 191 Value = 76.593 Hz
Deformation Scale 1 : 2.20481e-005

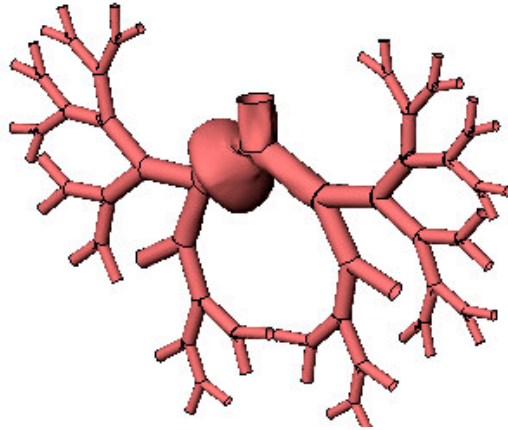


Figure 4.17 Mode shape 191 of the regional airway model from bronchus 3 to bronchus 9. Bronchus 4 left is excited in the radial mode at the frequency 76.6 Hz.

Model name: B3-9a
Study name: d=977
Plot type : Frequency Deformation - Plot192
Mode shape : 192 Value = 76.785 Hz
Deformation Scale 1 : 2.20481e-005

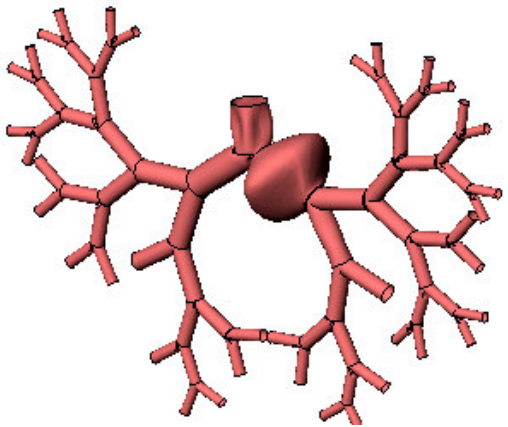


Figure 4.18 Mode shape 192 of the regional airway model from bronchus 3 to bronchus 9. Bronchus 4 right is excited in the radial mode at the frequency 76.8 Hz.

4.9 Closure

Finite element analysis (FEA) of COSMOS/Works is adopted in this work to link the relationship between the analytical and numerical modelling in the airway structure while searching for the radial natural frequencies in application to airway constriction and occlusion due to pulmonary disorders. COSMOS/Works was utilised in modelling and analysing Koval and Cranch's experimental sample. The first resonant mode shape was compared with the experimental, analytical and numerical results as shown in Table C.1 and Table 4.1. The FEA results may vary according to the mesh size in the analysis. In general, it is logically acceptable that the smaller the element size, the better the approximation to the analytical or real solution. Table 4.1 shows that COSMOS/Works provides a satisfactory frequency of 551 Hz versus the analytical value of 552 Hz which just lies above the experiment measurements.

In terms of the structure modelling of airways, the one-side branched model with expanded branched bronchial generation results small variation of frequencies when the angular branching angle at parent-to-daughter joints. Therefore the effect of such angles on the natural frequencies of a branched network like the airways is within the tolerance due to the fact that the complexity and the exact branching of human airways is not unique. The focus is on the trend of the pattern instead of the definite solutions.

In the model of a symmetric airway tree from bronchus 3 to 9, three analyses were run with homogeneous physical properties of bronchus 9, the updated properties of

the individual bronchus, and finally the updated properties with finer mesh for analysis. The frequency versus mode number graph (Figure 4.16) displayed a more continuous curve than curves of the updated properties and the updated properties with finer mesh. The discontinuous cluster is distinct with the finer mesh which acts like a magnifying glass or microscope when viewing curves. The mode frequencies of the tracheobronchial airway behave like photons of molecules in quantum mechanics [118].

In summary, numerical modelling can be a good approximation, depending on the chosen mesh size of elements, to the analytical solution as shown in the experimental data validation. Different mesh sizes lead to different results but have no obvious effect on the radial resonance of the assumed modelling of circular cylindrical thin shells. The branching angles of airways may be negligible in the preliminary investigation of airway resonances. Continuous branching airways may affect the resonances of tracheobronchial branches as a whole while compared to each branch individually in an acceptable range.

Chapter 5

Experimental Validation

5.1 Introduction

In spite of the fact that the main intention of this research is to conduct analytical and numerical investigations to determine the free vibrational characteristics of a branched structure, it is felt that conducting some experimental validations will enhance the results and give them more practicality. Obviously conducting in-vivo experimental validation tests is beyond the scope of this research due to the risks involved and the ethical requirements. Therefore, in this work samples of animal tissues are felt to be appropriate for the validation process.

Airway mechanics arises for investigation of lung disorders and develops with simple physical laws. Further theoretical advancement relies on the validation through other theoretical approaches, numerical modelling and/or experimental data. Rohrer [63] applied the fluid mechanics concept in measuring the air flow and pressure drop in the airways to determine the respiratory resistance of human lungs. This becomes the foundation of airway mechanics, especially in the experimental stream. The interrupter technique developed by Rohrer's student, von Neegaard,

force oscillation technique and plethysmograph by Dubois [69] are later techniques for experimental investigation of lungs so that control of lung disorders may be possible through improved modelling of the mechanical airway structure.

Lee et al. [111] concluded that there are better volume flow rates at the resonant frequency of the respiratory system in respiratory distress syndrome. The mean resonant frequency was 18.6 Hz and the median was 19 Hz for a sample of 18 infants. Fisher et al. [72] found that the resonant frequency was between 5 and 8 Hz for adults when determining the total respiratory resistance by the forced oscillation technique.

All the above experimental work has dealt with fluid flow measurements and the resistance-compliance, fluid mechanics approach with no relevance to the respiratory walls. No work has been done on determining the free vibration characteristics of the airway walls in particular as a branched structure. Since the intention of this work is to investigate the free vibration characteristics of branched structures with an application to the airway passages and not to investigate the vibration characterisations of airway passages as they are situated in the human body, measurements using animal tissues are justified for the present work. Also since the purpose of this experimentation is for validation only, trachea and tracheobronchial samples are used in the experimental validation conducted. It is felt that these suffice for the intention of the present validation.

This chapter describes the experimental work done on samples of pig tracheobronchi and identifies, in the concept of modal analysis and testing, the resonant frequencies

for comparison with values from the analytical and the numerical models. Two methods of measurements are used, one by mechanical excitation using a shaker and recording the dynamic response, while the second is by using acoustical excitation to avoid any direct contact of the samples with the exciting source.

5.2 Modal Analysis and Testing

Modal analysis involves a mathematical formulation for data dynamically characterising the system in terms of natural frequencies, damping factors and mode shapes [119-123]. An ideal and simple structure or system like a pendulum oscillates at one single frequency once displaced slightly from its equilibrium position. The periodic motion should continue for ever. However, the motion will eventually stop due to resistance of air as the damping effect. To maintain the oscillation or vibration, an external excitation is needed to drive the system in motion, and the system will resonate when the source drives at the natural frequency of the system. The pendulum moves in one plane and is restricted to motion in the orthogonal plane in space. Therefore, it is termed as the vibration of a single-degree of freedom (SDoF) system. The equation of motion for this system may be written as [123]

$$m \ddot{x}(t) + c \dot{x}(t) + kx(t) = f(t) \quad (5.2.1)$$

where m , c , k , x and t are the mass, damping factor, stiffness, displacement and time respectively.

The Laplace transformation of this time domain equation into the corresponding frequency domain ($s = j\omega$) expression is

$$X(s) = \frac{F(s)}{ms^2 + cs + k} = G(s)F(s) \quad (5.2.2)$$

Modal analysis assumes the vibration response is a set of simple harmonic motions and natural frequencies resulted from the linear time-invariant dynamic system as the Fourier series of any function. Each frequency is associated with a mode of vibration which is either a real or complex quantity. These modes are a function of the physical properties of mass, stiffness and damping, and the spatial distributions.

Modal testing is an experimental technique to investigate and validate modal models whose analytical solution is either difficult or impossible. Experiments include test preparation, frequency response measurements and modal parameter identification. The data produced from this method are sets of frequency response functions (FRF) to be analysed for modal parameters of the tested system.

5.3 Mechanical Excitation

The first experimental set-up in this chapter is to measure the deformation of samples excited by an electromagnetic shaker with a laser sensor head. The captured signals are processed by the vibrometer controller which outputs the conditioned voltage in the time domain to an oscilloscope for display. A block diagram and a photo of the experimental apparatus set-up are showed in Figure 5.1 and Figure 5.2 to Figure 5.5 respectively.

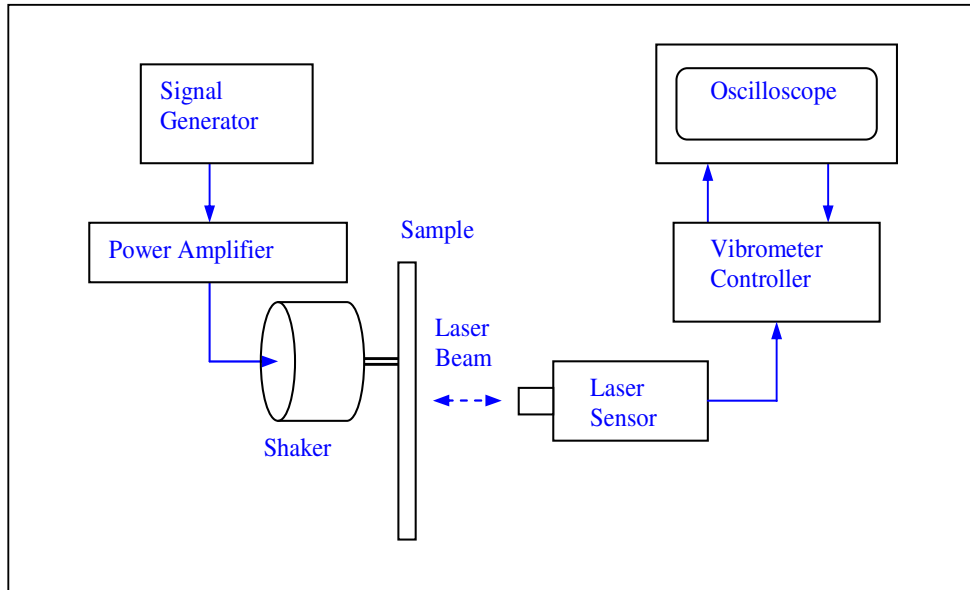


Figure 5.1 A block diagram of the experimental set-up.

Referring to Figure 5.2, the electromagnetic shaker (Ling Dynamic Systems Ltd., LDS V203) with an extended pointer was placed in contact with the sample at one end as a vibration exciter. The shaker is driven by a signal generator (TTi TG230) through a power amplifier (LDS PA25E Power Amplifier). A laser sensor head (Polytec OFV 505) of the vibrometer (Polytec OFV 5000) is used as the detection device of deformation which is then converted into the frequency domain through the Fast Fourier Transform (FFT) and displayed on the screen of an electronic oscilloscope (Tektronix TDS1012). Measurements are taken at the designated position of the sample with a reflective film where the laser beam is focused on for motion detection, Figure 5.9.

After checking the proper set-up connection, the Polytec OFV 5000 vibrometer is first turned on for at least twenty minutes of warm-up for stability of measurements. The Polytec OFV 505 sensor head in Figure 5.3 is calibrated to focus the reflective film in a distance of approximate 30 cm for the maximum lighted signal level displayed at the back of the sensor head. Once achieved, the laser spot on the reflective film is at the minimum size and in focus. A pre-caution was taken when switching on the LDS PA25E Power Amplifier which has its power on/off control together with the master gain knob. The power amplified was slightly turned just enough to click on the power to avoid overloading the fuse. The excited amplitude of the shaker was monitored by both outputs of the signal generator and the master gain of the LDS Power Amplifier. The shaker pointer was positioned just in-touch with the sample location and the vibrating amplitude was kept very small to avoid over-driving the sample, or over-loading the shaker. Data was then taken at step increments of frequency in Hertz of the signal generator and the corresponding intensity in decibels of the frequency spectrum displayed on the Tektronix TDS1012 oscilloscope set at the Mathematics Fast Fourier Transformation mode, Figure 5.5.

Although electromagnetic shakers and impact hammers are the two main types of excitation in general modal analysis and testing, it is possible to consider and design other source of excitation. Acoustic excitation is one of the sources that is used in the second part of the experimental validation.

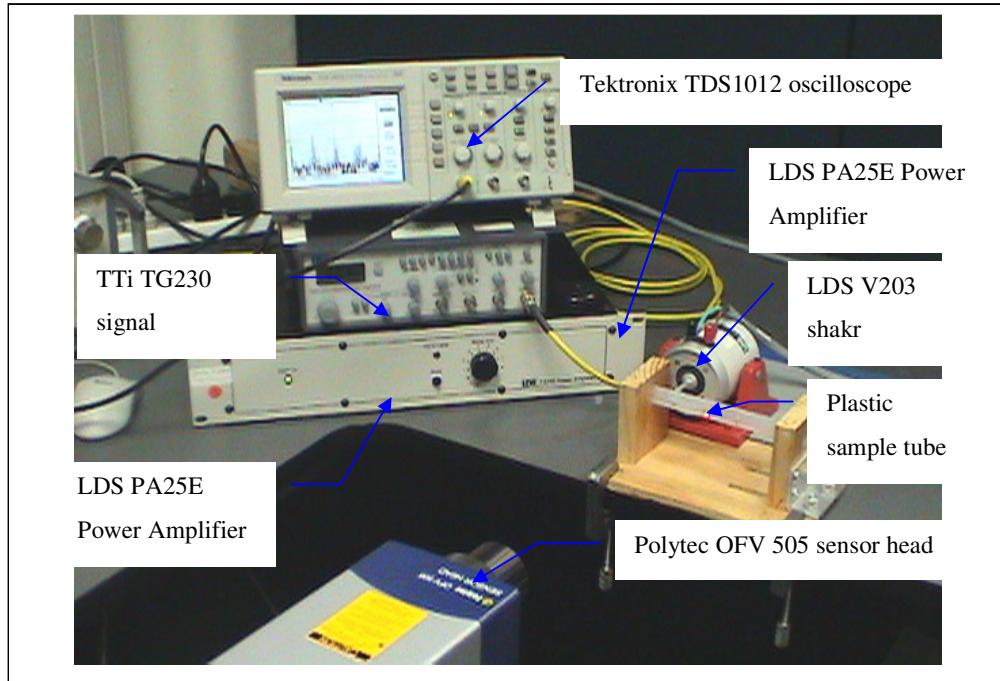


Figure 5.2 A photo of the experimental set-up.

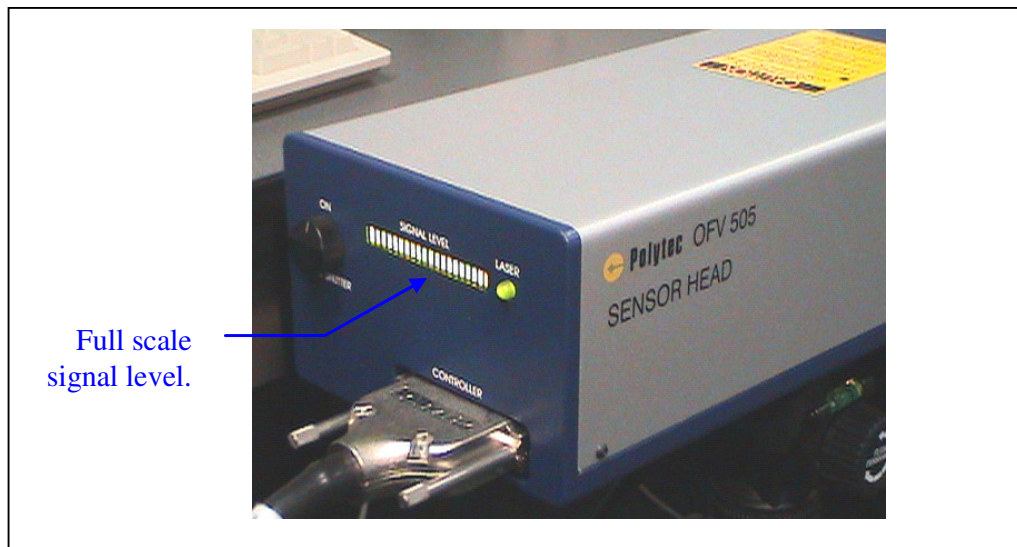


Figure 5.3 Polytec OFV 505 sensor head.



Figure 5.4 Polytec OFV 5000 vibrometer.

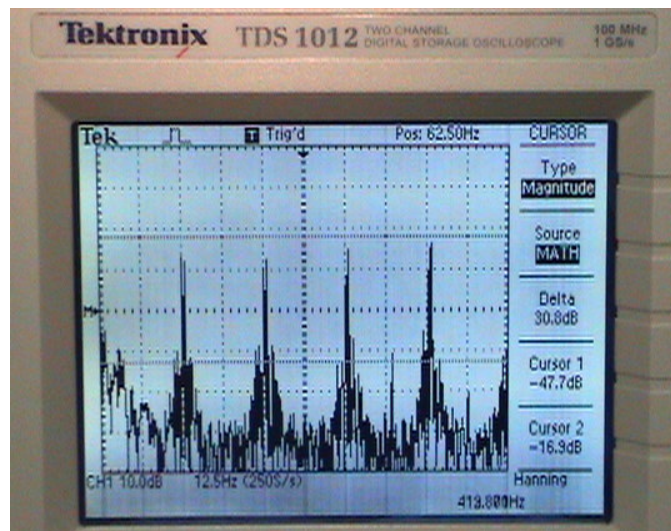


Figure 5.5 The Tektronix TDS1012 in Math FFT mode displays the frequency spectrum of signal input from the Polytec OFV 5000 vibrometer.

5.4 Acoustic Excitation

Due to the extended branching dimensions and the damping nature of the trachea-bronchia samples, the acoustic excitation is believed to generate more uniform driving power than the mechanical excitation using the shaker. The second experimental set-up in this work was to replace the shaker by an acoustic pressure chamber. The chamber was designed and built for the purpose of the experimentation. It consists of a transparent plastic enclosure which is firmly seated on a wooden board with a rubber seal, a speaker and clamps. The acoustic pressure is generated by the power speaker which is attached to the top of the enclosure. The inner air of the chamber is to be oscillated at the frequency of the speaker, Philips XB100 which is monitored by a signal generator TTi TG230. The sample is placed inside the chamber and excited by the speaker to produce the desired pressure and frequency. The chamber was firmly fixed in position using two elastic strings, one on each side, as shown in Figure 5.10.

5.5 Experimental Samples

Pig lungs have geometric and physical properties similar to the human lungs [124, 125]. Table 5.1 lists the average parameter values of the two lungs.

Table 5.1 Comparison of the average geometric and physical parameters between pig's and human trachea.

	Length mm	Diameter mm	Wall thickness mm	Young's modulus N/m ²	Density kg/m ³
Human	120	18	0.4	7300	1350
Pig	190	22	2.5	7300 [125]	1040

Experimental samples were dissected from pig lungs ordered from the local meat provider. The lungs were first dissected in the science laboratory with a scalpel. Excision of the trachea from the oesophagus was carefully performed and took about an hour but became more difficult from the trachea down to the primary bronchi and lower bronchi due to the increased branching and small bronchi size. Investigation showed that the pig's trachea had about 32 cartilaginous rings over its length of approximately 190 mm. Other than the normal primary bronchi at the carina, an extra or the third primary bronchus was branched out approximately at the 25th cartilaginous ring or 150 mm from the proximal. Although cartilaginous rings could be counted easily along the trachea, they were not so obvious or distinguishable from the soft tissue in the primary bronchi. Dimensions of length, radius, thickness and density were measured randomly for average values whenever possible. The morphological dimensions of pig tracheae are in general greater than those of human, referring to Table 5.1. The wall thickness was measured to be 2.5 mm average, which is one order of magnitude greater than that of the human measurements made by Weibel [42].

One of the pig tracheae was divided into two samples, i.e. sample 1 and sample 2, because there was a cut before the third primary bronchus. Sample 1 was a proximal sectioned trachea and sample 2 was a distal sectioned trachea with bronchi. Then sample 3 was the other pig trachea with bronchi. These three samples were to be used in the resonant frequency measurements with both mechanical and acoustic excitations as explained in the following sections.

5.6 Experimental Procedures

As previously described, the testing includes experiments on three samples from two pig tracheae and with two excitations, namely the mechanical excitation using an electromagnetic shaker and the acoustic excitation with an acoustic pressure chamber.

In summary, there were six experiments, three with mechanical excitation and three with acoustic excitation. Each experiment was run for two trials in general. The main focus was to measure the resonant frequency of the trachea although one experiment was performed on the bronchus. With the defined samples and two excitation approaches A and B, the six experiments are listed as follows,

A Mechanical Excitation

- 1 Resonant frequency measurements on the trachea of sample 1.
- 2 Resonant frequency measurements on the trachea of sample 2.
- 3 Resonant frequency measurements on the trachea of samples 3.

B Acoustic Excitation

- 1 Resonant frequency measurements on the trachea of sample 1.
- 2 Resonant frequency measurements on the trachea of sample 3.
- 3 Resonant frequency measurements on the bronchus of sample 3.

Experiments can now be coded or identified as A1, A2, A3, B1, B2 or B3 although descriptive detail may be included for clarity. The dimensions of the experimental samples are listed for mechanical excitation and acoustic excitation in Table 5.2 and Table 5.3, respectively.

Table 5.2 Dimensions on experiments with mechanical excitation.

Experiment	A1	A2	A3
Length, mm	90	60	151
Diameter, mm	24	24	21
Thickness, mm	3.1	3.1	2.8

Table 5.3 Dimensions on experiments with acoustic excitation.

Experiment	B1	B2	B3
Length (mm)	54	121	37
Diameter (mm)	23	21	12
Thickness (mm)	1.6	2.8	0.5

With reference to the experimental set-ups for mechanical and acoustic excitations, the experimental procedures for each experiment is quite typical with minor variations such as samples, sample mounting, measurements on trachea or bronchus and the type of excitation.

5.7 Mechanical Excitation Experimentation

The first experimental trial was experiment A1, on a sectioned pig trachea of sample 1 which was mounted on a circular tube at each end. One side was fixed and the other attached to a tiny cart pulled by a hanging mass over a string to eliminate any sagging of the sample as shown in Figure 5.6, but not too tight to contribute excessive tension altering the elasticity of the material. Precaution should be taken by varying the excitation position of the shaker to avoid exciting the vibration right at the node of the sample.

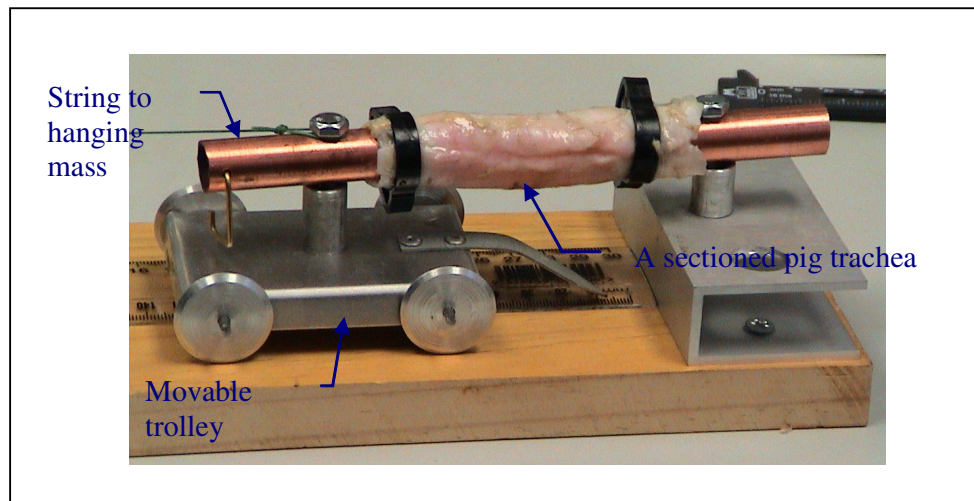


Figure 5.6 Mounting set-up of the pig trachea [126] adopted in natural frequency measurements.

In this work, the black circular clips were replaced with twisted wires to minimise the clamping effect. The effective length of the sample was considered to be between the inner supported edges.

This type of experimentation was conducted on a single trachea. However a tracheobronchial system excitation with a shaker was a bit difficult due to the geometrical complexity and the nature of damping of the sample. Therefore an acoustic pressure chamber was built for this purpose and was used in the second part of the experimental validation.

The second experiment was A2, on a tracheobronchial section of the first pig trachea and had a short tracheal part and the branched primary bronchi. The proximal trachea and distal bronchi were fitted with plastic tubing right into the lumen circumference of these three ends which were then nailed on a mounting board clamped on the laboratory bench. The carina was secured in place by three nails on the mounting board to serve as simple supports at the tracheobronchial junction, Figure 5.7. A light tension was applied before fixing the three end-points so that the hanging mass was eliminated.

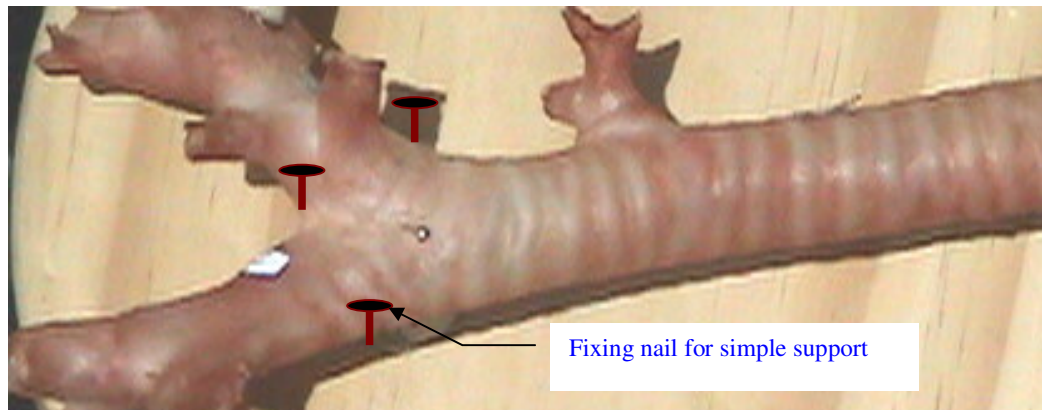


Figure 5.7 Nails were used to provide simple supports around the carina.

The third experiment was A3, and made on the trachea of the second pig sample. An improved fixture was designed to facilitate the mounting process. The sample was elevated above the mounting board as in the first trial and a circular split clamp was used for the simple support of the sample, Figure 5.8 and Figure 5.9.



Figure 5.8 A circular split clamp of 16.5 mm to support the pig trachea sample.

The width of the circular split clamp was about 2 mm with an inner shell structure. Therefore, it provided support at the edges and was not clamped tight during measurements.

It was obvious that the shaker excitation was stronger at the point of contact with the sample and became weaker at further positions. Therefore, certain mode shapes may have not been detected as the excitation position changes [127].

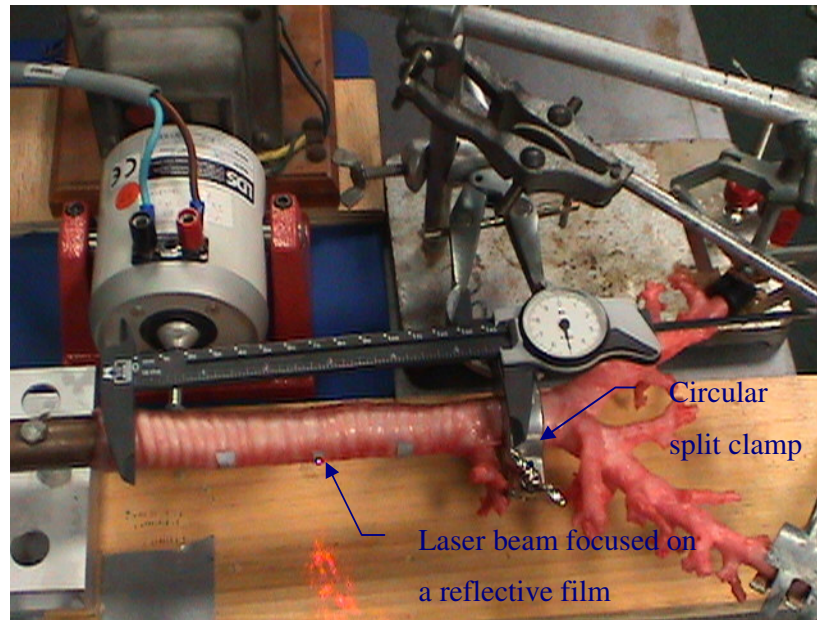


Figure 5.9 Fixture and mounting of the pig tracheobronchi for resonance measurements, with the laser beam focused at the mid position.

5.8 Acoustic Excitation Experimentation

Acoustic pressure was generated by longitudinal air wave motion of the power speaker mounted on top of the chamber. The deformed movement of the sample was detected by the laser head focused on a reflective film stuck to the sample.

The fourth experiment was B1, with acoustic excitation on the trachea of the first pig sample. Figure 5.10 shows the mounting of the sectioned tracheal sample placed inside the acoustic pressure chamber. The trachea ends were pinned to a support made of corks which were fixed to an aluminium base block. The cork was used due to its low resistance and it allowed the joining with the tissues without damage.

The fifth experiment was B2, measurement on the trachea of the second pig sample. Figure 5.11 is a view of the tracheobronchial sample mounted on the base board of the acoustic pressure chamber. Both ends and joint supports of the sample were pinned to cork supports which were fixed to the mounting base. It is worth mentioning that the pig trachea has an extra bronchus, which was removed and the connection point was sealed in the experimentation to generate a Y-shape which resembles to the theoretical model. The sixth experiment was B3 and had the same set-up as experiment B2, except that resonant frequency measurements were made on the bronchus instead of the trachea. The resonant frequency is expected to be higher because the effective length between boundaries is shorter.

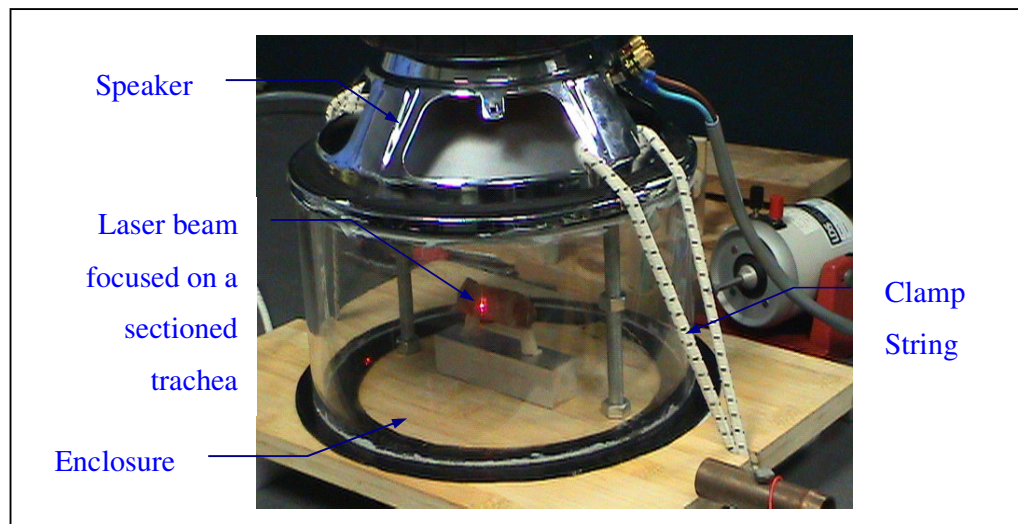


Figure 5.10 Mounting of the trachea section of sample 1 in the acoustic pressure chamber, with pinned supports on corks at the ends.

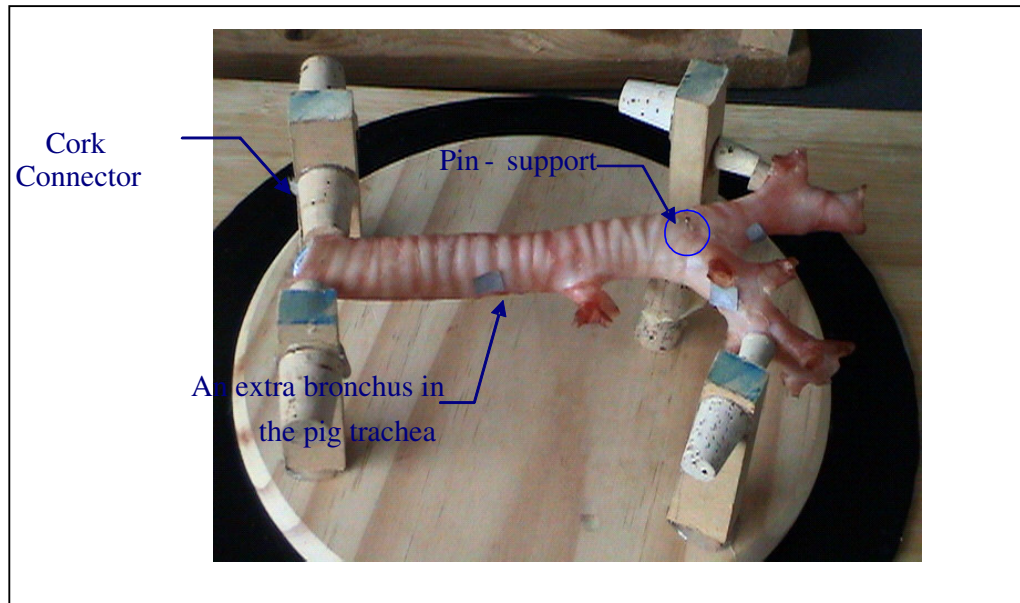


Figure 5.11 Mounted pig trachea with branched bronchi and simple supports at the carina and ends.

5.9 Mechanical Excitation Results

In all experiments with mechanical or acoustic excitation, the laser head was used to capture the sample deformation at the stimulated frequency which was varied in steps. Deformation intensity was measured through the oscilloscope which can be set at either in time domain or the Fast Fourier Transformation (FFT) mode. Figure 5.12 shows a sample graph of intensity versus frequency measured around the central position. The first peak is at 13 Hz and the second peak is at 50 Hz which has the highest relative peak.

To magnify these peaks, the abscissa is plotted with logarithmic frequency as shown in Figure 5.13. Below 13 Hz, there are two more peaks, 2 Hz and 4 Hz.

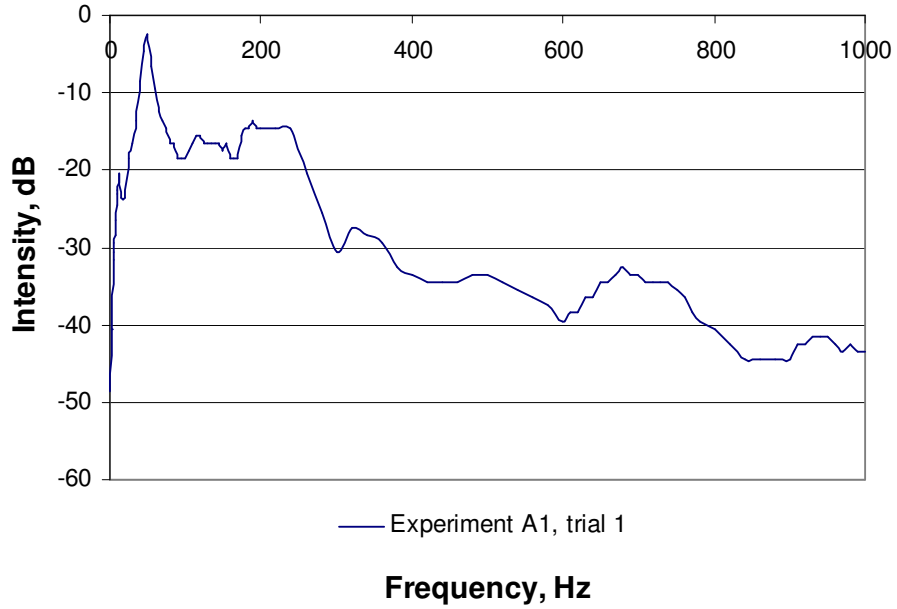


Figure 5.12 Trachea frequency spectrum of a sectioned pig trachea, sample 1, measured at the central position.

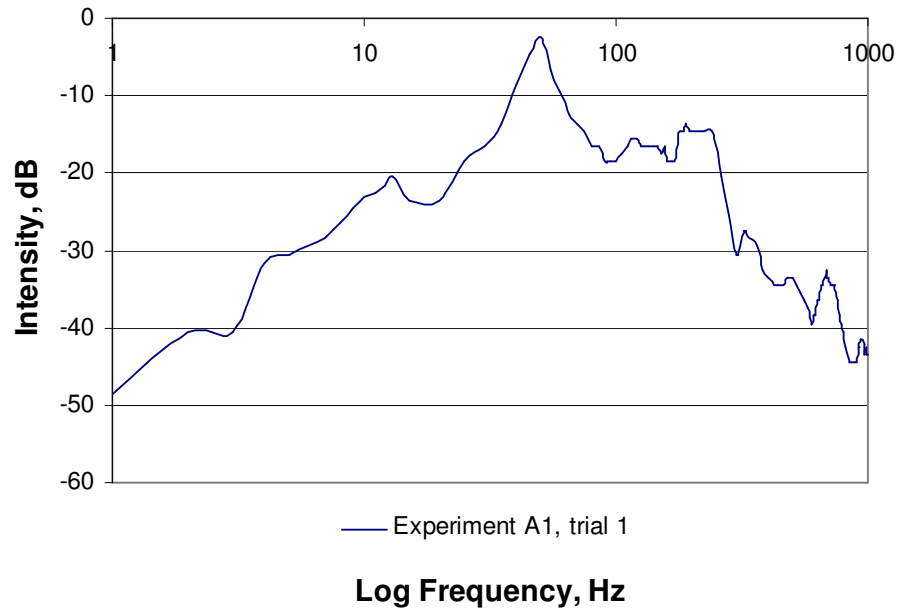


Figure 5.13 Logarithmic trachea frequency spectrum of the sectioned pig trachea, sample 1, measured at both the central and off-central positions (A1 for trachea of sample 1).

Table 5.4 Resonant frequency (f_x in Hertz) summary of experiments with mechanical excitation.

	Experiment						
	A1		A2		A3		
	Trial 1	Trial 2	Trial 1	Trial 2	Trial 1	Trial 2	Trial 3
f_1	2	-*	5	6	7	5	4
f_2	4	4	12	11	16	10	7
f_3	13	13	17	15	30	26	27
f_4	50	60	25	-*	65	68	96
f_5	85	120	90	90	80	93	93

* Frequency not observed.

Results are tabulated according to the relative resonant frequencies instead of the absolute mode shapes which are not detectable using the present techniques.

5.10 Acoustic Excitation Results

The first experiment with acoustic excitation was B1, measuring resonant frequency of the proximal sectioned trachea of the first pig sample. Figure 5.14 shows a sample of the frequency spectrum with several peaks ranging between 1.5 Hz and 19 Hz with the relative maximum at 11 Hz. The trend of the frequency spectrum in either mechanical or acoustic excitation is similar. However, the observable resonances may be different due to the excitation power transferable to the sample. Results by acoustic excitation are summarised in Table 5.5. Five matched resonant frequencies are listed for each experimental trial. In experiment B2, there were more unobservable resonances as compared with those results by mechanical excitation,

which has a stronger driving power, especially at points closer to the exciting position. However, the acoustic excitation is in general more uniform.

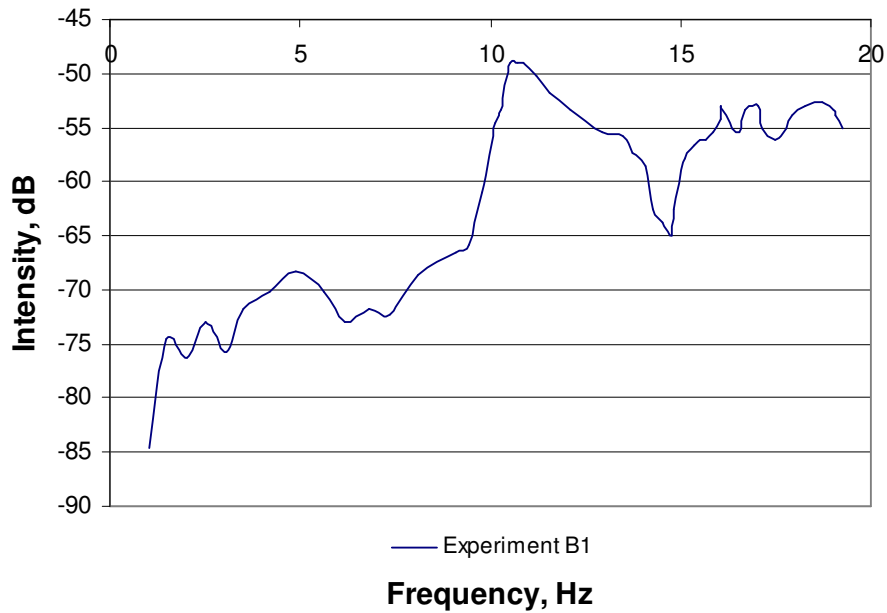


Figure 5.14 The acoustic (measured with the acoustic pressure chamber) frequency spectrum of the sectioned trachea of sample 1.

Table 5.5 Resonant frequency (f_x in Hertz) summary on experiments with acoustic excitation.

	Experiment				
	B1	B2		B3	
	Trial 1	Trial 1	Trial 2	Trial 1	Trial 2
f_1	5	-*	-*	6	6
f_2	11	12	11	10	11
f_3	16	-*	-	18	15
f_4	17	-*	-*	27	25
f_5	19	22	26	39	35

* Frequency not observed.

5.11 Closure

This chapter has presented a summary of the experimental validation method adopted in this research. Due to equipment unavailability, measurements were made to determine the natural frequencies only. No attempt was made to measure the mode shapes as they are beyond the scope of this research. The results of the experimental validation will be presented in chapter 6 and compared with the theoretical and numerical results.

Chapter 6

Discussion

6.1 Introduction

Since, to the best of our knowledge, no previous work in the open literature was found on the vibrations of branched circular cylindrical shells, the theoretical methods with some experimental validation are developed in this thesis. This includes analytical modelling of circular cylindrical thin shells, numerical modelling as an alternative solution to the analytical modelling, especially when the exact solutions are not available, and the experimental investigation to confirm and validate how and under what conditions that the analytical and numerical modelling are applicable. Although these approaches may not give an exact formulation of the present system, it is believed that a trend of variation of the natural frequencies of such a system is established. This process requires the integration of the three parts to characterise, deduce and conclude features of branched circular cylindrical shells as applied to airway modelling. This work is considered as the foundation for future

research on the vibration response of the lungs, identifying the range and limitation in modelling applications and monitoring dynamic progress and feedback in practice.

6.2 Analytical Modelling

The resonant frequencies of a circular cylindrical thin shell depend on the geometric dimensions and the material properties of the shell itself. The radial frequencies fall into the category of axisymmetric vibrations which occur in pipes, tanks, boilers, and other similar structural vessels subjected to asymmetrically internal loaded pressure. The derived natural frequency equation (3.4.3) of a circular ring as well as for an infinite long circular cylindrical thin shell could be written as [94, 98]

$$f_{ring} = \frac{1}{2\pi a} \sqrt{\frac{E}{\rho}} \quad (6.2.1)$$

The circular ring frequency equation depends on the radius, Young's modulus of elasticity and the density of the structure only. This is a single mode result regardless of the type of boundary conditions. However, it does not hold true when the longitudinal length and the radial thickness of the shell vary relatively in the finite range. In the case of a cylindrical membrane, the derived resonant frequency expression, equation (3.4.7), is found previously to be

$$f_m = \frac{1}{2\pi a} \sqrt{\frac{E}{\rho}} \left(\frac{a^2 m^2 \pi^2}{l^2 n^2} \right) \left(\frac{a^2 m^2 \pi^2}{l^2 n^2} + 1 \right)^{-1} \quad (6.2.2)$$

The dependent factors extend, from Young's modulus and the material density for the frequency of a ring, to the ratios of radius to length, the ratio of the longitudinal

mode number to the circumferential mode number, but not the membrane thickness as in the case of a thin shell. The analytical frequencies in Table 3.2 are listed again in Table 6.1, including two frequency ratios $f_{m\sim}/f_m$ and f_{r1}/f_1 , and the relevant frequency equations (3.4.7) to (3.5.1) for ready comparison.

This table shows the membrane frequency f_m using equation (3.4.7), the membrane approximate frequency $f_{m\sim}$ using equation (3.4.8), the frequency ratio $f_{m\sim}/f_m$, the lowest frequency using exact formulation f_1 in equation (3.5.1) and the lowest radial frequency f_{r1} in equation (3.5.2) and the ratio of f_{r1}/f_1 . The ratio of the approximate membrane frequency to the membrane frequency $f_{m\sim}/f_m$ ranges from 1.06 to 2.34 with an average of 1.30, and 1.24 excluding the highest ratio 2.34 of bronchus 3. This indicates that on average using membrane approximation generates frequencies 24% higher than those produced by exact membrane analysis. However, it is very interesting to notice that the ratio f_{r1}/f_1 is almost constant of a value 1.41 over the tracheobronchial airways under study. Both ratios are greater than 1, implying that the approximate membrane frequency $f_{m\sim}$ is greater than the exact membrane frequency f_m . Also it is noticed that the lowest radial frequency f_{r1} is greater than the lowest frequency f_1 of the shell. In fact, the radial frequency of a circular cylindrical shell, not too short and approaching to the ring shape, is greater than the first mode frequency as shown by the COSMOS/Works results (Table 6.2).

Table 6.1 Comparison of analytical frequencies and the frequency ratios.

Generation	rad/length a/l	Exact Membrane f _m	Membrane Approx. f _{m-}	f _{m-} /f _m	Simply supported Kraus: f ₁	Simply supported Kraus: f _{r1}	f _{r1} /f ₁
Z		Hz	Hz		Hz	Hz	
0	0.075	2.16	2.28	1.06	1.67	2.36	1.41
1	0.128	6.21	7.21	1.16	5.12	7.24	1.41
2	0.218	15.11	22.22	1.47	15.72	22.23	1.41
3	0.368	61.33	143.49	2.34	101.45	143.50	1.41
4	0.177	35.08	45.95	1.31	32.52	46.00	1.41
5	0.164	34.41	43.50	1.26	30.80	43.57	1.41
6	0.156	40.67	50.39	1.24	35.70	50.50	1.41
7	0.151	45.59	55.89	1.23	39.62	56.04	1.41
8	0.145	51.90	62.72	1.21	44.49	62.93	1.41
9	0.143	57.34	68.84	1.20	48.86	69.12	1.41
10	0.141	66.44	79.53	1.20	56.47	79.88	1.41
11	0.140	82.05	97.86	1.19	69.53	98.36	1.41
12	0.144	83.87	101.02	1.20	71.77	101.54	1.41
13	0.152	93.07	114.25	1.23	81.11	114.76	1.41
14	0.161	128.40	161.20	1.26	114.37	161.82	1.41
15	0.165	162.00	205.53	1.27	145.81	206.31	1.41
16	0.182	193.58	256.74	1.33	181.96	257.48	1.42

$$f_m = \frac{1}{2\pi a} \sqrt{\frac{E}{\rho}} \left(\pi^2 \frac{m^2 a^2}{n^2 l^2} \right) \left(\pi^2 \frac{m^2 a^2}{n^2 l^2} + 1 \right)^{-1}$$

$$f_{m-} = \frac{1}{2\pi a} \sqrt{\frac{E}{\rho}} \left(\pi^2 \frac{m^2 a^2}{n^2 l^2} \right)$$

where

$$f_1 = \frac{1}{2\pi a} \sqrt{\frac{E\Delta_1}{\rho(1-\nu^2)}}$$

$$f_{r1} = \frac{1}{2\pi a} \sqrt{\frac{E\Delta_{r1}}{\rho(1-\nu^2)}} \approx \frac{a\pi}{2} \sqrt{\frac{E}{\rho}} \left(\frac{1}{l^2} \right)$$

Refer to equations (3.4.7), (3.4.8), (3.5.1) and (3.5.2).

Figure 6.1 shows the frequency plots of the tracheobronchial generations together for the frequencies given in Table 6.1.

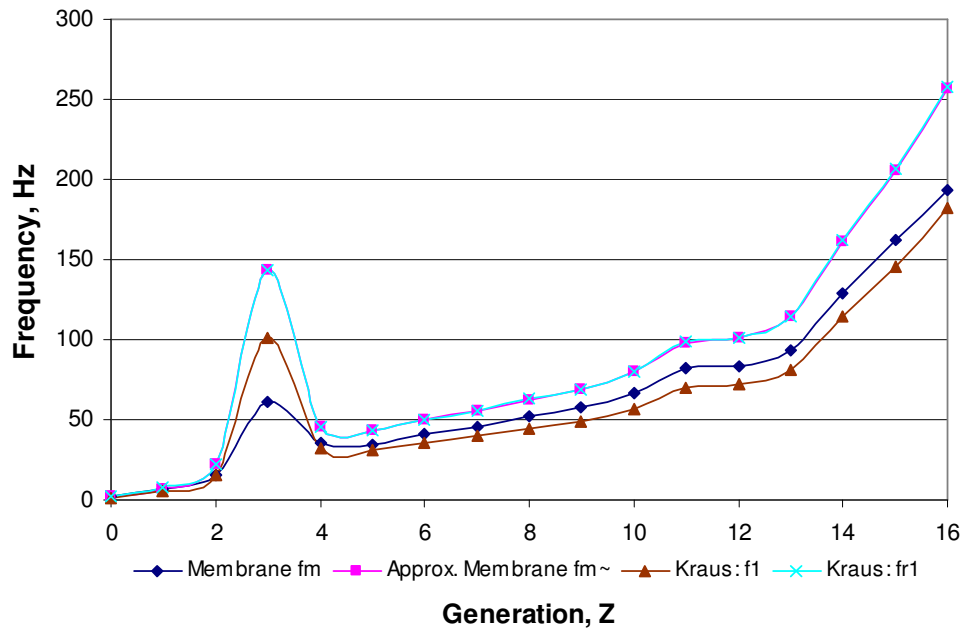


Figure 6.1 Comparison of analytical frequencies of airway from trachea to bronchus 16, where f_l , f_{r1} , $f_{m\sim}$ and f_m are the lowest frequency, the lowest radial frequency and the membrane frequency of circular cylindrical thin shells.

The lowest frequency f_l is based on the circular cylindrical thin shell with simply supported boundaries. When the longitudinal bending and the circumferential modes are ignored, the lowest radial frequency f_{r1} of the thin shell is greater than the lowest, the membrane and the membrane approximated frequencies f_l , f_m and $f_{m\sim}$ respectively. However, all these three frequencies including f_{r1} are lower than the ring frequency of equation (3.4.3) which is the upper limit of such a structure. They progress in the same trend from the trachea to bronchus 16, except at bronchus 2 and 3 where the membrane frequencies are the lowest. This is attributed to the

dimensions of the bronchus. The ‘bump’ at bronchus 3 is obvious in the ring frequency and is relatively less for the membrane frequency, most likely due to variation in its geometric and physical parameters.

So far, the analytical results presented for airways are based on the fundamental circular cylindrical shell. The complexity of the airway structure in numerous branching generations with various branching angles leads to the extreme difficulty in finding the exact solution of the natural frequencies of the tracheobronchial system. An approximate estimation formula for individual branch can be obtained using equation (6.2.2). The latter equation can be simplified with the circumferential mode number equal to one ($n = 1$) for radial modes to get

$$f_m = \frac{1}{2\pi a} \sqrt{\frac{E}{\rho}} \left(\frac{a^2 m^2 \pi^2}{l^2 + a^2 m^2 \pi^2} \right) \quad (6.2.3)$$

$$f_m = \frac{1}{2\pi a} \sqrt{\frac{E}{\rho}} \quad ; \text{ for } a^2 m^2 \pi^2 \gg l^2 \quad (6.2.4)$$

$$f_m = f_{ring} = \frac{1}{2\pi a} \sqrt{\frac{E}{\rho}}$$

For $l^2 \gg a^2 m^2 \pi^2$, the membrane radial frequency becomes

$$f_m = \frac{1}{2\pi a} \sqrt{\frac{E}{\rho}} m^2 \pi^2 \left(\frac{a^2}{l^2} \right) \quad (6.2.5)$$

The lowest membrane radial frequency occurs when $m = 1$

$$f_{m1} = \frac{1}{2\pi a} \sqrt{\frac{E}{\rho}} \pi^2 \left(\frac{a^2}{l^2} \right) \quad (6.2.6)$$

$$f_{m1} = f_{ring} \pi^2 \left(\frac{a^2}{l^2} \right) \quad (6.2.7)$$

$$f_{m1} = \frac{a\pi}{2} \sqrt{\frac{E}{\rho}} \left(\frac{1}{l^2} \right) \quad (6.2.8)$$

Therefore, it is possible to conclude that the first membrane radial frequency f_{m1} with simply-supported boundary conditions is the same as the lowest radial frequency f_{r1} of simply-supported cylindrical thin shells by Kraus. However, the membrane frequency is smaller than the lowest radial frequency and is approximately 0.8 of the exact value, and is about 1.1 of the exact lowest frequency.

6.3 Numerical Modelling

... that Rayleigh or his followers realized that the geometrical shape of many members made them difficult or impossible to handle with an appropriate untheoretical approximation. [128]

The demand of finite element analysis is increasing in science and engineering for numerical solutions due to the fact that theoretical analysis is limited to applications of simple and regular geometric constraints as well as the boundary conditions imposed on the structural system. In spite of the popularity, numerical analysis is in general the next option to the exact analytical approach. Confirmation of the result accuracy and skills in formulating the numerical analysis process are the draw-back of this versatile and rewardable approach.

6.3.1 Numerical Modelling and Analytical Modelling

The verification of results on the experimental sample by Koval and Cranch [105] shows that COSMOS/Works can be a reliable numerical software in investigating similar geometric structures like circular cylindrical thin shells which are assumed to make up the airway system. It has been shown in the previous section that COSMOS/Works resolves the fundamental resonant frequency of the verification sample in section 4.3 to be ranged from 663 Hz to 551 Hz as compared to 552 Hz by Kraus [93], which lies just above the experimental measurement [105].

Using the same assumptions as described in the Analytical Models, Chapter 3, namely a circular cylindrical thin shell is the basic unit in building up the whole airway network, the airway walls have negligible influence from the surrounding medium, and simple support is the type of boundary conditions at all ends and joints of branching, the numerical solutions were generated.

COSMOS/Works analyses of the trachea and each bronchus as an individual base unit had been achieved and the results of both default mesh and fine mesh of analysis are given in Appendix E. Appendix F also gives results with double shell thickness and half density of the parametric values. Both Table 6.2 and Table 6.3 summarise the generation frequencies of COSMOS/Works analysis mode 1 of clamped and simply-supported conditions, COSMOS/Works first radial mode, theoretical membrane frequency and the exact thin shell frequencies with clamped and simply-supported conditions. It is important to note that the radial resonant frequencies listed together with the lowest frequencies are for comparison purposes and in

general do not correspond to the lowest frequencies of generations. In fact, both COSMOS/Works $f_{r/l}$ and the membrane radial frequency f_m are greater in values than other lowest frequencies because the radial mode is not the first mode shape of vibrations in thin shell structures. In some cases, the exact shell frequency f_s is greater than f_m because

1. the membrane frequency is independent of the thickness while the shell frequency has a defined shell thickness for calculation, and
2. the relative radius to thickness ratio in calculating the shell frequency (referring to Appendix B).

The COSMOS/Works analysis also shows that the clamped frequency is higher than the simply-supported frequency unless the structural geometry is in the shape approaching to the limit of rings, i.e. the radius to length ratio is either too large or too small.

6.3.2 Sensitivity of Boundary Conditions and Physical Properties

Both COSMOS/Work and the analytical method were applied to a clamped-clamped as well as simply-simply boundary conditions for bronchi at different generations.

The simply-simply boundary conditions are $u = v = w = M_x = 0$, at $x = 0$ and $x = l$,

and the clamped boundary conditions are $u = v = w = \frac{\partial w}{\partial x} = 0$, at $x = 0$ and $x = l$.

These are summarized in Table 6.2. It is obviously clear that the effect of the boundary conditions is not critical in this case as the values of the frequency are very close. This may be attributed to the nature of the bronchial materials as they have

very low elasticity when compared to the stiffer materials such as steel and aluminium.

Table 6.2 Comparison of COSMOS/Works and theoretical fundamental or lowest resonant frequencies (with the clamped frequencies for reference).

The lowest frequencies (Hz)						
	COSMOS/Works			Membrane radial	Exact thin shell	
z	f (clamped)	f (supported)	f _{r1} (radial)	f _m (supported)	f _s (clamped)	f _s (supported)
0	1.96	1.97	5.61	2.16	2.41	1.67
1	3.49	3.46	10.38	6.21	6.01	5.00
2	6.97	6.87	18.77	15.11	12.79	7.12
3	24.95	23.88	71.83	61.33	45.42	31.80
4	17.71	17.38	47.84	35.08	29.07	19.50
5	17.82	17.52	49.05	34.41	29.37	21.19
6	21.61	21.27	59.75	40.67	36.14	27.43
7	24.61	24.23	68.13	45.59	41.65	32.45
8	28.80	28.38	79.62	51.90	49.98	40.51
9	32.46	32.00	89.06	57.34	57.24	47.35
10	48.02	47.33	122.48	66.44	68.65	57.71
11	47.33	47.67	129.18	82.05	88.30	74.13
12	49.70	48.96	129.47	83.87	92.13	77.00
13	54.11	53.18	138.81	93.07	98.76	82.84
14	73.53	72.11	184.87	128.40	133.60	109.78
15	92.93	91.03	229.82	162.00	170.79	140.31
16	108.27	105.56	260.55	193.58	197.64	155.03

Table 6.3 Comparison of COSMOS/Works and theoretical fundamental or lowest resonant frequencies, with double shell thickness and half density (with the clamped frequencies for reference).

The lowest frequencies (Hz)						
z	COSMOS/Works			Exact membrane	Exact thin shell	
	f (clamped)	f (supported)	f _{r1} (radial)	f _m (exact)	f _s (clamped)	f _s (supported)
0	3.92	3.88	8.03	6.57	5.44	2.60
1	7.00	6.92	14.85	17.10	8.51	7.07
2	12.00	11.57	26.84	34.84	18.09	10.08
3	48.78	45.66	102.77	115.22	64.23	44.97
4	30.88	30.08	68.46	87.53	41.11	27.58
5	32.18	31.45	70.22	88.26	41.54	29.97
6	40.40	39.61	85.58	106.08	51.11	38.79
7	46.83	45.97	97.61	119.96	58.90	45.90
8	56.59	55.65	114.13	138.32	70.69	57.29
9	64.90	63.87	127.13	153.73	80.95	66.96
10	77.82	76.63	149.00	178.69	97.09	81.61
11	98.54	98.54	185.53	221.51	124.88	104.83
12	103.92	102.26	186.15	224.70	130.30	108.90
13	110.72	108.65	199.68	245.48	139.66	117.15
14	148.21	144.95	266.16	332.72	188.94	155.25
15	188.98	184.54	331.16	416.56	241.53	198.42
16	214.46	208.05	375.84	481.75	279.50	219.25

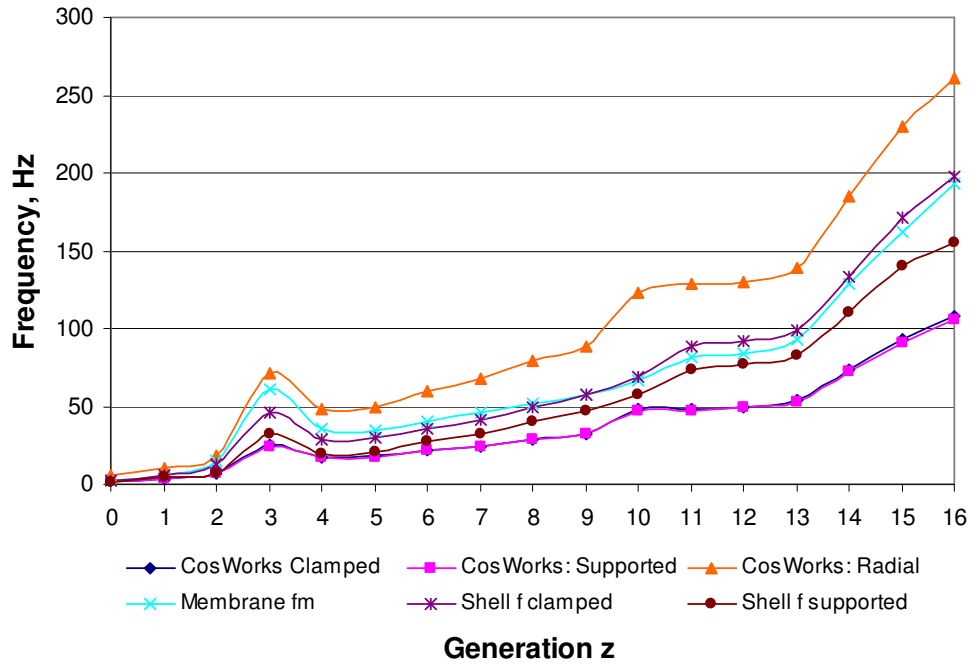


Figure 6.2 Comparison of frequencies by analytical and numerical modelling.

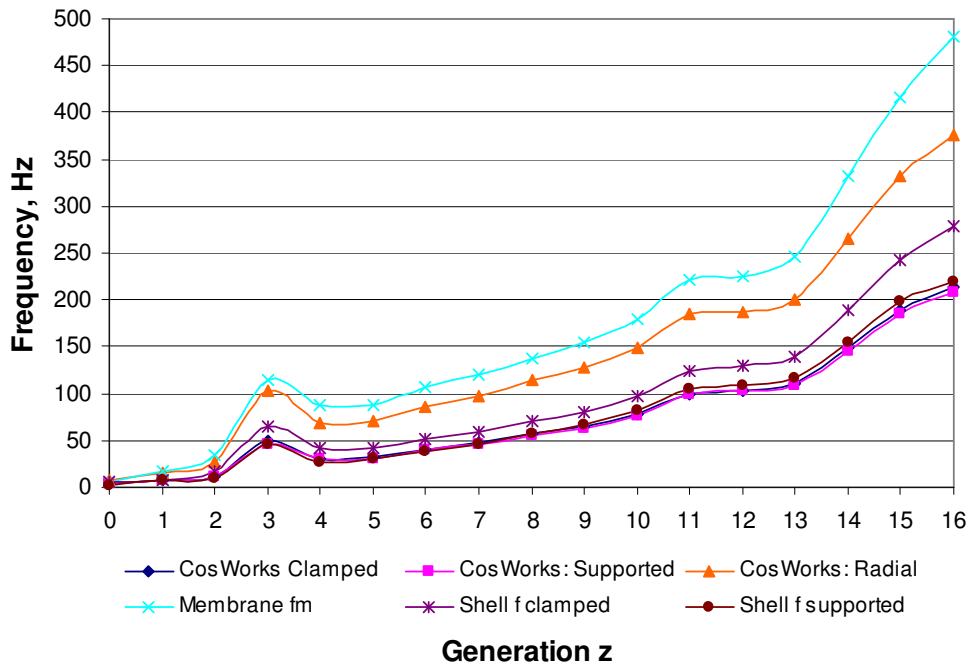


Figure 6.3 Comparison of frequencies by analytical and numerical modelling, with double shell thickness and half density.

Theoretically, the resonant ring frequency is proportional to the square root of Young's modulus or elasticity, and is inversely proportional to the square root of the density of the material. Comparison between Table 6.2 and Table 6.3 may be clear in terms of the corresponding frequency ratios which are listed in Table 6.4 and illustrated in Figure 6.4.

Table 6.4 Comparison of frequency ratios of results Table 6.2 to Table 6.3.

The lowest frequencies						
z	COSMOS/Workss			Exact membrane	Exact thin shell	
	f (clamped) ratio	f (supported) ratio	f _{r1} (radial) ratio	f _m (radial) ratio	f _s (clamped) ratio	f _s (supported) ratio
0	2.00	1.97	1.43	3.04	2.26	1.56
1	2.01	2.00	1.43	7.10	1.42	1.41
2	1.72	1.68	1.43	12.27	1.41	1.42
3	1.96	1.91	1.43	14.44	1.41	1.41
4	1.74	1.73	1.43	2.74	1.41	1.41
5	1.81	1.80	1.43	3.94	1.41	1.41
6	1.87	1.86	1.43	2.61	1.41	1.41
7	1.90	1.90	1.43	4.20	1.41	1.41
8	1.96	1.96	1.43	4.30	1.41	1.41
9	2.00	2.00	1.43	4.15	1.41	1.41
10	1.62	1.62	1.22	4.29	1.41	1.41
11	2.08	2.07	1.44	4.56	1.41	1.41
12	2.09	2.09	1.44	2.68	1.41	1.41
13	2.05	2.04	1.44	3.86	1.41	1.41
14	2.02	2.01	1.44	4.72	1.41	1.41
15	2.03	2.03	1.44	4.29	1.41	1.41
16	1.98	1.97	1.44	2.49	1.41	1.41
Average	1.93	1.92	1.42	5.04	1.46	1.42

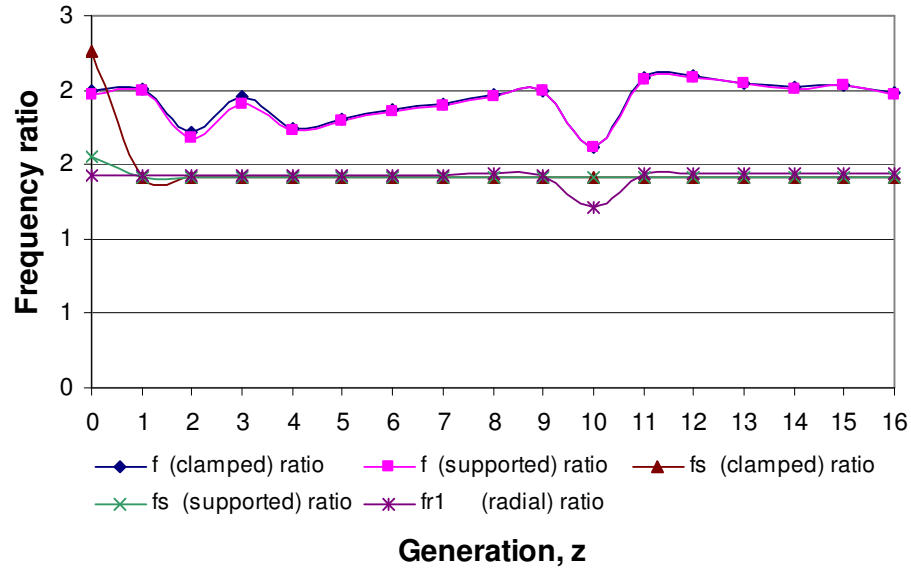


Figure 6.4 Frequency ratios of results from Table 6.2 and Table 6.3, the COSMOS/Work results of f and f_{r1} , and the analytical results of f_s .

Except for the trachea, the analytical frequency f_s expects the ratio of approximate 1.42 for half of the density and indicates that doubling the thickness has no effect on the resonant frequencies. It is, however, surprising to see that the COSMOS/Works radial frequency ratios are approximately equal to 1.42, implying that there is also no obvious effect of the thickness on the radial resonances and the change of resonant values depends on the change of elasticity only. The COSMOS/Works frequency ratios of clamped and simply-supported boundaries have fairly constant values implying that the numerical approximation by FEA is good and approaching to the analytical accuracy and relationship. The analytical membrane frequency ratios vary the most among others, especially for bronchus 2 and bronchus 3. This is due to the steep change of geometric and/or physical parameters from one generation to the

other as the membrane resonant frequency is factor of shell length or to be more specific, the radius to length ratio.

Table 6.5 compares the average ratio of resonant frequencies of COSMOS/Works results of Table 6.2 and Table 6.3 which has half of the density ρ and double of the wall thickness t (Column 1). Column 2 is the ratio of the first radial to lowest mode 1 frequency by COSMOS/Works. Column 3 is the ratio of the first radial by COSMOS/Works to the analytical membrane frequency. The average ratios are over the trachea up to bronchus 16. Such ratios indicate that constant relationship or trend is held between the relevant frequencies. Therefore one frequency can be predicted by the other with a given ratio.

Table 6.5 Average ratios of radial to simply supported frequencies, and radial to membrane frequencies of Table 6.2 and Table 6.3.

	Average frequency ratio	
	f_{r1} (radial) / f (supported)	f_{r1} (radial) / f_m (supported)
ρ and t	2.73	1.54
$\rho/2$ and $2t$	2.03	0.84

Figure 6.5 and Figure 6.6 are the graphs of the COSMOS/Works first radial frequencies of the tracheobronchi as listed in Table 6.2 and Table 6.3. Two linear curves are fitted to the data in each graph with the corresponding slopes and intercepts. With the assumed geometric and physical properties used in this work, linear relationships exist among the radial resonances of certain bronchi.

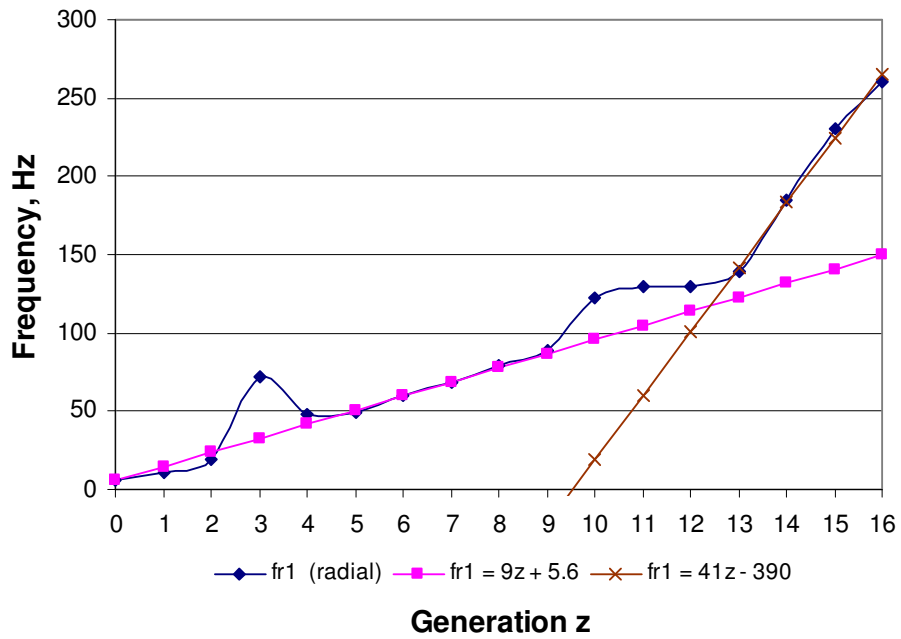


Figure 6.5 The tracheobronchial radial frequencies with linear curve fittings.

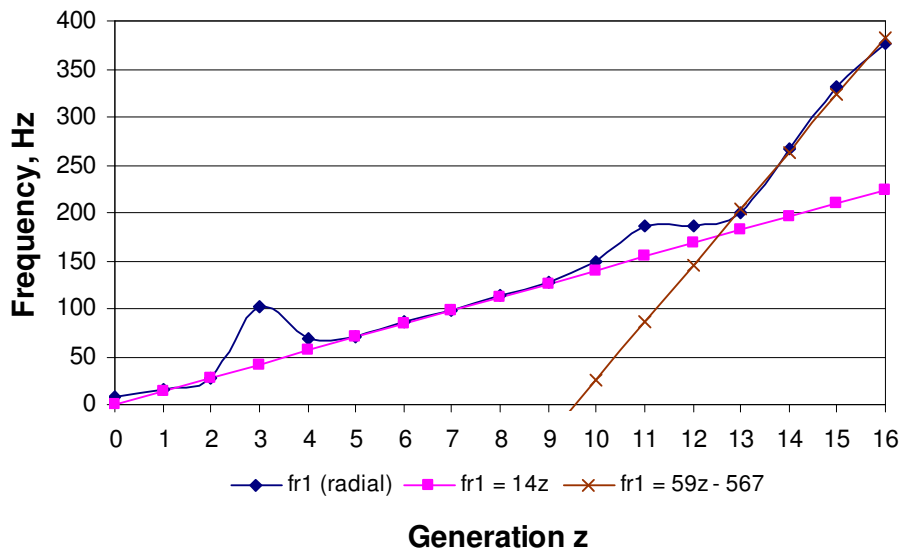


Figure 6.6 The tracheobronchial (of half density and double wall thickness) radial frequencies with linear curve fittings.

6.3.3 Numerical Modelling and Experimental Validation

With the two pig trachea samples used in the experimental validation, it is possible to obtain numerical results based on their measured geometric dimensions and densities, and the assumed Young's moduli of pigs to be the same as those of humans taken in previous modelling. Taking the average measurements of the sample dimensions, the COSMOS/Works results (refer to Appendix G) are summarised in Table 6.6 with the first column for each of the experimental measurements previously coded in Chapter 5, the Experimental Validation, second column for the first mode frequency f_1 , and the third column for the first radial resonant frequency f_{r1} . The harmonics of the radial frequency are multiples of the fundamental frequency as found in Appendix G.

Table 6.6 Resonant frequencies by COSMOS/Works on pig trachea samples with mode 1, f_1 and the first radial resonant frequency, f_{r1} .

Validation Experiment	COSMOS/Works Resonance, Hz	
	Mode 1 (f_1)	First Radial (f_{r1})
A1	5.22	8.59
A2	8.48	12.89
A3	2.40	5.12
B1	7.26	14.25
B2	3.36	6.39
B3 (Bronchus)	7.88	18.66

It is noticeable that the first radial resonant frequencies are greater than the first resonant frequencies, implying that the lowest resonant frequencies are not axisymmetric and may involve bending modes or its mixture. Also, the first radial

resonant frequencies are approximately double of the lowest or mode 1 frequencies although that is not the analytical result in theory.

6.4 Experimental Validation

In this work the experimental testing was performed to validate the theoretical results.

Experiments were performed based on the concept of vibrational resonance, and modal analysis and testing. Pig trachea samples were the optimal choice regarding the compatibility and the research resource capacity. As described in the previous chapter, the resonant frequencies resulting from different trials do not totally agree with each other, or able to correlate with the analytical and numerical models. Such phenomena are common and should be expected in most, especially preliminary research work. The valuable finding of this experimental work is the strong trend that reflects the physical behaviour of individual trials and the inter-relation among trials and other types of modelling.

The frequency response function (FRF) of a single degree of freedom (SDoF) is the basic building block of vibrations and modal analysis and testing of further complex systems with multiple degrees of freedom. A real system with a single degree of freedom has a flatter resonant peak with a band width relative to the damping than the ideal single frequency peak or spike. Analysis of the frequency spectrum of multiple degrees of freedom is quite manageable when the system is lightly coupled so that each resonant frequency is far enough from the others to be considered as a

system of a single degree of freedom. Otherwise intensities of close resonances suppress each other in a heavily coupled system.

Each of the experiments shows one or more distinct peak resonant frequencies. Figure 6.7 shows the logarithmic frequency spectrum of experiment A1 of a sectioned trachea of pig sample 1 run for two trials.

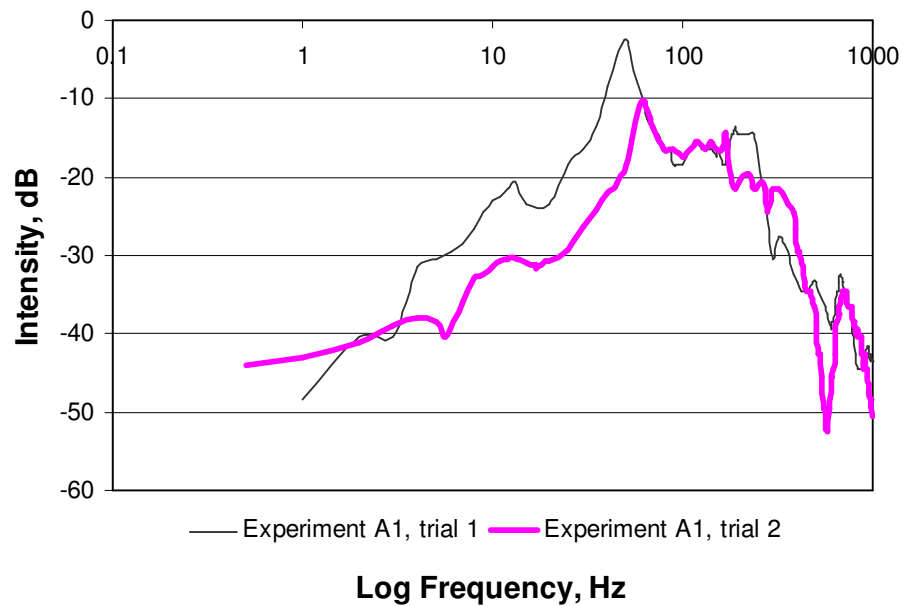


Figure 6.7 Logarithmic frequency spectra of experiment A1, the sectioned trachea of pig sample 1.

The curves follow the same trend with some frequency shifts and the highest peaks at 50 Hz and 60 Hz for trial 1 and trial 2, respectively. And logarithmic frequency spectra of other experiments are shown in Figure 6.8 to Figure 6.12.

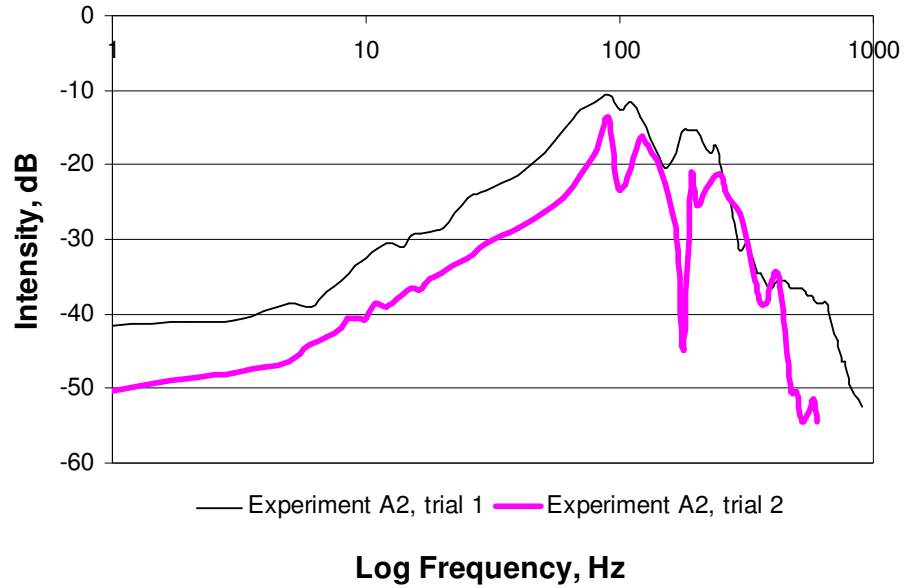


Figure 6.8 Logarithmic frequency spectra of experiment A2, the sectioned trachea with bronchi of pig sample 2.

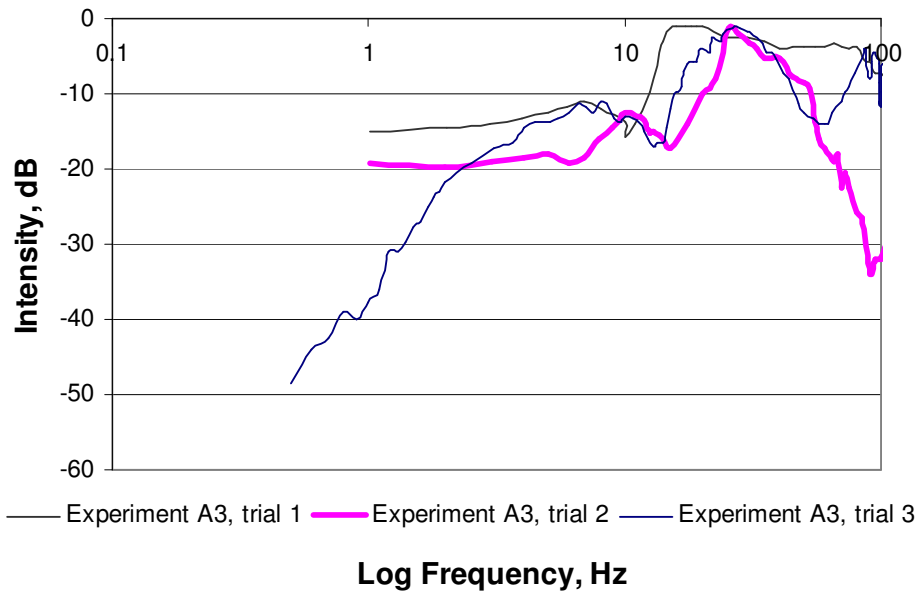


Figure 6.9 Logarithmic frequency spectra of experiment A3, the trachea with bronchi of pig sample 3.

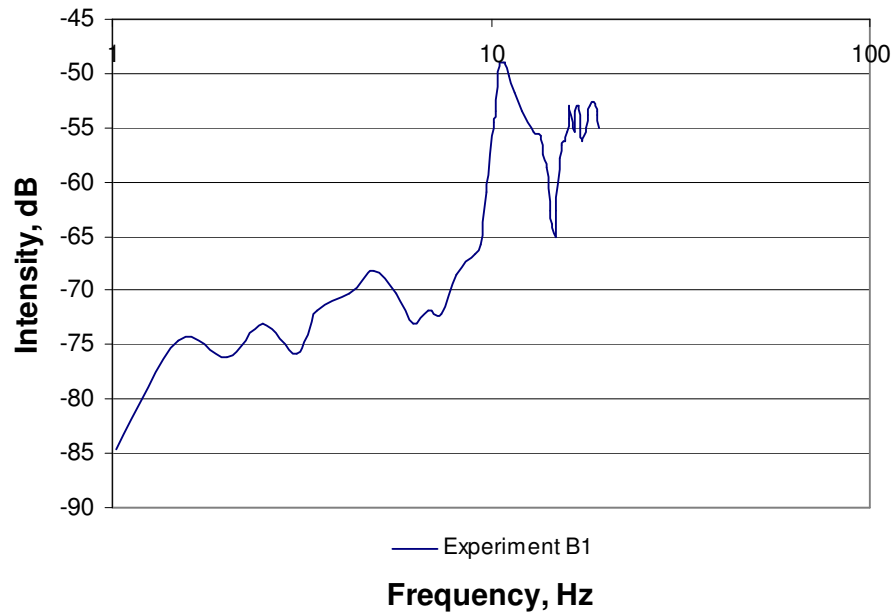


Figure 6.10 Logarithmic acoustic frequency spectrum of experiment B1, the sectioned trachea of pig sample 1.

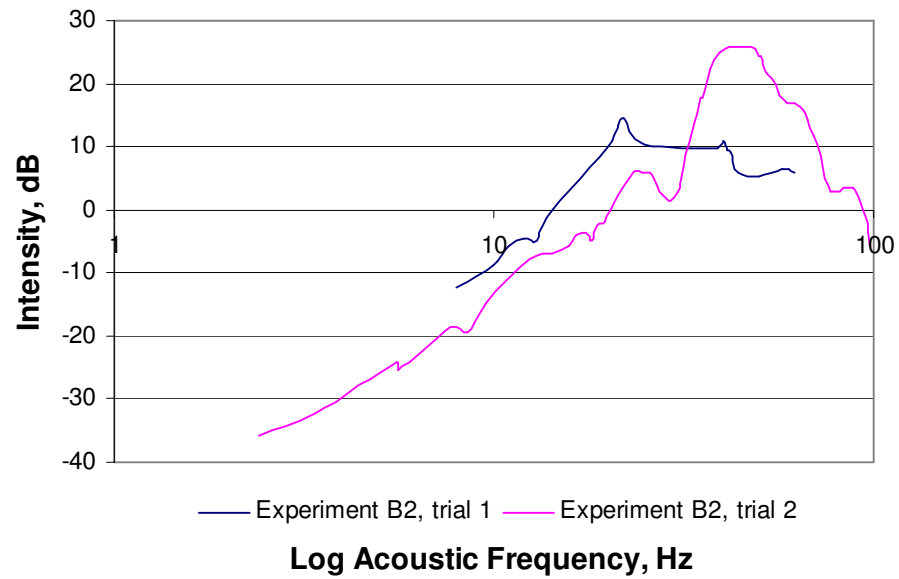


Figure 6.11 Logarithmic acoustic frequency spectra of experiment B2, the trachea with bronchi of pig sample 3.

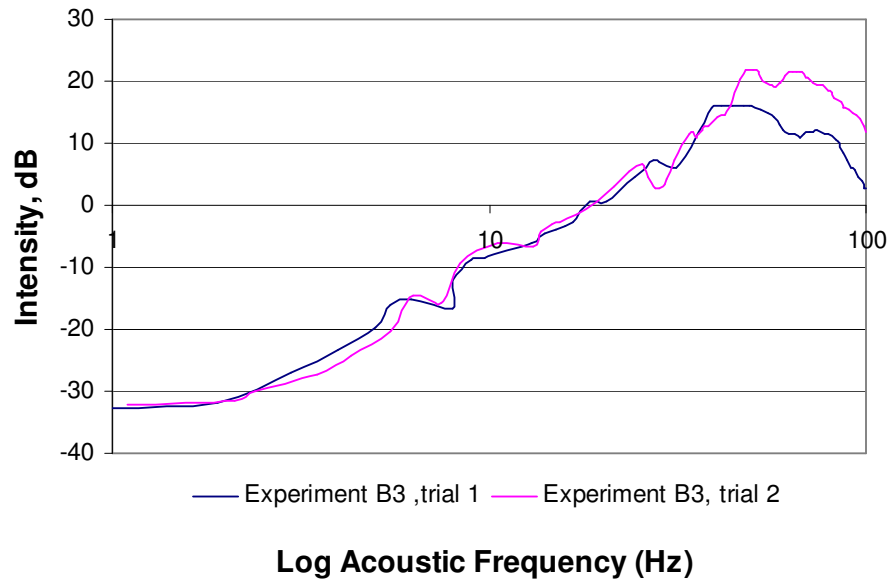


Figure 6.12 Logarithmic acoustic frequency spectra of experiment B3, the trachea with bronchi of pig sample 3.

All experimental frequency spectra on trials start with low frequencies rising to a peak and then decline. Measurements with the mechanical excitation resulted in distinct peaks. However, lower resonant frequencies were observed with the acoustic excitation and the peaks were flatter. Such phenomena could be understood through the modal analysis and testing concept. The sectioned trachea of pig sample 1 gave sharper peaks than other samples as shown in the spectral figures. Although all samples are complex with soft tissues and cartilaginous rings, sample 1 is closer to a simple thin shell model which should behave as a single degree of freedom (SDoF) system with only one fundamental resonant frequency. Sample 2 and sample 3 are trachea with bronchi and therefore would behave as a system with a multiple degrees of freedom (MDoF) which has more than one fundamental resonant

frequency. A MDoF system may have distinguishable fundamental frequencies over the spectral range if the system is lightly coupled. In the case of a heavily coupled MDoF system, the fundamental resonant frequencies can be so many and crowded together that interference among amplitudes of neighbouring resonant frequencies usually distort the mode shapes.

Figure 6.13 compares the frequency spectra of experiment A3 trial 1 and trial 2 with increasing and decreasing shaker frequency respectively. Both curves display similar patterns with a frequency shift and the characteristics of hysteresis that the lagging of response to the driving force and the current status depends on the path or history.

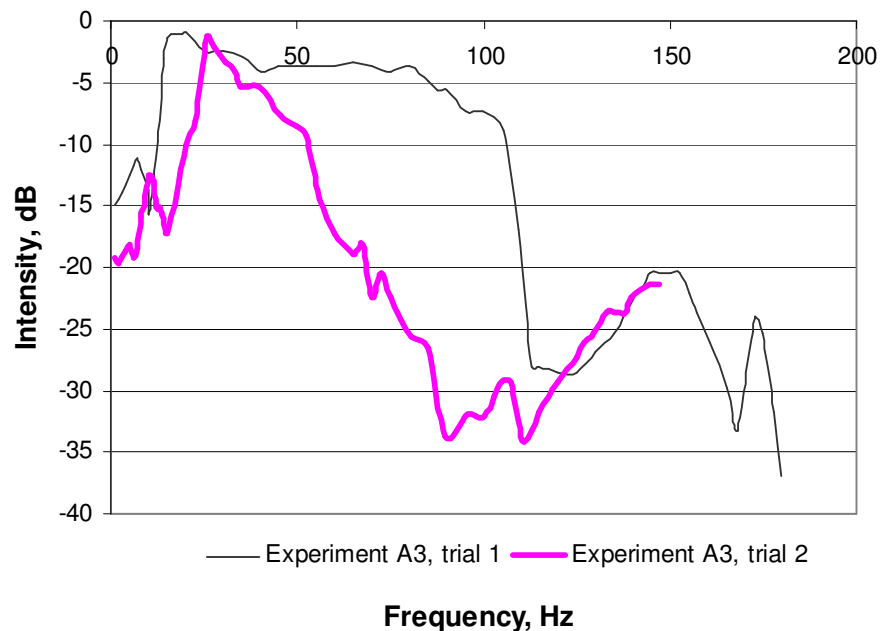


Figure 6.13 Frequency spectra of experiment A3 with increasing shaker frequency for trial 1 and decreasing frequency for trial 2.

Table 6.7 summarises the resonant frequencies observed and the average in the experimental trachea samples, and results from the numerical modelling by COSMOS/Works and analytical modelling.

Table 6.7 Comparison of resonant frequencies of experimental pig trachea samples with numerical and analytical results.

	Resonant Frequency, Hz						
	A1	A2	A3	B1	B2	B3	Average
Experimental	13	12	11	11	12	10	12
COSMOS/Workss radial	9	13	5	14	6	19	11
Membrane f_m	5	10	2	11	3	13	7
Membrane $f_{m\sim}$	6	14	2	16	3	16	10
Kraus f_1	5	10	3	12	3	12	8
Kraus f_{r1}	7	14	4	17	5	16	11

All values are rounded off to integers for easy comparison. The resonant frequencies match quite well in experiment A2 which is a sectioned trachea with bronchi. The analytical results (Appendix H) are lower than the observed values in experiment A3 and B2, which are samples with longer trachea dimensions. The observed frequencies from the experimental validation are chosen to have a relative match in values since identification of vibrational mode shapes is not possible without further detective equipment such as an electronic scanning device. It is worth noting that

from the COSMOS/Works results in Appendix H that the radial harmonics are multiples of the first radial frequency. The average values agree quite well with the previous theoretical and numerical analysis. Analytically, the membrane frequencies and Kraus's approximation are of the same order of magnitude and have the similar relationship in Table 3.2 that the approximate membrane frequency and the approximate radial frequency are about the same but higher than the membrane frequency and the lowest frequency.

Numerically, the COSMOS/Works radial frequency may be higher or lower than the membrane frequency depending on the Young's modulus of elasticity of the material as in Table 6.2 and Table 6.3.

Experimentally, trial 1 of experiment A1, the first radial resonance from COSMOS/Works is 8.59 Hz and the highest peak frequency from the experimental frequency spectrum is 50 Hz, which is about six times of the first resonance 8.59 Hz. Seven times of 8.59 Hz is 60.13 Hz which is the highest peak frequency 60 Hz of trial 2 of the same experiment. This relationship between the numerical radial frequency and the experimental peak frequency also holds quite well in other experiments. This finding is important because comparison is within the same experiment since each experimental setting is different in terms of geometric dimensions, especially the longitudinal length, and the actual physical properties.

Therefore, the resonant frequency of pigs' trachea can be estimated to be between 5 Hz and 13 Hz based on the integrated results presented in Table 6.7 and the inter-modelling analysis. The resonance of bronchus 1 would be between 10 Hz to 19 Hz.

Both tracheobronchial frequencies are in the same magnitude as found in the analytical and numerical resonance for human.

6.5 Conclusions

It is believed that the investigation of the natural frequencies of airways leads to better understanding of the dynamic response of such complex branching duct networks and could contribute to the study of relieving asthma by alternative means other than the traditional medical medications. The motion of airways is governed by their geometric and physical properties regardless whether the excitation is from the central nervous system or the external mechanically driven. This is a premier study of the dynamics and responses of airway walls through applying vibrations to branched circular cylindrical shells, analytically, numerically and experimentally for validation.

With Yu's approximation on cylindrical thin shells [91], the frequency equation of a circular cylindrical membrane with simple supports is derived by neglecting the inertia and bending effects of the Donnell-Mushtari equation [90-94]. The so-called analytical approach on cylindrical thin shells or membranes which can be manipulated for solutions is subjected to the assumed and limited approximation that reduces the eighth order differential equations to the fourth, applicable to clamped, simply-supported and free types of standard boundary conditions. Dichotomic or bifurcated structures beyond the simple circular cylindrical shells induce problems and difficulties in boundary matching between generations. Therefore searching for

the natural frequencies of the complex airways is not optimistic and in fact has no such solutions available in literature.

Analytically, the natural membrane frequency has the upper limit of the ring frequency of the same radius and physical properties of Young's modulus and density. This is a reference for a simple cylindrical membrane of one degree of freedom in vibration modes. It is this basic concept used in analysing a complex system with multiple degrees of freedom in either frequency analysis or modal analysis and testing. Mathematically, Fourier transformation decomposes the resulting response of a complex system into two or more components which may be lightly or heavily coupled. Therefore, the frequency spectrum of airways may suggest the type of coupling among branches of the tree structure.

Kraus [93] made the verification between analytical and experimental results through Koval and Cranch data on clamped cylindrical thin shells [93, 105]. Although there is no logical conclusion that similar agreement may work well with cylindrical membranes, verification and validation is needed in assuming a shell membrane as the fundamental building block of the airway tree

Finite element analysis (FEA) is overwhelming for its wide applications in fields and is a good tool in probing responses as well as analysing systems. COSMOS/Works is used in verifying Koval and Cranch's experimental sample and identifies the FEA drawback in approximation. Finer mesh improves results but requires more time and computing resources. FEA is not different from other numerical analysis where results are justified on their stability similar to the Simpson's rule in numerical

integration. With limited computing resources in the present time, only one radial mode of 77 Hz for bronchus 4 is identified in the bronchus 3-9 airway tree modelling as compared to the radial frequency of 68 Hz of modelling bronchus 4 itself (Appendix F). Results of COSMOS/Works analyses show that the mode 1 frequency changes as the mesh size of the study changes. Therefore, it may take a lot of work to reach the stability of analysis. However, simulations run with various mesh sizes do confirm one analytical and logical result that has been overlooked without attention to the fact that radial modes are the same and relatively independent of the analysis mesh size for individual shell structure of the airways.

The experimental validation comes in two parts, one with mechanical excitation by a shaker and the other with acoustic excitation by the acoustic pressure chamber, of two pig traheobronchial samples. In this section, resonant frequencies are identified by taking step-frequency responses instead of observing the peak or phase shift around the resonant frequency on the oscilloscope display or the frequency analyser. This approach is particularly suitable for systems with multiple degrees of freedom clustering together as tuning for the resonant frequency while observing for the relative peaks is not practical. The shift of resonant frequencies with the increasing and decreasing frequency trends for measurements reveals the tissue damping effect.

In conclusion, this work represents the initial stage of investigation of the free vibration characteristics of the respiratory walls and it sets the boundaries for the resonant frequencies of each individual generation of the respiratory system. The average radial resonance of the trachea is found to be about at 10 Hz as in Table 6.7,

and the radial frequencies of bronchi may be predicted with linear curve fitting to certain regions of generations. The radial frequencies found in this work agree quite well with literature values that fall between 5 and 8 Hz [72].

6.6 Future Work

To have more accurate results many of the assumptions made in the analytical and numerical modelling can be made more realistic. In further work, one could consider

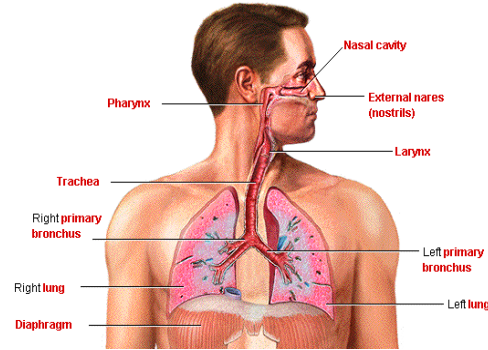
1. Use matching of boundary conditions rather than pure simple supported boundary conditions
2. Consider the respiratory walls to be embedded in a viscoelastic medium
3. Consider the properties as viscoelastic properties rather than purely elastic.

Appendices

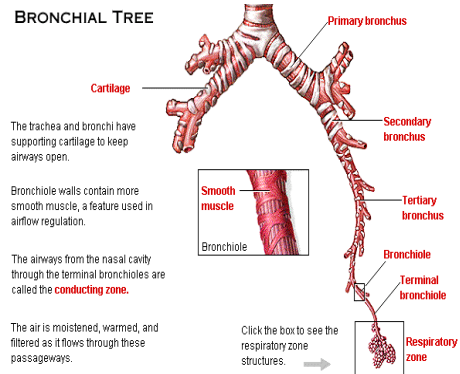
Appendix A Respiratory System and Tidal Breathing Cycle



OVERVIEW: RESPIRATORY SYSTEM ORGANS

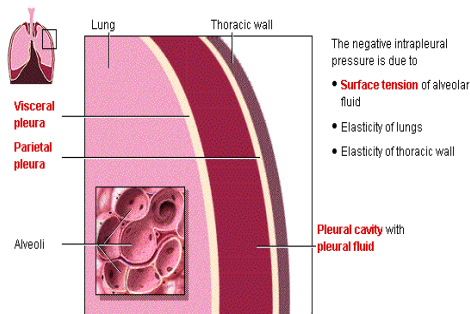


BRONCHIAL TREE



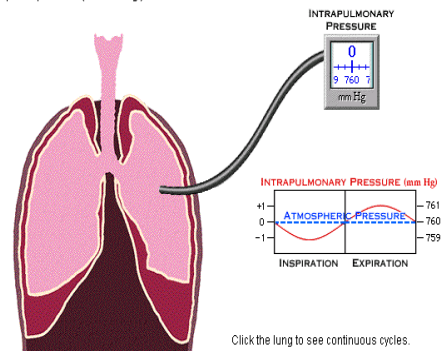
INTRAPLEURAL PRESSURE

Intrapleural pressure is the pressure within the pleural cavity. Intrapleural pressure is always negative, which acts like a suction to keep the lungs inflated.



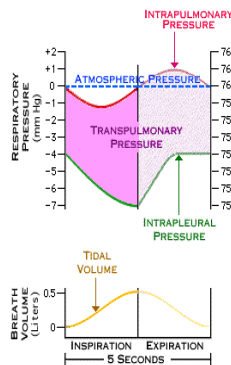
INTRAPULMONARY PRESSURE CHANGES

Intrapulmonary (intra-alveolar) pressure is the pressure within the alveoli. Between breaths, it equals atmospheric pressure (760 mm Hg).



EVENTS DURING INSPIRATION

- Diaphragm and external intercostal muscles contract
- ↓
- Volume of thoracic cavity increases
- ↓
- Intrapleural pressure becomes more negative
- ↓
- Lungs expand
- ↓
- Intrapulmonary pressure becomes negative
- ↓
- Air flows into the lungs



EVENTS DURING EXPIRATION

- Diaphragm and external intercostal muscles relax
- ↓
- Volume of thoracic cavity decreases
- ↓
- Intrapleural pressure becomes less negative
- ↓
- Lungs recoil
- ↓
- Intrapulmonary pressure rises above atmospheric pressure
- ↓
- Air flows out of the lungs

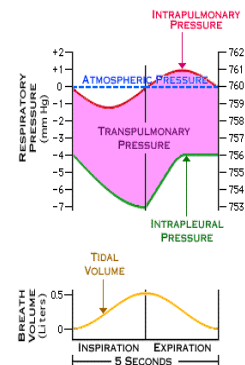


Figure A.1 An overview of the respiratory system organs and tidal breathing cycle [39].

Appendix B Morphological and Physical Data of Lungs

Table B.1 The geometric [42, 48] and physical [84] properties are listed for the generation z from 0 (the trachea) to the 16th bronchus.

Gen.	No. of Tubes	Diameter	Radius	Length	Thickness	Elasticity	Density
z	2^z	d , mm	a , mm	l , mm	t , mm	(kN/m ²)	(kg/m ³)
0	1	18.00	9.000	120.00	0.3870	7.3	1351
1	2	12.20	6.100	47.60	0.2684	5.7	1959
2	4	8.30	4.150	19.00	0.1826	4.7	3103
3	8	5.60	2.800	7.60	0.1260	4.7	1324
4	16	4.50	2.250	12.70	0.1035	4.7	1069
5	32	3.50	1.750	10.70	0.0823	3.9	1188
6	64	2.80	1.400	9.00	0.0686	3.9	1132
7	128	2.30	1.150	7.60	0.0575	3.9	1221
8	256	1.86	0.930	6.40	0.0484	3.2	1035
9	512	1.54	0.770	5.40	0.0416	3.2	1162
10	1024	1.30	0.650	4.60	0.0364	3.2	1178
11	2048	1.09	0.545	3.90	0.0322	3.2	1059
12	4096	0.95	0.475	3.30	0.0299	2.1	966
13	8192	0.82	0.410	2.70	0.0267	2.1	1256
14	16384	0.74	0.370	2.30	0.0252	2.1	976
15	32768	0.66	0.330	2.00	0.0234	2.1	835
16	65536	0.60	0.300	1.65	0.0225	2.1	955

Appendix C Kraus's Analytical Validation on Koval & Cranch's Experiment Measurements of a Cylindrical Thin Shell

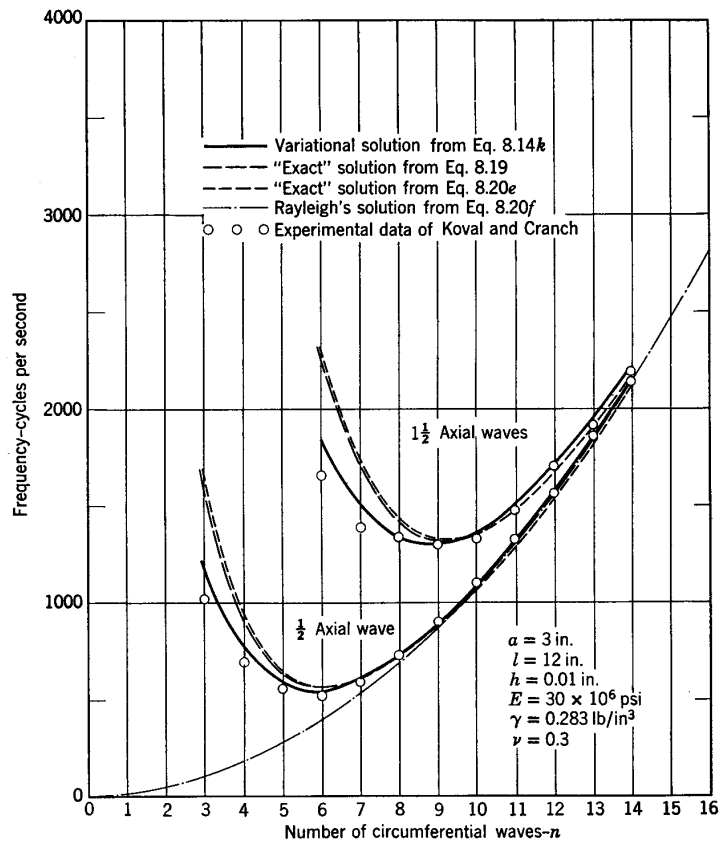
Kraus determined the lowest frequency on Koval and Cranch's sample to be 552 Hz with longitudinal parameter $m = 1$ and circumferential parameter $n = 6$, in the variational solutions as shown in Table C.1. For each set of parameters m and n , there are three frequency solutions with the second and the third frequencies much higher in order of magnitude than the first.

Table C.1 Natural Frequencies (Hertz or cycles/second) of Clamped Steel Cylinders [93] (radius $a = 3$ inch, thickness $h = 0.01$ inch, and length $l = 12$ inch.)

n	$\frac{1}{2}$ Axial Wave ($m = 1$)			$1 \frac{1}{2}$ Axial Waves ($m = 2$)		
	f_1	f_2	f_3	f_1	f_2	f_3
3	1,176	27,071	36,866	4,350	30,578	46,524
4	783	32,418	47,318	3,139	36,021	54,848
5	597	38,118	58,107	2,342	41,551	64,210
6	552	44,071	69,055	1,823	47,242	74,170
7	611	50,194	80,092	1,503	53,096	84,489
8	736	56,436	91,184	1,338	59,088	95,038
9	902	62,763	102,313	1,302	65,192	105,742
10	1,100	69,151	113,467	1,369	71,386	116,555
11	1,321	75,586	124,639	1,512	77,651	127,449
12	1,568	82,056	135,825	1,710	83,973	138,402
13	1,837	88,554	147,022	1,950	90,340	149,401
14	2,128	95,074	158,228	2,224	96,746	160,437

Table C.1 is a frequency graph, as a function of the circumferential parameter n , which compares results among the variational solutions, the approximate frequency solutions, the first approximate radial frequency solutions and the Rayleigh's

solutions [93] with the experimental results [105] for a clamped steel cylinder Kraus claimed that the variational solutions has a close fit to the experimental results. The two approximate exact solutions predict higher values than the variational solutions and the experimental results in the range of frequencies lower than minimum resonance of the sample. Rayleigh's minimum frequency is zero. However, all curves merges together with the experimental results as the circumferential parameter n increases beyond the minimum frequency.



FigureC.1 Natural frequencies for a freely vibrating circular cylindrical shell with clamped ends (with referring equations) [93, 105].

Appendix D A Sample of Analytical Calculation with Mathcad

Kraus “Exact” solutions on the experimental data of Koval and Cranch calculated in Mathcad. The lowest frequency is $f(6, m=1)$ of 564 Hz as compared to 552 Hz of the variational approach with clamped boundary conditions.

Kraus Exact Solution on Koval & Cranch's Experiment Measurements of a Cylindrical Thin Shell

$$E := 30 \cdot 10^6 \quad \nu := 0.3 \quad \rho := 0.00073$$

$$l := 12 \quad a := 3 \quad h := 0.01$$

$$\xi := \frac{12 \cdot a^2}{h^2} \quad n := 6 \quad m := 1.506$$

$$f(n, m) := \begin{array}{l} \text{for } m \in m \\ \quad K \leftarrow m \cdot \pi \\ \quad F \leftarrow \frac{K^4 \cdot a^4 \cdot (1 - \nu) \cdot (1 - \nu^2)}{l^4} \\ \quad \text{for } n \in n \\ \quad \quad v \leftarrow \left[-(1 - \nu) \cdot \frac{n^8}{\xi} - F \cdot (1 - \nu) \cdot n^2 \cdot (n^2 + 1) + (3 - \nu) \cdot \frac{n^6}{\xi} \cdot \left[2 + (3 - \nu) \cdot n^2 + \frac{2 \cdot n^4}{\xi} \right] \right]^{1/2} \\ \quad \quad v \leftarrow (v)^T \\ \quad \quad \Delta \leftarrow \text{polyroots}(v) \\ \quad \quad f \leftarrow \sqrt{\frac{\Delta \cdot E}{4 \cdot \pi^2 \cdot \rho \cdot a^2 \cdot (1 - \nu^2)}} \\ f \end{array}$$

$$f(1, m) = \begin{pmatrix} 6.34 \times 10^3 - 5.31 \times 10^3 \\ 6.34 \times 10^3 + 5.31 \times 10^3 \\ 1.657 \times 10^4 \end{pmatrix} \quad f(2, m) = \begin{pmatrix} 3.523 \times 10^3 \\ 1.27 \times 10^4 \\ 2.53 \times 10^4 \end{pmatrix} \quad f(3, m) = \begin{pmatrix} 1.595 \times 10^3 \\ 1.992 \times 10^4 \\ 3.567 \times 10^4 \end{pmatrix}$$

$$f(4, m) = \begin{pmatrix} 928.445 \\ 2.666 \times 10^4 \\ 4.649 \times 10^4 \end{pmatrix} \quad f(5, m) = \begin{pmatrix} 647.45 \\ 3.334 \times 10^4 \\ 5.749 \times 10^4 \end{pmatrix} \quad f(6, m) = \begin{pmatrix} 564.276 \\ 4.002 \times 10^4 \\ 6.858 \times 10^4 \end{pmatrix}$$

$$f(7, m) = \begin{pmatrix} 607.734 \\ 4.669 \times 10^4 \\ 7.972 \times 10^4 \end{pmatrix} \quad f(8, m) = \begin{pmatrix} 727.369 \\ 5.336 \times 10^4 \\ 9.089 \times 10^4 \end{pmatrix} \quad f(9, m) = \begin{pmatrix} 892.651 \\ 6.003 \times 10^4 \\ 1.021 \times 10^5 \end{pmatrix}$$

Appendix E Frequency mode 1 to 100 of the Tracheobronchial Generation 0 to 16 by COSMOS/Works Analysis

Table E.1 Results of COSMOS/Works of individual tracheobronchus from the trachea (T0) to the 16th bronchus (B1-B16). Analyses include default mesh and fine mesh data of mode 1 to 100. The radial frequencies (in bold) are the same for each branch and independent of the mesh size of the analysis.

Frequency mode 1 to 25 of the tracheobronchial generation T0 to B8 by COSMOS/Work Analysis

Frequency Number	T0	T0 fine	B1	B1 fine	B2	B2 fine	B3	B3 fine	B4	B4 fine	B5	B5 fine	B6	B6 fine	B7	B7 fine	B8	B8 fine
1	2.40	1.97	3.66	3.46	7.22	6.87	24.34	23.88	17.64	17.38	17.83	17.52	21.87	21.27	24.95	24.23	29.23	28.38
2	2.41	1.97	3.66	3.46	7.22	6.87	24.34	23.88	17.64	17.38	17.85	17.53	21.87	21.27	24.96	24.23	29.27	28.38
3	2.72	2.71	6.26	5.35	7.27	7.17	29.91	28.58	21.68	20.09	23.96	22.12	32.39	28.91	38.34	34.28	47.34	42.76
4	2.72	2.71	6.26	5.35	7.28	7.17	29.93	28.59	21.73	20.10	24.09	22.12	32.51	28.92	38.44	34.29	47.59	42.77
5	3.47	3.19	6.31	6.26	7.22	10.72	30.17	30.05	30.57	29.11	31.29	30.48	37.74	37.73	42.79	42.78	49.56	49.55
6	3.48	3.19	6.34	6.26	11.43	10.72	30.17	30.05	30.59	29.11	31.30	30.48	37.75	37.73	42.80	42.78	49.57	49.55
7	5.32	4.69	7.18	6.63	11.81	11.18	43.00	40.75	30.93	30.92	32.14	31.28	41.27	38.35	48.12	44.59	57.73	54.01
8	5.33	4.70	7.19	6.63	11.82	11.18	43.03	40.75	30.94	30.92	32.16	31.28	41.36	38.36	48.17	44.59	57.74	54.01
9	5.61	4.95	7.48	7.07	12.45	12.45	44.90	42.68	36.11	34.29	36.36	36.15	43.93	43.56	49.80	49.37	58.10	57.22
10	6.04	4.95	7.50	7.07	12.45	12.45	44.91	42.68	36.12	34.29	36.36	36.15	43.93	43.56	49.81	49.37	58.19	57.22
11	6.04	5.14	9.67	8.97	13.88	12.90	45.10	44.52	37.65	35.94	42.88	38.75	56.32	51.50	65.05	61.53	77.14	73.53
12	6.08	5.14	9.69	8.97	13.89	12.90	45.10	44.52	37.71	35.94	43.07	38.76	56.37	51.51	65.08	61.55	77.22	73.53
13	6.11	5.54	10.38	9.79	14.75	14.70	48.19	48.19	42.35	38.48	45.27	42.53	59.47	53.95	68.13	61.96	79.62	77.53
14	6.34	5.54	11.66	9.79	14.75	14.70	48.19	48.19	42.39	38.49	45.35	42.54	59.62	53.95	70.45	61.96	87.82	77.55
15	6.36	5.61	11.66	10.34	17.36	16.64	53.87	50.74	44.23	42.75	47.07	43.83	59.75	55.81	70.61	66.25	88.09	79.62
16	6.82	6.04	11.86	10.34	17.37	16.64	53.90	50.75	44.25	42.75	47.17	43.84	63.96	55.82	75.40	66.26	92.86	82.75
17	6.85	6.04	11.92	10.38	17.67	16.72	58.46	57.46	47.84	46.21	49.06	49.05	64.06	59.75	75.56	68.13	92.90	82.76
18	7.64	6.51	12.41	11.44	17.69	16.72	58.46	57.47	50.55	46.21	54.37	49.76	70.26	64.04	80.00	75.29	93.29	92.46
19	7.64	6.51	12.46	11.44	18.61	16.99	62.20	58.35	50.57	47.84	54.62	49.76	70.28	64.05	80.01	75.29	93.46	92.46
20	7.69	7.50	12.57	11.58	18.62	16.99	62.36	58.35	57.53	54.38	58.33	58.08	71.24	70.20	84.09	79.68	100.56	92.78
21	7.70	7.50	12.59	11.58	18.77	18.13	64.96	62.01	57.54	54.39	58.34	58.08	71.27	70.20	84.21	79.69	100.58	92.78
22	8.89	7.83	12.86	12.02	20.17	18.13	64.98	62.01	59.99	56.96	61.48	59.66	76.13	72.99	86.52	83.44	100.79	98.22
23	8.90	7.84	12.86	12.02	20.20	18.77	67.96	65.49	60.02	56.97	61.49	59.67	76.15	72.99	86.54	83.44	100.83	98.22
24	9.66	8.96	13.65	12.86	22.17	20.67	67.97	65.50	60.18	57.25	62.87	60.06	76.81	76.05	87.34	86.53	104.99	100.57
25	9.95	8.96	13.71	12.86	22.19	20.67	69.18	66.73	60.23	57.26	62.88	60.07	76.85	76.05	87.36	86.53	105.07	100.57

Frequency mode 26 to 50 of the tracheobronchial generation T0 to B8 by COSMOS/Work Analysis

Frequency Number	T0	T0 fine	B1	B1 fine	B2	B2 fine	B3	B3 fine	B4	B4 fine	B5	B5 fine	B6	B6 fine	B7	B7 fine	B8	B8 fine
26	9.96	9.09	14.95	13.14	22.91	21.46	69.21	66.74	61.76	57.32	65.25	61.75	83.64	76.14	98.32	88.61	118.78	107.71
27	10.16	9.10	14.97	13.14	22.91	21.46	71.83	67.01	61.77	57.32	65.36	61.77	83.73	76.14	98.40	88.62	118.85	107.72
28	10.17	9.34	16.22	15.35	23.46	22.85	73.66	67.01	62.07	58.46	69.04	62.87	96.30	82.26	110.17	98.38	128.98	124.09
29	10.40	9.35	16.23	15.35	23.52	22.85	73.81	71.83	62.07	58.46	69.49	62.87	96.41	82.28	110.27	98.41	129.00	124.12
30	10.41	9.42	16.57	15.43	23.73	23.17	81.39	77.69	63.74	61.77	72.20	64.38	96.68	85.33	111.18	101.79	130.73	125.23
31	11.23	9.42	16.58	15.43	23.75	23.17	81.40	77.69	63.75	61.77	72.58	64.39	96.86	85.35	111.21	101.81	130.80	125.24
32	11.74	9.65	17.26	15.73	24.44	24.25	83.66	79.13	70.06	62.39	77.92	69.23	98.08	90.70	114.02	105.32	134.56	126.72
33	11.74	9.78	17.28	15.74	24.44	24.26	83.67	79.13	70.08	62.40	78.32	69.24	98.11	90.70	114.38	105.34	138.90	126.74
34	11.90	9.78	17.65	16.14	26.48	24.31	84.64	81.02	75.66	69.48	78.42	72.59	98.53	91.22	114.87	106.59	139.30	127.97
35	11.94	9.95	19.12	16.15	26.51	24.32	84.79	81.02	75.68	69.49	78.49	72.60	98.58	91.23	115.79	106.60	142.50	127.99
36	12.01	9.95	19.40	16.35	27.07	24.44	85.07	83.01	76.85	70.27	78.76	76.25	100.24	93.29	116.16	107.99	142.70	128.74
37	12.03	10.07	19.61	16.35	27.63	24.44	85.19	83.01	76.90	70.29	79.04	76.26	100.56	93.30	118.10	108.00	146.85	128.74
38	12.25	10.07	19.66	16.88	28.42	25.43	87.82	83.65	78.15	74.48	80.13	76.46	100.60	96.94	118.53	110.41	147.30	134.48
39	12.27	10.40	19.98	16.88	28.76	25.43	87.92	83.65	78.16	74.49	80.18	76.48	106.34	96.95	125.26	110.42	155.00	134.94
40	12.62	10.40	19.99	17.63	28.95	26.78	89.43	85.02	79.22	77.72	82.27	79.67	106.72	99.34	125.76	114.80	155.61	134.95
41	12.64	11.10	20.04	17.95	29.06	26.78	89.46	85.03	79.25	77.72	86.79	79.68	115.52	99.34	133.19	117.29	155.75	145.45
42	12.86	11.11	20.06	17.95	29.70	27.51	93.14	86.62	79.68	79.28	86.96	82.20	115.71	100.49	133.23	117.30	155.79	145.46
43	12.86	11.22	20.22	18.00	29.72	27.52	93.36	86.63	87.76	79.29	93.37	85.41	116.40	107.66	133.69	124.29	158.27	148.63
44	13.28	11.29	20.23	18.00	30.07	28.77	95.36	87.16	87.81	79.61	93.52	85.42	116.57	107.68	134.10	124.32	158.41	148.66
45	13.31	11.29	20.73	18.96	30.08	28.77	96.77	87.17	90.63	79.82	95.36	87.07	116.67	110.59	135.93	129.61	159.24	152.69
46	13.74	12.20	20.77	18.96	30.40	29.09	96.87	95.30	90.63	79.84	95.43	87.07	116.70	110.59	136.26	129.63	162.36	152.70
47	13.79	12.21	20.90	19.53	31.12	29.09	97.90	96.74	91.09	81.84	95.48	90.16	118.76	113.47	136.27	129.92	162.63	155.77
48	14.06	12.74	21.13	19.53	31.30	29.87	97.91	96.74	91.15	81.85	95.50	90.18	119.03	113.48	137.26	129.94	163.62	155.77
49	14.06	12.74	21.15	20.22	31.53	29.87	98.88	96.85	91.34	83.68	98.12	92.49	119.49	116.68	137.51	133.21	163.67	159.23
50	14.20	13.08	21.95	20.22	31.69	30.38	98.88	96.85	91.52	83.70	98.15	92.49	122.50	116.68	139.77	133.21	168.71	159.57

Frequency mode 51 to 75 of the tracheobronchial generation T0 to B8 by COSMOS/Work Analysis

Frequency Number	T0	T0 fine	B1	B1 fine	B2	B2 fine	B3	B3 fine	B4	B4 fine	B5	B5 fine	B6	B6 fine	B7	B7 fine	B8	B8 fine
51	14.24	13.08	22.16	20.76	34.41	30.53	103.02	98.16	92.25	86.05	99.04	92.52	122.52	119.49	139.84	136.26	169.47	159.57
52	15.01	13.39	22.73	20.81	34.42	30.54	103.24	98.18	92.27	86.09	99.14	92.53	130.50	120.19	150.63	138.59	183.70	162.53
53	15.05	13.39	22.77	20.81	34.47	32.30	106.38	98.68	93.07	89.81	99.56	95.48	131.15	120.22	151.92	138.60	184.21	162.54
54	15.48	14.06	23.39	20.97	34.57	32.31	106.57	98.68	93.16	89.83	99.65	95.48	133.57	121.19	157.11	143.74	187.47	172.12
55	15.50	14.06	23.42	20.97	35.26	33.23	106.60	101.10	95.67	91.55	101.15	96.49	133.77	121.19	157.96	143.78	187.83	172.14
56	15.82	14.55	24.04	21.43	35.33	33.24	110.21	101.11	95.90	91.59	105.13	96.51	138.78	122.90	158.73	143.85	188.21	177.20
57	15.83	14.56	24.16	21.43	35.60	33.75	110.29	104.74	95.93	92.26	107.14	97.17	138.95	122.93	158.97	143.90	189.38	177.22
58	16.44	14.66	25.36	22.46	35.71	33.76	110.54	104.74	96.95	92.26	108.36	97.19	141.74	123.59	164.39	145.76	194.30	179.46
59	16.50	14.67	25.39	22.46	35.92	34.31	110.74	105.99	97.10	92.36	108.90	98.10	142.29	123.61	164.48	145.77	194.37	179.48
60	16.84	14.72	25.57	23.08	35.95	34.32	111.13	106.00	104.82	92.40	110.79	98.83	143.90	126.18	168.01	146.84	201.48	181.28
61	17.28	14.72	25.64	23.09	36.17	34.41	111.76	106.14	105.04	95.19	111.41	98.84	143.98	126.20	168.11	146.88	201.55	181.32
62	17.32	14.87	26.30	23.46	36.74	34.41	112.01	106.14	105.31	95.19	111.80	101.55	144.89	127.83	168.86	152.18	206.00	184.80
63	18.04	14.88	26.33	23.46	36.83	34.47	112.37	106.27	105.60	95.67	112.01	101.56	145.26	127.86	170.29	152.21	206.79	184.85
64	18.11	15.01	26.70	23.65	37.35	34.48	112.53	108.11	107.04	98.07	113.46	102.57	147.37	132.81	170.70	152.23	208.50	190.93
65	18.12	15.01	26.80	23.65	37.53	34.58	113.96	108.14	107.04	98.10	113.80	102.58	148.32	132.82	170.75	152.26	210.57	190.97
66	18.13	15.19	26.81	23.86	38.84	34.60	114.02	109.20	108.78	100.75	115.95	107.85	148.50	134.88	171.83	160.02	212.88	192.11
67	18.21	15.20	27.03	23.86	38.85	35.36	118.07	109.21	108.88	100.78	116.03	107.86	148.54	134.91	172.30	160.07	213.83	192.12
68	18.26	15.40	27.22	24.11	39.64	35.36	118.09	110.66	110.79	104.04	118.70	109.97	151.62	139.11	177.70	161.94	214.32	195.26
69	18.45	15.40	27.30	24.11	39.76	36.23	118.19	111.26	110.83	104.09	119.49	109.98	151.83	139.14	178.08	161.99	214.59	195.29
70	18.51	15.61	27.92	25.05	39.92	36.24	119.86	111.26	112.18	104.79	119.77	110.55	152.23	141.88	178.72	162.89	214.63	198.98
71	18.64	15.62	28.35	25.06	40.00	37.53	120.26	114.27	112.19	104.80	119.81	110.57	152.48	141.88	178.75	162.90	214.84	199.04
72	18.84	16.16	28.43	25.15	40.16	37.89	122.88	114.29	115.00	108.78	122.63	114.87	153.95	144.14	180.50	166.43	215.07	200.06
73	18.87	16.16	29.13	25.16	40.27	37.90	123.10	116.46	115.02	108.80	122.67	114.88	153.98	144.15	180.61	166.45	216.10	200.11
74	18.94	16.17	29.15	25.78	40.89	38.77	123.44	116.46	116.07	109.47	123.98	116.61	158.17	144.83	181.76	170.51	220.79	201.49
75	18.99	16.17	29.24	25.78	40.90	38.80	123.64	117.12	116.13	109.48	124.65	116.63	158.32	144.87	182.09	170.58	220.90	201.49

Frequency mode 76 to 100 of the tracheobronchial generation T0 to B8 by COSMOS/Work Analysis

Frequency Number	T0	T0 fine	B1	B1 fine	B2	B2 fine	B3	B3 fine	B4	B4 fine	B5	B5 fine	B6	B6 fine	B7	B7 fine	B8	B8 fine
76	19.24	16.84	29.41	26.22	41.15	38.81	123.73	119.65	120.89	110.92	127.24	119.73	161.10	148.48	185.93	170.69	222.40	205.14
77	19.67	16.86	29.47	26.23	41.21	38.81	128.12	119.65	120.92	110.99	127.74	119.73	161.79	148.48	186.16	170.70	222.92	205.17
78	19.99	16.86	30.44	26.33	41.39	38.97	128.17	120.27	122.01	111.31	128.77	120.41	163.29	151.16	188.39	173.53	230.11	211.84
79	20.03	16.95	30.58	26.34	41.94	38.98	132.41	120.28	122.09	111.34	129.33	120.47	163.40	151.18	188.93	173.56	232.08	211.90
80	20.36	16.96	30.58	26.80	41.98	39.50	132.58	123.17	122.39	112.11	129.67	122.33	167.71	153.89	191.27	178.66	234.04	214.52
81	20.49	17.59	30.63	26.81	42.58	39.50	132.74	126.37	122.44	112.11	130.35	122.34	168.40	153.89	191.89	178.66	234.12	214.52
82	20.52	17.59	31.09	26.93	42.66	39.72	132.97	126.39	123.74	112.74	131.00	122.57	170.03	155.24	196.56	181.27	234.88	217.40
83	20.77	17.78	31.15	26.93	43.28	39.73	133.11	126.53	123.87	112.79	131.27	122.57	170.08	155.25	196.61	181.34	236.38	217.41
84	20.83	17.78	31.27	27.91	43.29	39.79	134.17	126.54	124.56	114.96	131.84	123.82	170.82	156.98	199.25	183.30	236.87	218.15
85	21.31	17.97	31.64	27.92	43.37	39.80	134.41	127.56	124.81	114.96	133.99	123.85	171.25	157.00	201.34	183.32	238.84	218.20
86	21.62	17.98	31.96	28.80	43.67	40.85	135.65	127.57	125.12	115.29	135.91	124.01	172.54	159.27	201.73	183.68	239.85	224.30
87	21.70	18.12	31.98	28.80	44.22	40.85	135.77	127.58	125.24	115.32	135.95	124.04	174.29	159.27	202.30	183.80	240.16	224.39
88	21.75	18.12	32.23	28.84	44.27	42.55	139.91	127.58	126.63	117.64	138.17	126.13	175.42	163.62	203.20	188.15	242.13	226.81
89	21.83	18.61	32.34	28.85	44.97	42.59	140.10	128.02	126.64	117.71	138.75	126.17	175.75	163.67	204.39	188.18	242.66	226.88
90	21.90	18.62	32.44	29.12	45.49	43.16	141.01	128.03	128.41	118.76	140.38	128.23	176.81	165.11	204.61	193.96	246.36	229.82
91	21.92	18.85	32.62	29.13	45.68	43.17	142.20	129.68	128.71	118.80	140.81	128.23	179.23	165.15	205.38	194.00	247.02	229.85
92	22.04	18.88	32.67	29.80	45.97	43.49	142.98	133.45	128.81	120.96	141.93	130.07	182.27	167.76	206.46	196.42	250.93	233.92
93	22.19	18.88	33.07	29.81	45.97	43.49	143.45	133.46	131.54	120.98	142.21	130.13	182.58	167.79	207.07	196.42	252.80	233.93
94	22.38	19.31	33.35	30.08	46.10	43.57	143.65	134.04	132.04	121.31	142.68	131.63	184.66	168.73	213.66	197.46	256.47	236.73
95	22.44	19.31	33.67	30.09	46.25	43.59	145.50	134.09	134.42	121.32	142.68	131.69	184.69	168.76	213.79	197.51	256.54	238.84
96	22.45	19.72	33.97	30.57	46.83	43.60	145.89	134.48	134.48	123.32	143.71	132.42	187.19	169.59	214.30	199.04	258.00	239.25
97	22.57	19.72	34.12	30.57	47.01	43.61	151.44	134.50	135.66	123.39	143.94	132.46	187.96	169.64	214.37	199.15	259.78	239.26
98	22.84	20.41	34.28	31.14	47.05	43.65	152.21	134.74	135.71	126.44	146.56	135.68	190.19	169.88	219.61	199.17	262.90	242.29
99	23.03	20.41	34.42	31.78	47.12	44.10	152.79	134.79	136.95	126.44	146.70	135.73	190.82	169.89	220.32	200.49	263.20	242.36
100	23.11	20.71	34.80	31.80	47.42	44.11	153.46	137.48	137.02	127.60	146.71	135.79	191.03	172.44	220.69	200.53	269.65	244.63

Frequency mode 1 to 25 of the tracheobronchial generation B9 to B16 by COSMOS/Work Analysis

Frequency Number	B9	B9 fine	B10	B10 fine	B11	B11 fine	B12	B12 fine	B13	B13 fine	B14	B14 fine	B15	B15 fine	B16	B16 fine
1	33.04	32.00	48.76	47.33	49.21	47.67	50.39	48.96	54.57	53.18	73.22	72.11	92.39	91.03	106.72	105.56
2	33.06	32.00	48.78	47.34	49.23	47.67	50.40	48.96	54.59	53.18	73.33	72.11	92.53	91.03	106.75	105.57
3	55.20	50.27	75.56	75.54	79.69	79.66	80.44	80.41	87.27	87.25	117.59	115.85	146.88	146.62	167.45	161.44
4	55.21	50.28	75.58	75.54	79.70	79.66	80.45	80.41	87.29	87.25	117.61	115.87	146.90	146.63	167.75	161.45
5	55.63	55.18	90.60	85.16	87.62	80.26	90.11	83.24	94.39	87.67	121.59	117.56	153.68	146.85	169.21	169.17
6	55.76	55.18	90.65	85.17	87.86	80.27	90.34	83.25	94.59	87.69	121.77	117.57	154.07	146.85	169.22	169.17
7	64.55	62.37	91.75	89.77	94.08	93.10	95.80	94.81	104.32	103.40	141.19	140.33	177.42	176.38	206.17	205.27
8	64.56	62.37	91.92	89.78	94.10	93.10	95.82	94.81	104.32	103.40	141.20	140.34	177.43	176.39	206.23	205.28
9	67.22	63.90	106.77	100.46	103.89	96.88	106.63	100.35	113.89	107.33	149.80	143.90	189.41	182.38	212.78	206.76
10	67.30	63.91	106.93	100.46	104.07	96.88	106.82	100.35	114.00	107.33	149.92	143.90	189.55	182.38	212.85	206.77
11	88.06	83.70	122.49	122.48	129.19	126.78	129.48	129.47	138.82	138.81	184.88	184.87	229.83	229.82	260.57	260.55
12	88.14	83.71	134.61	128.29	133.57	126.80	136.78	130.89	148.28	141.62	197.87	191.71	250.28	242.88	287.18	280.55
13	89.06	89.06	134.67	128.31	133.65	129.18	136.88	130.91	148.35	141.63	198.12	191.71	250.56	242.89	287.36	280.58
14	103.52	91.67	144.49	143.64	150.79	147.43	152.89	152.07	166.18	160.03	223.21	210.23	280.99	265.73	303.41	289.12
15	103.69	91.70	144.51	143.65	150.81	147.47	152.91	152.07	166.21	160.06	223.60	210.26	281.08	265.76	303.93	289.14
16	103.77	97.38	153.87	153.88	162.27	149.95	163.34	152.80	174.32	165.28	224.26	223.35	281.98	279.92	324.60	314.39
17	103.86	97.40	153.91	153.88	162.31	149.96	163.39	152.83	174.51	165.29	224.32	223.36	282.81	279.94	324.68	314.39
18	109.59	103.24	171.36	157.15	163.38	155.65	168.61	161.54	176.41	170.21	236.60	225.07	294.96	285.07	329.90	323.51
19	109.82	103.24	171.63	157.18	163.70	155.68	168.88	161.57	176.45	170.22	236.65	225.07	295.02	285.07	330.33	323.52
20	112.18	108.30	171.98	165.24	172.03	162.27	176.38	163.36	185.73	176.42	239.79	236.62	302.74	294.99	337.40	337.43
21	112.21	108.32	172.07	165.26	172.18	162.28	176.43	163.36	185.95	176.43	239.95	236.63	303.18	295.00	337.46	337.43
22	114.81	111.09	180.22	165.31	173.31	165.84	177.52	170.67	193.06	185.51	258.88	251.58	327.03	318.64	373.93	360.06
23	114.95	111.11	180.45	165.34	173.39	165.87	177.67	170.71	193.15	185.52	259.08	251.60	327.55	318.65	374.15	360.10
24	121.74	112.19	196.64	180.40	189.53	171.33	195.42	178.04	206.66	189.25	269.75	252.89	341.63	320.81	384.20	370.80
25	121.82	112.20	196.96	180.41	189.84	171.35	195.53	178.06	207.06	189.27	270.13	252.92	342.26	320.85	384.56	370.83

Frequency mode 26 to 50 of the tracheobronchial generation B9 to B16 by COSMOS/Work Analysis

Frequency Number	B9	B9 fine	B10	B10 fine	B11	B11 fine	B12	B12 fine	B13	B13 fine	B14	B14 fine	B15	B15 fine	B16	B16 fine
26	137.11	124.77	201.41	200.30	209.86	194.70	212.40	202.49	229.63	217.20	307.77	292.42	384.96	371.92	433.43	424.95
27	137.36	124.79	201.47	200.32	209.92	194.72	212.46	202.51	229.70	217.23	307.92	292.47	385.18	371.98	439.77	425.03
28	144.45	141.27	207.54	202.98	213.92	209.34	216.32	211.60	234.12	228.69	310.65	307.05	385.47	383.72	439.97	433.22
29	144.51	141.29	214.73	202.99	214.19	209.35	216.46	211.61	237.07	228.70	312.18	307.07	395.17	383.74	446.55	438.43
30	147.57	143.97	214.89	207.42	218.85	209.97	219.01	215.48	237.28	233.98	312.72	310.48	396.32	385.30	446.95	438.45
31	147.77	143.98	222.01	207.65	219.38	210.00	227.60	215.52	243.68	234.28	328.44	318.09	415.07	402.18	481.47	458.22
32	150.68	145.85	222.29	207.69	219.52	218.71	227.94	218.89	243.86	234.31	328.63	318.12	415.49	402.21	481.82	458.26
33	159.73	145.86	239.68	232.56	246.93	225.11	251.87	234.16	271.55	252.93	356.68	334.80	447.72	422.70	486.15	467.72
34	160.01	146.81	239.76	232.57	247.08	225.13	251.98	234.18	271.63	252.99	360.75	334.84	447.83	422.76	486.34	467.76
35	167.96	146.85	244.98	239.72	252.70	236.07	253.41	244.34	275.60	255.42	360.84	342.79	450.53	436.55	501.89	478.36
36	168.58	150.59	251.88	239.72	252.77	236.12	253.49	244.39	275.83	255.47	361.84	342.88	457.26	436.63	502.00	478.38
37	172.73	151.14	251.91	244.96	258.37	242.52	258.95	251.31	277.63	263.49	366.27	346.57	459.66	438.20	507.79	501.90
38	173.57	151.16	256.71	251.26	264.58	242.56	268.44	251.35	280.46	263.53	367.61	346.61	464.28	438.25	508.16	501.91
39	174.22	158.96	256.77	251.31	264.70	252.73	268.55	253.44	281.26	271.58	369.76	360.79	465.07	447.77	521.12	505.05
40	174.27	158.99	262.44	251.92	265.49	252.74	273.32	253.45	289.75	271.59	372.68	360.80	469.25	447.78	530.55	505.17
41	178.12	170.29	262.66	251.97	265.71	253.97	273.67	258.94	289.83	277.62	375.84	367.36	474.62	459.65	531.39	513.95
42	178.76	170.31	277.07	254.54	267.74	253.99	274.63	261.82	290.88	277.77	385.94	367.41	481.34	465.36	544.26	513.95
43	179.00	170.67	277.22	254.55	267.88	255.54	275.02	261.87	291.53	277.80	386.12	369.74	481.48	465.41	544.49	521.11
44	181.31	170.68	284.48	257.85	272.01	255.58	280.49	263.62	296.30	284.35	397.15	383.47	501.29	478.06	549.14	540.37
45	182.15	172.24	284.65	257.89	272.27	258.36	280.94	263.64	296.38	284.39	398.70	383.49	503.41	478.09	550.32	540.40
46	183.75	172.27	291.04	267.49	286.10	260.87	290.84	267.82	308.10	287.60	399.23	385.62	504.60	487.25	585.20	565.48
47	183.86	174.24	291.26	267.51	286.38	260.90	291.20	267.83	309.01	287.60	401.01	385.66	507.24	487.30	585.51	565.53
48	186.49	174.25	298.67	269.54	286.68	265.87	295.35	271.32	321.95	294.48	429.32	397.95	545.06	505.27	603.94	566.13
49	186.97	178.11	299.28	269.55	287.04	265.88	295.86	271.35	322.48	294.55	431.77	398.00	545.46	505.31	603.98	566.21
50	196.24	182.26	305.80	286.59	307.49	271.09	316.79	281.90	334.65	298.86	434.84	400.89	550.84	511.02	609.20	596.13

Frequency mode 51 to 75 of the tracheobronchial generation B9 to B16 by COSMOS/Work Analysis

Frequency Number	B9	B9 fine	B10	B10 fine	B11	B11 fine	B12	B12 fine	B13	B13 fine	B14	B14 fine	B15	B15 fine	B16	B16 fine
51	197.05	182.26	305.83	286.60	308.24	271.09	317.58	281.91	334.89	298.87	437.00	401.01	553.61	511.17	610.13	596.27
52	210.10	186.32	309.60	296.57	313.15	293.96	318.09	306.21	342.92	326.79	454.43	438.25	561.15	557.70	622.49	603.62
53	210.33	186.34	309.85	296.63	313.48	294.01	318.37	306.27	343.09	326.81	454.60	438.31	561.29	557.74	622.60	603.63
54	214.33	196.89	312.90	303.38	318.53	300.26	324.92	308.03	348.14	334.04	455.71	450.15	565.93	560.51	627.23	622.26
55	214.70	196.91	313.01	303.39	318.83	300.30	325.16	308.08	348.26	334.08	455.83	450.19	566.03	560.54	628.04	622.27
56	215.86	202.65	319.73	306.60	329.73	300.90	328.73	312.29	349.66	339.39	466.89	452.64	572.39	561.00	637.04	629.52
57	216.20	202.68	320.42	306.63	329.84	300.95	328.84	312.31	349.81	339.40	467.00	452.69	572.52	561.01	637.34	629.56
58	219.18	205.88	334.05	309.43	330.16	316.31	334.66	317.84	363.40	340.07	469.94	455.64	594.13	572.00	684.06	632.61
59	219.67	205.91	334.54	309.48	330.62	316.32	335.26	317.85	363.46	340.16	471.54	455.65	594.52	572.06	685.30	632.70
60	226.33	214.50	339.21	312.92	336.20	322.43	347.23	328.73	366.30	348.11	483.54	464.26	613.74	572.26	689.80	663.06
61	226.40	214.55	339.26	312.93	336.83	322.51	348.78	328.74	367.19	348.12	487.35	464.42	616.39	572.26	689.82	663.13
62	237.50	216.05	347.49	337.78	357.73	329.75	351.29	336.38	375.15	361.17	500.37	466.77	631.71	592.30	692.11	664.73
63	238.99	216.06	347.94	337.87	357.79	329.76	351.35	336.46	375.71	361.23	500.74	466.77	633.27	592.46	695.11	664.81
64	241.69	218.47	350.61	339.11	359.29	341.97	363.22	351.19	390.40	363.28	509.54	486.18	639.63	613.21	696.50	681.59
65	242.46	218.52	350.70	339.11	359.66	342.01	363.35	351.19	390.56	363.28	516.04	486.27	639.78	613.31	708.19	681.67
66	243.17	224.21	356.94	340.72	364.03	344.46	372.60	353.31	401.50	371.63	516.30	487.65	641.98	621.75	709.39	688.58
67	243.21	224.24	357.26	340.78	364.32	344.55	372.92	353.37	401.63	371.69	520.49	487.68	643.51	621.79	720.83	688.58
68	245.48	225.49	367.18	346.53	372.00	345.14	379.81	355.81	402.94	379.15	520.67	497.13	644.31	627.58	721.73	691.83
69	246.22	225.53	367.29	346.54	372.90	345.20	380.96	355.84	403.22	379.21	521.18	497.20	645.40	627.67	728.66	695.02
70	247.76	226.33	367.45	348.50	377.45	350.48	383.18	356.04	405.73	382.79	525.90	508.92	657.65	633.79	730.02	695.23
71	247.93	226.34	370.16	348.52	377.75	350.55	383.29	356.12	408.35	382.84	539.73	508.96	683.05	633.83	733.61	711.35
72	249.43	229.23	379.60	365.77	386.57	356.05	386.40	361.56	409.62	384.73	540.59	515.95	683.92	638.96	734.01	711.42
73	249.88	229.27	380.39	365.84	386.68	356.16	386.88	361.58	412.33	384.74	541.82	516.01	686.27	638.96	747.61	713.42
74	251.91	232.00	383.35	367.01	387.54	357.62	387.80	362.56	413.02	388.37	546.89	518.88	689.45	645.17	747.90	713.52
75	252.96	232.03	383.64	367.02	388.64	357.62	388.41	362.63	416.42	388.48	548.13	518.95	693.10	652.16	757.29	714.14

Frequency mode 76 to 100 of the tracheabronchial generation B9 to B16 by COSMOS/Work Analysis

Frequency Number	B9	B9 fine	B10	B10 fine	B11	B11 fine	B12	B12 fine	B13	B13 fine	B14	B14 fine	B15	B15 fine	B16	B16 fine
76	260.71	235.61	391.66	367.44	390.20	360.27	400.57	371.88	421.25	392.07	554.59	520.07	694.76	652.22	768.47	714.22
77	261.49	235.64	391.74	369.97	390.26	360.28	402.92	371.97	422.06	392.13	554.68	520.07	695.41	656.48	770.20	744.56
78	264.04	243.09	404.26	371.18	395.61	360.86	404.74	373.77	427.52	401.18	566.29	525.69	696.04	656.54	781.63	744.58
79	264.12	243.09	404.36	371.29	397.05	360.92	404.84	373.83	428.44	401.18	566.36	531.25	697.88	678.47	781.79	756.91
80	265.30	245.15	405.73	372.05	402.54	375.89	408.15	382.96	435.31	401.34	568.87	531.43	713.53	678.60	782.67	759.76
81	266.95	245.16	405.84	372.10	402.65	375.95	408.73	382.97	435.55	401.44	570.61	542.66	714.30	687.63	783.04	759.88
82	267.16	248.80	406.81	382.62	407.25	384.86	417.95	386.69	438.08	405.52	571.11	542.73	717.82	687.65	794.09	764.81
83	267.38	248.85	407.98	382.67	407.60	384.86	419.18	388.41	439.03	410.74	572.01	545.56	722.29	689.47	794.65	764.93
84	270.62	251.31	413.44	383.95	409.29	386.39	421.45	389.97	439.14	410.82	578.00	545.61	724.72	693.34	804.23	780.90
85	271.16	251.33	414.83	384.01	410.76	386.40	421.53	390.03	439.88	416.42	580.47	554.61	728.69	693.35	805.09	781.66
86	274.48	256.83	422.73	385.46	416.22	387.54	422.43	397.66	455.42	425.24	595.11	562.99	731.94	696.27	805.95	789.06
87	275.08	256.85	423.86	385.50	417.20	388.22	423.18	397.73	457.28	425.27	598.50	563.03	736.07	696.41	810.54	789.09
88	277.64	260.31	426.14	392.45	425.55	388.29	427.54	400.56	457.87	431.34	598.59	564.95	736.61	702.43	811.64	792.12
89	277.72	260.34	426.95	392.46	426.31	390.04	428.77	400.59	459.54	431.40	601.35	564.95	750.52	702.48	827.60	792.25
90	279.31	263.91	428.58	397.95	426.52	393.94	433.54	400.92	463.75	435.18	602.96	578.66	756.29	724.47	828.76	799.72
91	280.36	263.91	430.05	398.00	426.64	394.04	434.10	400.95	464.18	435.27	611.10	578.67	768.05	731.72	833.71	799.95
92	290.20	265.79	431.28	405.12	430.30	396.41	444.01	410.48	464.30	438.00	613.90	585.35	770.42	731.75	842.18	801.97
93	290.30	265.81	431.30	405.13	430.87	396.50	444.13	410.52	465.52	438.01	617.09	585.46	773.22	734.28	844.26	807.61
94	291.22	266.80	433.72	409.18	442.17	398.88	445.35	413.17	468.10	438.54	620.48	594.94	776.31	734.35	855.59	807.88
95	292.96	267.16	434.33	409.33	442.20	398.89	446.22	413.24	474.56	438.66	621.82	595.58	782.40	741.96	856.99	819.90
96	296.85	270.42	440.35	418.26	452.31	420.43	446.64	420.70	474.83	446.96	630.48	595.61	783.22	742.04	867.00	820.09
97	297.35	270.43	447.66	418.32	452.45	420.50	446.66	420.70	487.59	447.10	630.58	600.58	786.15	749.98	867.27	829.24
98	298.50	278.83	448.23	420.58	452.99	425.87	455.11	435.99	489.17	462.10	630.92	600.71	788.02	766.74	874.15	845.76
99	298.65	278.87	452.83	420.60	453.14	425.88	464.64	436.01	490.17	462.11	635.87	610.42	788.35	767.74	890.21	845.83
100	306.94	285.59	453.05	428.08	456.47	428.41	466.10	437.73	491.24	463.74	636.28	610.50	791.73	767.90	890.54	865.09

**Appendix F Frequency mode 1 to 100 of the
Tracheobronchial Generation 0 to 16 by
COSMOS/Works Analysis (Half density and
double wall thickness)**

Table F.1 Results of COSMOS/Works of individual tracheobronchus from the trachea (T0) to the 16th bronchus (B1-B16). Analyses include default mesh and fine mesh data of mode 1 to 100. The radial frequencies (in bold) are the same for each branch and independent of the mesh size of the analysis.

Frequency mode 1 to 25 of the tracheobronchial generation T0 to B16 by COSMOS/Work Analysis
(half density and double wall thickness)

Mode	T0	B1	B2	B3	B4	B5	B6	B7	B8	B9	B10	B11	B12	B13	B14	B15	B16
1	3.88	6.92	11.57	45.66	30.08	31.45	39.61	45.97	55.65	63.87	76.63	98.54	102.26	108.65	144.95	184.54	208.05
2	3.89	6.92	11.57	45.66	30.08	31.49	39.61	45.99	55.65	63.89	76.66	98.58	102.29	108.70	144.99	184.63	208.20
3	5.27	8.96	17.03	48.83	44.29	44.81	54.09	61.34	71.08	79.20	92.19	114.49	115.68	125.59	169.36	211.72	244.21
4	5.29	8.96	17.04	48.83	44.30	44.82	54.09	61.35	71.09	79.21	92.20	114.51	115.71	125.61	169.39	211.76	244.24
5	6.51	11.48	17.82	69.06	53.47	56.69	69.32	79.20	93.25	105.20	124.19	156.82	161.38	174.53	236.18	299.29	346.27
6	6.51	11.49	17.82	69.07	53.50	56.72	69.34	79.23	93.29	105.24	124.25	156.91	161.49	174.67	236.40	299.64	346.61
7	8.03	14.85	22.30	74.33	55.66	60.14	80.19	95.50	114.13	127.73	149.00	185.53	186.15	199.68	266.16	331.16	375.84
8	8.64	15.38	22.31	74.35	55.68	60.23	80.24	95.59	120.13	140.77	171.64	224.27	233.55	242.76	317.08	404.34	438.48
9	8.65	15.41	22.68	80.84	65.00	70.22	85.58	97.61	120.25	140.83	171.72	224.46	233.70	242.84	317.19	404.50	438.65
10	8.86	16.94	22.68	80.87	65.00	70.80	92.19	108.62	134.68	156.75	187.69	233.36	235.24	254.27	341.48	426.28	488.72
11	8.86	16.95	26.84	88.82	68.46	70.80	92.22	108.64	134.75	156.79	187.74	233.43	235.31	254.35	341.57	426.39	488.85
12	12.01	17.84	30.13	88.84	84.42	88.67	107.97	123.02	144.04	161.10	189.24	238.39	244.16	265.27	357.89	454.38	506.92
13	12.02	17.85	30.14	98.20	84.47	88.72	108.01	123.08	144.11	161.14	189.35	238.52	244.32	265.49	358.17	454.87	507.30
14	13.81	18.40	31.42	98.20	87.12	89.34	109.18	124.11	144.32	161.76	190.95	247.46	257.93	270.72	359.93	457.75	529.12
15	14.24	18.41	31.43	102.78	87.16	89.48	109.21	124.14	144.36	161.83	190.98	247.53	257.98	270.83	360.32	458.10	529.68
16	14.24	19.94	33.73	112.88	88.53	90.11	113.64	132.39	161.49	186.21	224.43	289.86	301.99	321.58	430.61	550.86	625.43
17	14.25	19.94	33.74	112.90	88.55	90.13	113.72	132.45	161.55	186.36	224.54	290.02	302.21	322.03	431.32	551.54	625.81
18	14.30	24.22	34.59	121.28	97.72	111.17	142.68	164.76	193.07	216.28	252.40	314.48	315.04	336.97	447.53	555.79	626.19
19	14.64	24.22	34.60	121.29	97.79	111.25	142.80	164.89	198.65	223.41	262.28	328.97	336.34	364.84	493.83	624.09	724.31
20	14.68	24.84	35.04	122.21	105.27	113.90	144.19	165.02	198.84	223.51	262.43	329.17	336.59	365.13	494.39	624.89	725.08
21	15.38	24.85	35.05	122.27	105.31	113.93	148.71	169.69	198.95	227.51	272.53	349.85	364.52	392.77	523.20	650.83	733.37
22	15.43	25.26	39.89	129.22	109.33	117.91	148.76	169.76	199.04	227.73	272.83	350.24	364.99	392.85	523.35	651.03	733.56
23	15.62	28.97	39.92	129.25	109.42	118.21	149.27	178.14	224.01	250.72	292.53	364.30	366.07	393.03	530.57	662.31	751.67
24	15.63	28.98	41.98	132.25	114.23	118.21	149.41	178.36	224.09	250.80	292.62	364.42	366.20	393.30	531.29	679.09	784.38
25	16.05	28.99	42.01	132.33	118.42	121.72	157.31	186.91	224.62	255.46	297.99	371.06	372.30	399.36	532.31	680.57	785.66

Frequency mode 26 to 50 of the tracheobronchial generation T0 to B16 by COSMOS/Work Analysis
(half density and double wall thickness)

Mode	T0	B1	B2	B3	B4	B5	B6	B7	B8	B9	B10	B11	B12	B13	B14	B15	B16
26	16.61	29.24	43.62	136.38	118.44	121.79	157.42	187.09	224.82	263.20	320.88	418.69	429.23	449.75	584.17	743.14	798.64
27	16.64	29.41	46.00	136.43	118.94	130.72	167.71	191.48	228.26	263.45	321.15	418.99	429.56	450.13	584.78	743.79	799.09
28	18.27	29.41	46.02	137.75	118.97	130.97	167.76	191.55	234.63	274.44	330.88	420.18	434.99	464.53	615.01	782.39	850.35
29	18.29	29.70	47.71	148.77	132.65	137.20	171.15	195.23	234.74	274.63	331.22	420.47	435.27	464.98	615.56	783.36	850.53
30	19.52	30.09	47.78	148.78	132.68	137.23	171.78	202.79	243.15	277.43	334.35	423.29	440.88	470.31	627.61	793.53	876.53
31	19.53	30.31	48.61	157.18	136.92	140.44	171.90	202.94	243.44	277.79	334.39	423.85	441.56	470.62	628.39	794.58	876.57
32	20.12	31.85	48.63	160.59	137.29	142.01	176.59	203.30	252.76	284.71	334.83	435.68	452.98	478.68	650.93	818.58	919.64
33	20.13	31.86	49.64	160.72	137.39	142.14	176.79	203.56	252.82	284.86	334.92	435.90	453.10	479.29	651.15	818.66	920.56
34	20.45	32.03	49.65	166.15	137.76	149.01	187.90	215.00	253.30	294.77	358.27	466.13	477.91	507.67	666.13	832.50	921.93
35	20.45	32.21	50.74	166.23	137.77	149.23	187.99	215.11	253.39	295.01	358.35	466.36	478.08	507.85	666.26	832.72	922.23
36	23.00	34.97	50.79	167.38	148.05	153.00	193.42	226.80	280.24	325.09	382.61	477.72	484.94	508.24	669.02	833.05	941.21
37	23.01	35.09	53.21	167.40	148.14	153.12	193.54	226.91	280.32	325.15	382.74	477.89	484.98	508.27	669.71	834.90	941.40
38	23.44	35.22	53.24	167.84	155.55	171.18	212.92	244.59	291.14	327.20	393.62	505.82	505.10	522.85	674.12	853.10	972.60
39	23.46	35.22	53.68	167.92	155.63	171.37	213.05	244.94	291.23	327.31	393.76	506.57	505.16	522.90	674.27	854.54	974.15
40	24.08	38.48	56.08	170.88	161.46	172.90	214.56	246.62	291.93	332.78	396.42	508.24	519.59	561.60	746.95	933.05	1003.10
41	25.85	38.50	56.09	170.93	161.48	172.94	214.63	246.69	292.23	333.09	396.84	508.55	520.01	562.09	748.17	954.60	1060.10
42	25.88	38.51	56.14	174.45	161.85	173.58	220.67	256.20	304.33	343.12	404.01	510.94	527.02	563.48	759.13	956.00	1060.10
43	25.95	38.52	56.18	175.83	161.89	174.00	220.70	256.23	304.50	343.32	404.24	511.17	527.83	563.78	759.38	960.84	1070.60
44	25.96	39.01	56.25	179.42	162.33	175.91	221.70	257.24	307.72	348.86	409.49	513.82	532.31	574.89	759.78	961.68	1071.50
45	26.98	39.07	56.26	179.63	162.38	175.94	221.86	257.30	307.77	348.90	409.54	513.88	532.38	575.72	777.16	963.48	1107.60
46	27.21	41.20	59.03	183.17	165.87	176.63	224.71	258.44	316.44	365.02	440.63	556.57	557.38	585.05	777.34	964.11	1117.50
47	27.32	41.22	59.08	183.25	165.90	178.74	224.89	258.67	316.51	365.19	440.73	561.53	558.42	593.99	783.82	993.41	1118.80
48	27.35	43.75	59.46	188.27	167.07	181.90	238.87	285.18	340.31	383.17	446.98	565.28	563.61	594.14	786.53	1005.00	1127.40
49	27.39	43.75	59.46	188.27	167.25	182.03	239.26	285.41	341.12	383.67	449.11	565.45	563.76	599.01	798.42	1006.60	1170.10
50	27.75	43.92	62.80	205.53	173.96	183.09	246.00	286.18	341.22	384.99	451.36	569.43	594.59	634.70	848.12	1053.10	1180.60

Frequency mode 51 to 75 of the tracheobronchial generation T0 to B16 by COSMOS/Work Analysis
(half density and double wall thickness)

Mode	T0	B1	B2	B3	B4	B5	B6	B7	B8	B9	B10	B11	B12	B13	B14	B15	B16
51	28.07	43.94	63.93	207.51	174.00	184.96	246.48	286.54	342.37	385.11	451.50	569.53	594.83	634.95	851.58	1080.50	1183.10
52	28.38	44.55	63.95	207.65	175.07	194.15	247.79	286.62	342.97	391.55	466.02	593.20	608.07	657.68	862.76	1080.60	1200.60
53	28.52	44.79	64.86	209.97	175.20	196.16	248.06	287.25	343.16	391.81	466.50	593.70	608.63	658.30	869.47	1086.90	1201.10
54	28.94	44.82	64.87	210.09	184.98	198.36	248.13	287.73	353.06	398.87	470.59	595.32	619.74	663.89	869.58	1088.70	1237.20
55	28.97	45.90	65.08	211.48	185.92	198.56	249.68	292.83	353.29	399.10	470.90	596.12	620.49	663.98	891.15	1106.20	1238.20
56	29.27	46.08	65.13	211.68	185.93	198.60	249.84	292.98	359.29	413.75	498.04	632.89	631.29	676.87	891.95	1132.60	1244.30
57	29.30	46.10	66.08	211.88	190.14	199.77	256.62	293.26	359.59	414.49	498.29	633.04	631.38	678.91	904.91	1134.00	1244.50
58	30.38	46.17	66.10	215.50	190.19	199.81	256.71	296.53	360.89	420.35	504.04	641.37	657.10	680.13	913.71	1135.80	1246.60
59	30.42	46.84	66.76	215.51	190.73	204.59	257.16	296.79	361.13	421.08	504.14	641.52	670.69	705.95	920.44	1135.90	1246.90
60	31.08	47.26	68.47	216.28	190.75	205.06	258.93	297.84	368.30	428.95	511.72	665.96	671.28	706.01	920.57	1159.40	1247.20
61	31.12	47.31	69.56	216.32	198.12	209.38	259.44	298.18	368.64	429.04	512.53	666.32	672.81	710.33	926.24	1162.00	1288.20
62	31.40	48.46	70.01	219.34	198.36	209.59	259.63	307.15	379.02	430.65	523.95	669.04	672.86	710.70	928.41	1175.40	1293.10
63	31.42	48.47	70.53	219.42	201.32	210.63	260.08	307.42	379.09	431.35	524.81	676.64	689.86	710.78	930.94	1189.80	1293.50
64	31.84	49.53	70.72	228.24	201.48	210.67	273.57	316.81	384.57	448.55	532.80	676.76	690.43	720.64	943.31	1192.00	1324.50
65	31.90	49.72	71.37	229.77	203.43	211.82	273.62	316.86	384.93	449.45	535.81	677.78	692.26	721.23	945.74	1195.30	1326.40
66	32.11	49.84	71.39	229.79	203.50	218.00	277.80	327.78	395.37	452.29	535.99	678.24	695.38	729.16	954.32	1206.30	1356.90
67	32.24	50.58	71.40	234.27	203.93	218.01	278.09	328.29	395.40	452.36	538.92	681.41	695.77	729.55	966.18	1207.20	1359.50
68	32.27	50.65	72.77	234.48	205.37	223.58	283.88	330.82	399.40	453.53	539.39	681.77	699.49	734.91	966.58	1210.50	1360.00
69	33.68	50.74	73.42	238.15	211.49	230.17	287.54	330.98	400.75	453.97	539.66	689.45	699.71	734.95	971.72	1227.20	1374.20
70	33.76	51.76	74.14	238.28	212.59	230.66	287.73	331.34	401.03	454.26	539.73	690.35	706.01	738.26	973.10	1244.90	1374.40
71	34.65	51.78	74.25	244.42	212.60	232.28	292.14	336.92	405.57	459.09	545.66	699.51	706.54	755.81	992.55	1248.40	1389.40
72	34.71	51.83	76.38	244.43	218.18	232.48	292.18	337.18	405.61	459.13	546.38	699.64	716.73	756.51	996.68	1260.30	1404.70
73	35.55	53.27	76.42	251.29	218.37	232.93	294.15	338.83	408.00	470.18	557.34	706.17	717.47	763.86	1002.80	1273.90	1406.10
74	35.61	53.48	76.46	251.58	218.88	233.01	294.22	338.89	408.24	471.25	557.36	709.05	718.12	764.46	1028.90	1276.40	1411.40
75	35.95	53.55	76.57	259.75	221.76	233.75	296.19	341.75	413.31	474.79	561.41	709.87	734.85	772.14	1029.50	1285.70	1411.50

Frequency mode 76 to 100 of the tracheobronchial generation T0 to B16 by COSMOS/Work Analysis
(half density and double wall thickness)

Mode	T0	B1	B2	B3	B4	B5	B6	B7	B8	B9	B10	B11	B12	B13	B14	B15	B16
76	36.00	55.02	77.55	259.94	221.86	236.98	297.55	341.78	413.92	474.81	564.78	724.92	735.34	788.94	1043.60	1312.60	1438.10
77	36.30	55.64	77.65	261.74	225.05	237.08	298.16	346.08	419.31	476.26	564.97	725.10	744.50	790.85	1048.70	1313.90	1439.70
78	36.33	55.65	77.87	265.17	225.17	237.89	303.04	352.38	420.13	476.82	577.47	729.16	744.74	796.01	1057.30	1324.40	1489.60
79	36.44	55.95	78.28	265.26	228.21	238.65	303.53	352.39	420.15	477.21	578.29	742.03	749.16	796.17	1058.00	1331.10	1489.90
80	36.46	56.19	78.32	266.23	228.56	239.62	305.02	355.56	431.90	491.79	579.08	744.17	749.47	798.60	1063.10	1332.40	1503.00
81	37.96	56.31	80.52	266.36	228.83	244.84	305.15	356.32	440.17	499.82	589.66	744.25	759.06	813.17	1064.40	1351.60	1523.10
82	38.02	56.61	80.57	271.45	230.76	244.86	305.22	356.46	440.49	499.97	589.81	749.31	760.10	813.86	1072.10	1354.10	1524.40
83	38.50	56.84	81.98	271.70	230.95	248.49	315.52	366.99	440.71	507.31	595.92	750.11	777.59	814.75	1082.60	1354.20	1548.10
84	38.51	57.08	82.83	277.60	231.25	249.95	317.24	367.28	441.01	509.79	597.95	753.74	778.08	819.85	1085.60	1364.30	1549.30
85	38.51	57.63	83.07	277.86	231.34	252.91	317.30	368.11	445.61	509.94	603.88	763.86	780.44	821.12	1108.10	1379.60	1557.10
86	39.13	57.64	84.03	278.84	231.66	253.10	327.22	376.44	449.78	510.85	604.13	764.58	790.17	823.98	1112.40	1386.30	1579.60
87	39.18	59.39	84.04	278.86	231.80	255.49	327.40	376.83	449.84	511.34	614.44	784.92	790.77	857.08	1113.00	1389.10	1580.10
88	40.13	59.48	84.15	295.01	238.52	258.11	329.32	378.93	450.76	511.67	614.79	788.11	806.07	859.47	1113.10	1429.00	1635.00
89	40.53	59.71	85.22	295.20	238.87	258.76	330.83	379.14	450.97	516.34	619.04	789.14	816.27	860.24	1113.50	1431.50	1637.60
90	40.56	59.74	86.34	298.81	239.26	260.20	331.14	383.19	456.45	516.57	619.76	802.15	816.64	874.55	1156.10	1433.20	1639.80
91	40.97	59.95	86.36	298.82	239.30	263.91	333.96	388.60	463.10	527.10	621.93	802.78	820.70	874.86	1161.40	1433.50	1641.40
92	41.03	60.00	86.49	299.38	241.33	264.82	335.38	389.27	469.48	533.92	636.42	805.71	820.82	878.79	1161.50	1471.10	1642.60
93	41.62	60.58	86.60	300.11	242.51	265.24	340.09	390.40	470.41	535.09	636.92	805.93	831.93	879.31	1166.40	1481.90	1642.60
94	41.69	60.77	87.89	301.24	242.85	266.49	340.33	390.59	475.01	539.72	641.10	818.35	833.23	879.38	1174.90	1483.70	1672.10
95	42.23	61.89	87.95	301.32	243.08	266.82	341.98	391.43	475.41	540.10	641.55	818.63	833.56	879.56	1176.20	1491.40	1672.90
96	42.24	61.95	88.14	308.19	254.81	268.05	342.25	396.52	480.74	550.14	649.11	819.30	841.13	888.35	1176.80	1493.80	1674.80
97	42.25	62.33	88.17	308.80	255.67	269.25	343.63	396.85	481.09	555.66	668.70	843.69	845.79	889.68	1177.30	1505.80	1739.20
98	42.49	63.14	89.36	308.83	255.93	272.68	343.77	399.24	483.30	556.81	671.22	846.20	845.82	889.75	1180.80	1507.50	1741.40
99	42.59	63.23	90.49	313.25	258.42	272.80	347.37	411.13	497.85	567.02	671.54	850.12	858.96	908.18	1245.10	1546.10	1760.50
100	42.66	63.58	91.27	314.39	258.52	275.27	347.81	413.38	500.64	568.69	671.99	850.17	860.08	909.77	1248.20	1546.20	1761.60

Appendix G Experimental Data and Results

Intensity versus frequency measurements on experimental samples.

Experiment A1, trial 1							
f_{Shaker} (Hz)	Intensity (dB)	f_{Shaker} (Hz)	Intensity (dB)	f_{Shaker} (Hz)	Intensity (dB)	f_{Shaker} (Hz)	Intensity (dB)
1.00	-48.50	85.00	-16.50	280.00	-25.50	710.00	-34.50
2.00	-40.50	90.00	-18.50	300.00	-30.50	720.00	-34.50
3.00	-40.50	95.00	-18.50	320.00	-27.50	730.00	-34.50
4.00	-31.50	100.00	-18.50	340.00	-28.50	740.00	-34.50
5.00	-30.50	105.00	-17.50	360.00	-29.50	750.00	-35.50
6.00	-29.50	110.00	-16.50	380.00	-32.50	760.00	-36.50
7.00	-28.50	115.00	-15.50	400.00	-33.50	770.00	-38.50
8.00	-26.50	120.00	-15.50	420.00	-34.50	780.00	-39.50
9.00	-24.50	125.00	-16.50	440.00	-34.50	800.00	-40.50
10.00	-23.00	130.00	-16.50	460.00	-34.50	820.00	-42.50
11.00	-22.50	135.00	-16.50	480.00	-33.50	840.00	-44.50
12.00	-21.50	140.00	-16.50	500.00	-33.50	860.00	-44.50
13.00	-20.50	145.00	-16.50	520.00	-34.50	880.00	-44.50
15.00	-23.50	150.00	-17.50	540.00	-35.50	900.00	-44.50
20.00	-23.50	155.00	-16.50	560.00	-36.50	910.00	-42.50
25.00	-18.50	160.00	-18.50	580.00	-37.50	920.00	-42.50
30.00	-16.50	165.00	-18.50	600.00	-39.50	930.00	-41.50
35.00	-13.50	170.00	-18.50	610.00	-38.50	940.00	-41.50
40.00	-8.50	175.00	-15.50	620.00	-38.50	950.00	-41.50
45.00	-4.50	180.00	-14.50	630.00	-36.50	960.00	-42.50
50.00	-2.50	185.00	-14.50	640.00	-36.50	970.00	-43.50
55.00	-6.50	190.00	-13.50	650.00	-34.50	980.00	-42.50
60.00	-9.50	195.00	-14.50	660.00	-34.50	990.00	-43.50
65.00	-12.50	200.00	-14.50	670.00	-33.50	1000.00	-43.50
70.00	-13.50	220.00	-14.50	680.00	-32.50		
75.00	-14.50	240.00	-14.50	690.00	-33.50		
80.00	-16.50	260.00	-20.50	700.00	-33.50		

Experiment A1, trial 2							
f_{Shaker} (Hz)	Intensity (dB)	f_{Shaker} (Hz)	Intensity (dB)	f_{Shaker} (Hz)	Intensity (dB)	f_{Shaker} (Hz)	Intensity (dB)
0.50	-44.10	80.00	-16.50	440.00	-33.50	730.00	-35.50
0.99	-43.00	90.00	-16.50	450.00	-34.50	740.00	-36.50
1.98	-41.10	100.00	-17.50	460.00	-34.50	750.00	-36.50
3.01	-39.00	110.00	-16.50	470.00	-34.50	760.00	-36.50
3.99	-38.10	120.00	-15.50	480.00	-35.50	770.00	-36.50
5.00	-38.50	130.00	-16.50	490.00	-36.50	780.00	-37.50
5.60	-40.30	140.00	-15.50	500.00	-38.50	790.00	-38.50
6.99	-36.10	150.00	-16.50	510.00	-39.50	800.00	-38.50
8.02	-33.00	160.00	-16.50	520.00	-42.50	810.00	-39.50
9.01	-32.40	170.00	-14.50	530.00	-42.50	820.00	-39.50
10.00	-31.50	180.00	-20.50	540.00	-45.50	830.00	-40.50
11.02	-30.80	190.00	-21.50	550.00	-49.50	840.00	-39.50
12.00	-30.60	200.00	-20.50	560.00	-49.50	850.00	-40.50
12.96	-30.30	220.00	-19.50	570.00	-51.50	860.00	-40.50
14.98	-30.90	240.00	-21.50	580.00	-52.50	870.00	-40.50
16.01	-31.30	260.00	-20.50	590.00	-49.50	880.00	-42.50
16.98	-31.30	270.00	-21.50	600.00	-45.50	890.00	-42.50
17.03	-31.70	280.00	-24.50	610.00	-45.50	900.00	-44.50
18.01	-31.30	290.00	-22.50	620.00	-44.50	910.00	-42.50
19.01	-30.80	300.00	-21.50	630.00	-42.50	920.00	-44.50
20.00	-30.70	320.00	-21.50	640.00	-39.50	930.00	-44.50
25.00	-29.30	340.00	-22.50	650.00	-38.50	940.00	-45.50
30.00	-26.30	360.00	-23.50	660.00	-37.50	950.00	-46.50
35.00	-24.20	380.00	-24.50	670.00	-37.50	960.00	-47.50
40.00	-22.10	390.00	-26.50	680.00	-35.50	970.00	-48.50
45.00	-20.80	400.00	-29.50	690.00	-34.50	980.00	-48.50
50.00	-18.50	410.00	-29.50	700.00	-34.50	990.00	-50.50
60.00	-10.50	420.00	-30.50	710.00	-34.50		
70.00	-13.50	430.00	-31.50	720.00	-34.50		

Experiment A2, trial 1			
f_{Shaker} (Hz)	Intensity (dB)	f_{Shaker} (Hz)	Intensity (dB)
0.50	-42.50	180.10	-15.50
1.00	-41.70	190.10	-15.50
1.99	-41.10	200.00	-15.50
3.01	-40.90	225.00	-18.50
4.01	-39.70	240.00	-17.50
5.00	-38.50	250.00	-20.50
6.10	-39.00	261.00	-23.50
6.97	-37.10	270.00	-24.50
8.01	-35.60	280.00	-26.50
9.01	-33.60	300.00	-31.50
10.00	-32.50	320.00	-30.50
10.99	-31.30	341.00	-33.50
11.98	-30.60	350.00	-34.50
13.05	-30.80	360.00	-34.50
14.01	-31.00	382.00	-36.50
15.00	-29.50	399.00	-36.50
16.50	-29.30	420.00	-35.50
18.01	-28.90	448.00	-35.50
19.02	-28.80	475.00	-36.50
20.20	-28.50	499.00	-36.50
25.20	-24.50	525.00	-36.50
30.00	-23.50	550.00	-37.50
40.00	-21.50	574.00	-37.50
50.20	-18.50	601.00	-38.50
59.90	-15.50	625.00	-38.50
70.00	-12.50	651.00	-38.50
79.90	-11.50	675.00	-40.50
90.00	-10.50	699.00	-42.50
100.00	-12.50	724.00	-43.50
110.30	-11.50	750.00	-46.50
119.90	-13.50	774.00	-46.50
130.30	-16.50	802.00	-49.50
139.90	-18.50	824.00	-50.50
150.00	-20.50	876.00	-51.50
160.10	-19.50	899.00	-52.50
170.10	-17.50		

Experiment A2, trial 2			
f_{Shaker} (Hz)	Intensity (dB)	f_{Shaker} (Hz)	Intensity (dB)
0.97	-50.50	120.00	-16.50
1.99	-48.70	129.90	-17.50
3.02	-47.80	139.70	-19.50
3.97	-47.20	150.10	-22.50
5.00	-46.50	160.00	-26.50
6.03	-44.10	169.90	-31.50
7.01	-43.00	180.00	-44.50
7.99	-41.80	190.20	-21.50
8.43	-40.70	202.00	-25.50
9.02	-40.70	225.00	-22.50
9.99	-40.50	240.00	-21.50
10.97	-38.60	250.00	-21.50
12.01	-39.00	261.00	-23.50
13.04	-38.10	269.00	-24.50
13.97	-37.30	281.00	-25.50
15.01	-36.50	300.00	-26.50
16.02	-36.90	320.00	-30.50
17.02	-36.10	341.00	-35.50
17.98	-35.30	348.00	-36.50
19.00	-34.80	360.00	-38.50
19.80	-34.50	381.00	-38.50
25.10	-32.50	401.00	-35.50
30.00	-30.50	421.00	-34.50
40.10	-28.50	440.00	-39.50
49.70	-26.50	475.00	-50.50
59.90	-24.50	499.00	-50.50
69.90	-21.50	523.00	-54.50
80.00	-18.50	550.00	-53.50
90.10	-13.50	575.00	-51.50
100.20	-23.50	599.00	-54.50

Experiment A3, trial 1					
f_{Shaker} (Hz)	Intensity (dB)	f_{Shaker} (Hz)	Intensity (dB)	f_{Shaker} (Hz)	Intensity (dB)
0.50	-48.50	16.04	-9.70	93.20	-4.50
0.60	-44.10	16.57	-8.90	94.80	-4.50
0.70	-42.50	17.01	-6.90	97.00	-5.30
0.80	-38.90	17.53	-6.10	97.60	-6.10
0.90	-40.10	17.95	-5.70	97.90	-8.50
1.00	-37.70	18.55	-5.70	98.20	-11.30
1.10	-36.10	19.04	-5.70	98.50	-10.90
1.20	-30.90	19.86	-4.10	99.20	-11.70
1.30	-30.90	21.60	-4.50	100.50	-9.70
1.40	-29.70	22.00	-2.50	100.80	-6.90
1.50	-27.70	23.60	-2.90	101.80	-6.10
1.60	-26.90	24.20	-2.10	102.20	-6.10
1.70	-24.90	26.30	-1.30	104.60	-6.50
1.80	-23.70	26.90	-0.90	106.20	-6.50
1.90	-22.90	28.20	-1.30	108.80	-6.50
2.00	-21.70	30.40	-1.70	111.00	-6.10
2.51	-19.30	31.30	-2.10	112.50	-13.70
3.10	-17.30	34.30	-3.30	113.40	-13.70
3.68	-16.50	35.50	-4.50	117.30	-15.30
4.06	-14.50	37.70	-4.50	117.70	-13.70
4.47	-13.70	39.10	-5.30	120.20	-10.10
5.10	-13.70	41.80	-7.30	123.20	-8.10
5.48	-13.30	43.50	-8.10	125.00	-7.70
6.02	-12.50	47.90	-11.30	130.50	-6.90
6.58	-11.30	50.40	-12.50	134.70	-6.90
7.00	-11.70	54.30	-13.30	137.80	-6.10
7.60	-12.50	57.70	-14.10	144.10	-6.90
8.03	-10.90	60.30	-14.10	147.90	-6.90
8.55	-11.30	62.20	-14.10	150.70	-6.90
9.11	-13.30	64.70	-12.50	156.20	-6.50
9.55	-13.70	69.80	-10.90	161.80	-7.30
10.10	-12.90	72.80	-9.70	165.30	-7.30
10.73	-13.30	75.20	-8.90	170.40	-7.70
11.35	-13.70	78.70	-7.30	176.00	-7.30
11.97	-14.90	83.90	-5.30	179.00	-8.10
12.42	-16.10	85.70	-4.10	185.10	-9.30
12.98	-16.90	87.10	-4.10	189.00	-9.30
13.48	-16.50	87.50	-5.30	195.20	-10.10
14.13	-16.50	88.90	-6.90	210.00	-14.10
14.49	-14.50	89.80	-8.10	233.00	-21.30
15.03	-12.10	91.30	-7.30		
15.61	-10.10	92.60	-5.70		

Experiment A3, trial 2			
f_{Shaker} (Hz)	Intensity (dB)	f_{Shaker} (Hz)	Intensity (dB)
1.007	-19.3	55.4	-13.7
1.998	-19.7	57.7	-16.1
3.01	-19.1	60.1	-17.3
4.02	-18.6	65.2	-18.9
5.01	-18.1	67.7	-18.1
6.01	-19.3	69.9	-22.5
6.98	-18.4	72.6	-20.5
7.99	-15.9	74.9	-22.5
9	-14.6	80.4	-25.7
9.98	-12.5	84.9	-26.5
11.2	-12.9	89.7	-33.7
11.7	-13.3	95.2	-32.1
12.3	-14.8	97.7	-32.1
12.54	-15.3	100	-32.1
13	-15.1	102.7	-30.5
13.56	-15.5	104.9	-29.3
13.98	-16.0	107.5	-29.3
14.56	-16.9	110.4	-34.1
14.96	-17.3	112.7	-33.3
17.54	-14.1	115.1	-31.7
20.1	-10.1	119.7	-29.3
22.5	-8.1	124.9	-27.3
25.5	-1.3	127.2	-26.1
27.7	-2.1	129.7	-25.3
30.5	-3.3	132.8	-23.7
33	-4.1	135.1	-23.7
35	-5.3	137.9	-23.7
40	-5.3	139.5	-22.5
45.5	-7.7	144.6	-21.3
50	-8.5	147.1	-21.3
52.4	-9.3		

Experiment A3, trial 3					
f_{Shaker} (Hz)	Intensity (dB)	f_{Shaker} (Hz)	Intensity (dB)	f_{Shaker} (Hz)	Intensity (dB)
0.50	-48.50	16.04	-9.70	93.20	-4.50
0.60	-44.10	16.57	-8.90	94.80	-4.50
0.70	-42.50	17.01	-6.90	97.00	-5.30
0.80	-38.90	17.53	-6.10	97.60	-6.10
0.90	-40.10	17.95	-5.70	97.90	-8.50
1.00	-37.70	18.55	-5.70	98.20	-11.30
1.10	-36.10	19.04	-5.70	98.50	-10.90
1.20	-30.90	19.86	-4.10	99.20	-11.70
1.30	-30.90	21.60	-4.50	100.50	-9.70
1.40	-29.70	22.00	-2.50	100.80	-6.90
1.50	-27.70	23.60	-2.90	101.80	-6.10
1.60	-26.90	24.20	-2.10	102.20	-6.10
1.70	-24.90	26.30	-1.30	104.60	-6.50
1.80	-23.70	26.90	-0.90	106.20	-6.50
1.90	-22.90	28.20	-1.30	108.80	-6.50
2.00	-21.70	30.40	-1.70	111.00	-6.10
2.51	-19.30	31.30	-2.10	112.50	-13.70
3.10	-17.30	34.30	-3.30	113.40	-13.70
3.68	-16.50	35.50	-4.50	117.30	-15.30
4.06	-14.50	37.70	-4.50	117.70	-13.70
4.47	-13.70	39.10	-5.30	120.20	-10.10
5.10	-13.70	41.80	-7.30	123.20	-8.10
5.48	-13.30	43.50	-8.10	125.00	-7.70
6.02	-12.50	47.90	-11.30	130.50	-6.90
6.58	-11.30	50.40	-12.50	134.70	-6.90
7.00	-11.70	54.30	-13.30	137.80	-6.10
7.60	-12.50	57.70	-14.10	144.10	-6.90
8.03	-10.90	60.30	-14.10	147.90	-6.90
8.55	-11.30	62.20	-14.10	150.70	-6.90
9.11	-13.30	64.70	-12.50	156.20	-6.50
9.55	-13.70	69.80	-10.90	161.80	-7.30
10.10	-12.90	72.80	-9.70	165.30	-7.30
10.73	-13.30	75.20	-8.90	170.40	-7.70
11.35	-13.70	78.70	-7.30	176.00	-7.30
11.97	-14.90	83.90	-5.30	179.00	-8.10
12.42	-16.10	85.70	-4.10	185.10	-9.30
12.98	-16.90	87.10	-4.10	189.00	-9.30
13.48	-16.50	87.50	-5.30	195.20	-10.10
14.13	-16.50	88.90	-6.90	210.00	-14.10
14.49	-14.50	89.80	-8.10	233.00	-21.30
15.03	-12.10	91.30	-7.30		
15.61	-10.10	92.60	-5.70		

Experiment B1							
f_{Shaker} (Hz)	Intensity (dB)	f_{Shaker} (Hz)	Intensity (dB)	f_{Shaker} (Hz)	Intensity (dB)	f_{Shaker} (Hz)	Intensity (dB)
1.02	-84.60	9.10	-66.60	13.74	-57.40	16.37	-55.00
1.50	-74.60	9.44	-65.80	14.08	-58.60	16.55	-55.40
2.00	-76.20	9.77	-61.00	14.28	-62.60	16.68	-53.40
2.50	-73.00	10.14	-54.60	14.54	-63.80	17.04	-53.00
3.05	-75.80	10.28	-53.40	14.75	-65.00	17.16	-55.00
3.49	-71.80	10.51	-49.00	14.82	-62.60	17.48	-56.20
4.20	-70.20	10.71	-49.00	15.10	-57.80	17.77	-55.00
4.91	-68.20	10.85	-49.00	15.37	-56.60	17.92	-53.80
5.64	-70.20	11.21	-50.20	15.52	-56.20	18.25	-53.00
6.19	-73.00	11.57	-51.80	15.65	-56.20	18.74	-52.60
6.81	-71.80	12.11	-53.40	15.87	-55.40	19.03	-53.40
7.36	-72.20	12.93	-55.40	16.03	-54.20	19.08	-53.80
8.08	-68.60	13.48	-55.80	16.07	-53.00	19.24	-55.00

Experiment B2, trial 1							
f_{Shaker} (Hz)	Intensity (dB)	f_{Shaker} (Hz)	Intensity (dB)	f_{Shaker} (Hz)	Intensity (dB)	f_{Shaker} (Hz)	Intensity (dB)
8.00	-12.20	13.80	-1.39	40.00	11.00	58.00	6.61
9.00	-10.60	20.60	11.00	41.00	9.41	60.00	6.61
10.00	-8.59	21.10	13.40	42.00	9.01	62.00	5.81
11.00	-5.79	22.00	14.60	44.00	5.81		
12.00	-4.59	25.00	10.20	50.00	5.41		
13.00	-4.99	39.00	9.81	57.00	6.61		

Experiment B2, trial 2							
f_{Shaker} (Hz)	Intensity (dB)	f_{Shaker} (Hz)	Intensity (dB)	f_{Shaker} (Hz)	Intensity (dB)	f_{Shaker} (Hz)	Intensity (dB)
1.00	-36.50	20.30	-0.21	37.30	22.20	69.10	11.80
2.20	-35.00	21.30	2.21	39.30	25.00	72.80	8.61
2.40	-35.80	22.60	5.01	41.70	25.80	74.10	5.01
3.40	-32.30	23.50	6.21	42.70	25.80	76.90	3.01
5.50	-24.20	24.50	5.81	43.40	25.80	78.00	3.01
5.60	-25.40	25.70	5.81	44.60	25.80	79.30	3.01
7.70	-18.60	26.50	5.01	46.00	25.80	81.10	3.01
8.50	-19.30	27.00	3.81	48.50	25.40	83.20	3.41
9.50	-14.60	28.00	2.21	49.70	24.20	86.20	3.41
12.40	-7.79	29.20	1.41	50.50	24.20	88.50	3.41
14.30	-6.99	30.40	3.01	52.40	21.80	90.60	2.61
15.80	-5.79	31.00	4.21	55.10	19.80	92.80	1.01
16.50	-3.99	31.70	7.01	56.70	18.20	95.10	-1.39
17.50	-3.79	32.80	10.60	59.50	17.00	98.20	-5.79
18.00	-4.99	34.20	15.00	62.30	17.00		
18.80	-2.59	35.00	17.80	65.80	15.80		
19.50	-1.79	35.50	17.80	67.30	14.20		

Experiment B3, trial 1			
f_{Shaker} (Hz)	Intensity (dB)	f_{Shaker} (Hz)	Intensity (dB)
1.00	-32.60	47.20	16.20
1.90	-31.80	48.80	16.20
2.97	-27.00	49.70	16.20
3.99	-23.40	52.50	15.40
5.01	-19.70	54.90	15.00
5.50	-16.20	57.10	14.20
6.20	-15.00	58.90	13.00
7.99	-16.70	60.60	12.20
8.01	-12.20	62.30	11.40
8.98	-8.77	64.70	11.40
9.70	-8.59	66.90	11.00
13.00	-6.19	68.60	11.40
13.99	-4.58	70.80	11.80
14.97	-3.96	72.70	11.80
16.01	-3.24	74.20	12.20
16.60	-2.59	77.40	11.40
18.40	0.61	79.40	11.40
20.60	0.61	82.80	10.60
24.40	4.61	84.60	10.20
27.40	7.41	87.50	8.61
28.30	7.01	89.60	7.41
31.50	6.21	91.60	6.21
35.30	10.60	93.40	5.81
38.90	15.80	95.80	4.61
41.10	16.20	97.20	3.81
43.60	16.20	99.10	2.61
44.40	16.20	100.00	2.61

Experiment B3, trial 2			
f_{Shaker} (Hz)	Intensity (dB)	f_{Shaker} (Hz)	Intensity (dB)
1.10	-32.00	43.50	16.20
2.10	-31.50	46.20	20.20
2.40	-30.00	47.70	21.80
3.50	-27.20	50.10	21.80
4.30	-24.20	51.70	21.40
5.50	-20.40	52.70	20.60
6.30	-14.60	54.10	19.80
7.50	-15.80	56.00	19.40
8.40	-9.39	57.70	19.00
10.50	-6.19	58.90	19.80
13.10	-6.59	59.20	19.80
13.70	-4.19	60.10	20.20
14.70	-2.99	61.10	21.00
15.40	-2.59	62.80	21.40
17.00	-1.39	64.20	21.40
19.30	0.61	65.30	21.40
21.40	3.01	66.80	21.40
23.60	5.41	68.00	21.40
25.40	6.61	69.50	20.60
25.80	6.21	70.30	20.60
26.30	4.61	72.80	19.80
27.60	2.61	73.80	19.40
28.30	2.61	75.50	19.40
29.10	3.41	76.80	19.40
29.60	4.21	79.50	18.50
31.10	7.41	81.10	18.20
33.80	11.40	82.60	17.40
34.50	11.80	85.80	16.60
34.80	11.80	87.40	15.80
35.50	11.00	88.60	15.80
36.00	11.40	90.00	15.40
36.80	12.20	92.60	15.00
37.20	12.60	94.30	14.60
38.00	12.60	96.40	13.80
40.30	14.20	98.80	12.60
42.10	14.60	99.90	11.80

Appendix H Analytical Results on Experimental Validation

Sample A1

Experiment A1:

Analytical solutions of membrane radial frequency, the lowest frequency and the lowest radial frequency on experiment A1.

$$\begin{aligned}
 E &:= 7300 & \nu &:= 0.5 & \rho &:= 1040 \\
 l &:= 0.09 & a &:= \frac{.02287}{2} & h &:= 0.00217 & m &:= 1 \\
 \xi &:= \frac{12 \cdot a^2}{h^2} & K &:= m \cdot \pi & n &:= 0.1, 0.2.. 50 & f_R &:= \frac{1}{2 \cdot \pi \cdot a} \cdot \sqrt{\frac{E}{\rho}}
 \end{aligned}$$

$$a = 0.01 \quad E = 7.3 \times 10^3 \quad \rho = 1.04 \times 10^3 \quad l = 0.09 \quad K = 3.14 \quad f_R = 36.87$$

Membrane shell based on thin shell theory

$$f_m(n) := \frac{1}{2 \cdot \pi \cdot a} \cdot \sqrt{\frac{E}{\rho}} \cdot \frac{K^2 \cdot a^2}{n^2 \cdot l^2} \left(1 + \frac{K^2 \cdot a^2}{n^2 \cdot l^2} \right)^{-1}$$

Membrane frequency : $f_m(1) = 5.07$

$$f_{mm}(n) := \frac{1}{2 \cdot \pi \cdot a} \cdot \sqrt{\frac{E}{\rho}} \cdot \frac{K^2 \cdot a^2}{n^2 \cdot l^2}$$

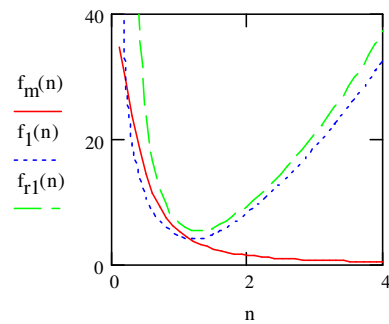
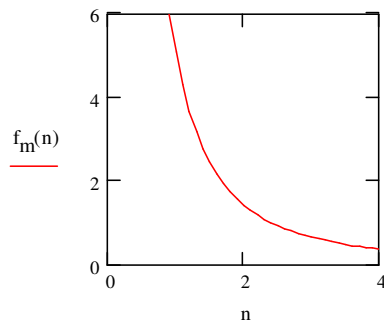
Membrane frequency : $f_{mm}(1) = 5.88$

$$f_1(n) := f_R \sqrt{\frac{\frac{n^8}{\xi} + (1 - \nu^2) \cdot \left(\frac{K \cdot a}{l} \right)^4}{n^2(n^2 + 1) + (3 - \nu) \frac{n^6}{\xi \cdot (1 - \nu)}}} \cdot \frac{1}{1 - \nu^2}$$

Lowest frequency : $f_1(1) = 4.45$

$$f_{r1}(n) := f_R \sqrt{\left[\frac{n^8}{\xi} + (1 - \nu^2) \cdot \left(\frac{K \cdot a}{l} \right)^4 \right]} \cdot \frac{1}{n^4} \cdot \frac{1}{1 - \nu^2}$$

Lowest radial frequency : $f_{r1}(1) = 6.32$



Appendix I COSMOS/Works Validation

Resonant frequencies on experimental samples by COSMOS/Works.
Lengths, diameters and thicknesses are measured in mm. Radial frequencies (Hz) are in bold.

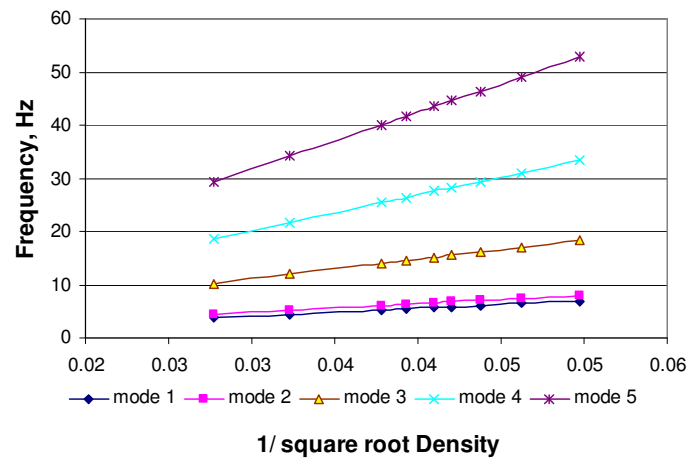
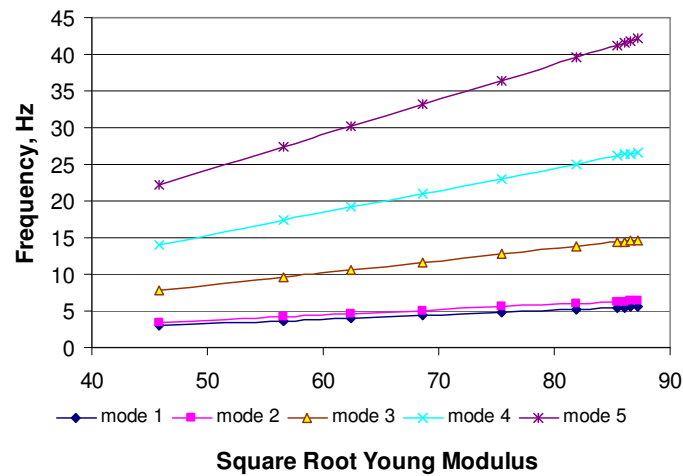
Length	90	60	151	Length	54	121	37
Diameter	24	24	21	Diameter	23	21	12
Thickness	3.1	3.1	2.8	Thickness	1.6	2.8	0.5
Mode No.	A1	A2	A3	Mode No.	B1	B2	B3
	Hertz	Hertz	Hertz		Hertz	Hertz	Hertz
1	5.22	8.48	2.40	1	7.26	3.36	7.88
2	5.22	8.48	2.40	2	7.27	3.36	7.88
3	8.58	9.86	5.12	3	9.44	6.39	11.87
4	8.58	9.86	5.41	4	9.44	7.29	11.87
5	8.59	12.89	5.41	5	12.93	7.29	14.21
6	10.77	14.96	8.77	6	12.93	8.98	14.21
7	10.77	14.97	8.93	7	13.57	8.99	14.62
8	10.90	17.09	8.94	8	13.57	10.00	14.63
9	10.91	17.09	8.98	9	14.25	10.00	16.95
10	14.53	21.21	8.99	10	16.59	10.91	16.95
11	14.71	22.09	9.49	11	16.59	11.90	18.66
12	14.73	22.09	9.51	12	18.68	11.90	21.73
13	17.10	22.29	10.25	13	18.68	11.91	21.73
14	17.10	22.31	10.62	14	19.95	11.93	23.05
15	17.19	25.11	10.65	15	19.95	12.79	23.05
16	19.52	25.13	12.35	16	21.55	14.64	23.89
17	19.54	25.78	12.40	17	21.56	14.66	23.90
18	21.39	25.81	12.80	18	23.31	16.68	26.01
19	21.39	25.81	12.81	19	24.29	16.68	26.01
20	22.64	28.65	14.60	20	24.29	17.97	27.62
21	22.65	28.65	14.67	21	26.46	18.00	27.62
22	23.04	30.29	15.37	22	26.46	19.18	27.93
23	23.05	30.31	16.68	23	27.00	21.09	27.94
24	24.71	30.72	16.69	24	27.00	21.35	30.54
25	24.72	30.74	17.18	25	27.08	21.36	30.55
26	24.87	32.89	17.25	26	27.08	21.71	31.36
27	24.89	33.32	17.33	27	27.91	21.74	31.69
28	24.90	33.32	20.18	28	27.92	23.43	31.69
29	24.93	36.91	20.28	29	28.50	23.43	34.79
30	25.78	37.31	20.45	30	30.21	24.01	34.79
31	26.45	37.35	20.47	31	30.21	24.02	34.94
32	28.10	38.50	20.49	32	30.50	25.04	34.95
33	28.13	38.50	23.33	33	30.50	25.04	36.48
34	28.35	38.66	23.43	34	33.01	25.04	36.48
35	28.36	39.78	23.70	35	33.01	25.05	37.33
36	30.62	39.80	23.77	36	34.08	25.57	39.74
37	30.65	39.88	24.03	37	34.09	25.71	39.74
38	32.23	40.05	24.05	38	34.35	25.73	40.24
39	32.27	40.05	24.05	39	35.15	25.73	40.24
40	32.46	40.86	24.11	40	35.16	25.75	41.27

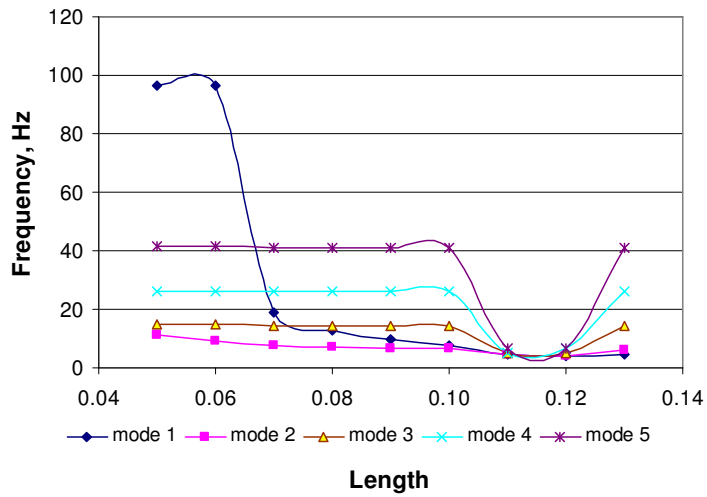
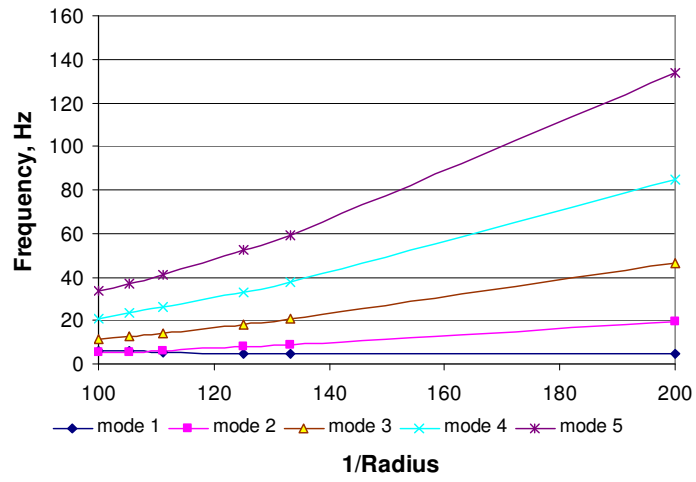
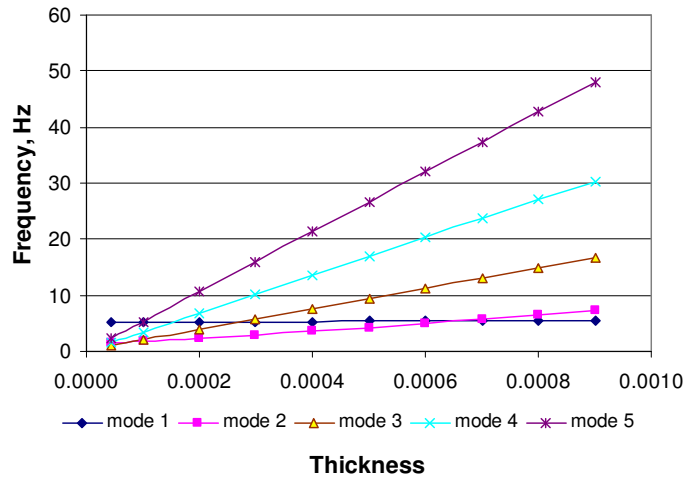
Mode No.	A1	A2	A3	Mode No.	B1	B2	B3
	Hertz	Hertz	Hertz		Hertz	Hertz	Hertz
41	32.54	40.87	24.30	41	35.46	26.56	41.27
42	32.54	41.84	24.31	42	35.47	26.59	42.27
43	33.20	41.84	24.69	43	37.12	28.61	42.28
44	33.20	42.73	24.70	44	37.51	28.65	42.61
45	34.37	43.04	24.74	45	37.51	29.28	42.61
46	35.09	44.88	25.61	46	37.67	29.71	44.97
47	36.59	44.91	25.66	47	37.67	29.72	44.97
48	36.62	44.95	25.68	48	39.56	29.89	46.18
49	37.13	44.95	26.62	49	39.56	29.93	46.18
50	37.17	45.71	26.73	50	39.58	30.08	46.60
51	37.32	45.75	26.96	51	41.27	30.08	46.61
52	37.87	48.44	26.96	52	41.28	31.16	46.98
53	37.87	48.44	27.37	53	41.99	31.21	46.99
54	38.03	49.39	27.40	54	42.00	31.96	47.20
55	38.03	49.42	27.87	55	42.39	33.43	47.20
56	38.88	49.94	27.88	56	42.74	33.43	48.38
57	38.89	50.54	28.57	57	42.75	34.18	48.39
58	39.64	50.58	28.61	58	42.78	34.20	49.75
59	40.25	51.54	30.02	59	42.78	34.23	49.76
60	40.26	52.16	30.14	60	42.84	34.25	52.87
61	40.61	52.16	30.50	61	42.84	34.27	52.88
62	40.63	53.30	30.50	62	43.06	35.90	52.92
63	41.24	53.30	30.53	63	43.07	35.90	52.93
64	41.46	55.03	30.54	64	44.73	36.86	53.17
65	42.62	55.08	30.60	65	44.73	37.00	53.58
66	42.67	55.13	30.73	66	46.06	37.00	53.59
67	42.79	56.94	32.33	67	47.13	37.60	53.71
68	42.83	56.94	32.34	68	47.13	37.66	53.72
69	42.92	57.07	32.83	69	47.33	38.35	55.99
70	42.92	57.08	32.92	70	47.34	38.54	57.35
71	42.96	57.64	33.48	71	49.00	38.63	57.36
72	43.10	57.69	33.50	72	49.01	38.68	57.84
73	43.13	58.53	33.53	73	49.22	40.06	57.84
74	43.16	58.53	33.65	74	49.22	40.58	58.37
75	43.16	59.08	34.20	75	49.41	40.58	58.38
76	45.00	59.09	35.40	76	49.57	41.36	59.59
77	45.63	59.53	35.56	77	49.58	41.43	59.60
78	46.35	59.56	35.85	78	51.58	41.52	59.94
79	46.39	59.58	36.29	79	51.60	41.52	59.95
80	47.09	62.45	36.31	80	53.14	41.73	60.25

Mode No.	A1	A2	A3	Mode No.	B1	B2	B3
	Hertz	Hertz	Hertz		Hertz	Hertz	Hertz
81	47.09	62.47	36.37	81	53.14	41.74	60.84
82	47.14	63.06	37.05	82	53.15	41.74	60.85
83	47.15	63.06	37.05	83	53.17	42.23	61.35
84	48.58	63.84	37.10	84	54.88	42.24	61.36
85	48.63	63.85	37.24	85	54.88	43.07	61.41
86	48.79	64.05	37.81	86	55.34	43.08	61.42
87	48.79	64.05	38.26	87	55.35	43.17	62.59
88	49.24	64.41	38.43	88	56.65	43.23	63.01
89	49.28	65.17	39.01	89	56.68	43.57	63.01
90	49.89	65.21	39.20	90	56.68	44.27	64.20
91	50.31	65.38	39.22	91	57.00	44.27	64.77
92	50.36	65.38	40.23	92	57.32	44.27	64.79
93	51.54	65.92	40.77	93	57.32	44.29	65.16
94	52.74	65.98	40.90	94	57.50	44.74	65.16
95	52.74	67.18	40.96	95	57.50	44.87	65.30
96	53.32	67.22	41.38	96	57.80	45.42	65.30
97	53.33	67.27	41.44	97	57.81	45.50	65.77
98	54.01	68.12	41.44	98	58.00	45.76	65.77
99	54.92	68.12	41.54	99	58.02	45.84	66.05
100	54.92	69.67	41.57	100	60.11	45.87	66.10

Appendix J COSMOS/Works Resonant Characterisation on Geometric and Physical Parameters of the Trachea

The following are graphs of COSMOS/Works frequency analyses versus the tracheobronchial parameters of the Young's modulus (N/m^2), density (kg/m^3), thickness (m), radius (m) and length (m).





Reference

1. Al-Jumaily, A.M. and Y. Al-Fakhri, *Occlusion identification in respiratory system using asymmetric model*. Communications in Nonlinear Science and Numerical Simulation, 2003. **8**(1): p. 37-47.
2. Aljuri, N., L. Freitag, and J.G. Venegas, *Modeling expiratory flow from excised tracheal tube laws*. J Appl Physiol, 1999. **87**(5): p. 1973-1980.
3. Bowes, C., et al., *Gas mixing in a model of the pulmonary acinus with asymmetrical alveolar ducts*. J Appl Physiol, 1982. **52**(3): p. 624-633.
4. Fredberg, J.J. and J.A. Moore, *The distributed response of complex branching duct networks*. Journal of Acoustic Society of America, 1978. **63**: p. 954 - 961.
5. Fredberg, J.J., et al., *Airway area by acoustic reflections measured at the mouth*. Journal of Applied Physiology, 1980. **48**: p. 748 - 75.
6. Fung, Y.C., *Biomechanics : motion, flow, stress, and growth*. 1990, Springer-Verlag: New York. p. 569.
7. Fung, Y.C., *Biomechanics : circulation*. 1997, New York: Springer-Verlag. 571.
8. Hantos, Z., et al., *Mechanical impedance of the lung periphery*. J Appl Physiol, 1997. **83**(5): p. 1595-1601.
9. Horsfield, K., A. Davies, and G. Cumming, *Role of conducting airways in partial separation of inhaled gas mixtures*. J Appl Physiol, 1977. **43**(3): p. 391-396.
10. Howatson, M., *An anatomically accurate mathematical model of the human pulmonary acinus*, in *Engineering Science*. 1995, University of Auckland: Auckland. p. 99.
11. Jackson, A.C., et al., *Branching airway network models for analyzing high-frequency lung input impedance*. J Appl Physiol, 1993. **75**(1): p. 217-227.
12. Kitaoka, H. and B. Suki, *Branching design of the bronchial tree based on a diameter-flow relationship*. J Appl Physiol, 1997. **82**(3): p. 968-976.
13. Kitaoka, H., R. Takaki, and B. Suki, *A three-dimensional model of the human airway tree*. J Appl Physiol, 1999. **87**(6): p. 2207-1693.
14. Margolis, D.L. and M. Tabrisi, *Acoustic modelling of lung dynamics using bond graphs*. Journal of Biomechanical Engineering, 1983. **105**(1): p. 84 - 91.
15. Raphael, D.T., *An explicit resonance condition for a rigid symmetric Nth order branching network*1988. Journal of Acoustic Society of America, 1988. **83**(1): p. 335 - 337.
16. Raphael, D.T. and M.A.F. Epstein, *Volume estimation of symmetrical branching structures by resonance mode analysis*. Journal of Acoustic Society of America, 1987. **82**(3): p. 800 - 806.
17. Tawhai, M.H., *An anatomically based mathematical model of the human lungs, applied to gas mixing and water vapour and heat transport*, in *Engineering Science*. 2001, University of Auckland: Auckland. p. 234.

18. Tawhai, M.H., et al., *CT-based geometry analysis and finite element models of the human and ovine bronchial tree*. J Appl Physiol, 2004. **97**(6): p. 2310-2321.
19. Cochrane, G.M., W.F. Jackson, and P.J. Rees, *Asthma Current Perspectives*. 1996, London: Mosby-Wolfe.
20. Johnston, M., *Asthma rate triple world average*, in *The New Zealand Herald*. 2004: Auckland.
21. Arnold, V., et al., *Increase in Perforin-positive Peripheral Blood Lymphocytes in Extrinsic and Intrinsic Asthma*. Am. J. Respir. Crit. Care Med., 2000. **161**(1): p. 182-186.
22. Holt, S. and R. Beasley, *The Burden of Asthma in New Zealand*. 2001, Asthma and Respiratory Foundation of New Zealand.
23. Johnston, M., *Asthma drug wrong for some*, in *The New Zealand Herald*. 2001: Auckland.
24. Johnston, M., *Asthma quick-fix worries doctors*, in *The New Zealand Herald*. 2004: Auckland.
25. Johnston, M. and A. Gregory, *Asthma causes remain mystery*, in *The New Zealand Herald*. 2002: Auckland.
26. Crane, J., *Editorial: Inhaled corticosteroids in asthma action plans - double or quits?* The New Zealand Medical Journal, 2004. **117**(1196).
27. Nadel, J.A. and W.W. Busse, *Asthma*. Am. J. Respir. Crit. Care Med., 1998. **157**(4): p. 130S-138.
28. Saunders, K.B., *Clinical Physiology of The Lung*. 1977, Oxford: Blackwell Scientific Publications.
29. Tiddens, H., M. Silverman, and A. Bush, *The Role of Inflammation in Airway Disease . Remodeling*. Am. J. Respir. Crit. Care Med., 2000. **162**(2): p. 7S-10.
30. Tobin, M.J., *Asthma, Airway Biology, and Nasal Disorders in AJRCCM 2001* Am. J. Respir. Crit. Care Med., 2002. **165**(5): p. 598-618.
31. Van Wynsberghe, D., C.R. Noback, and R. Carola, *Human Anatomy & Physiology*. 3 ed. 1995, United States: McGraw-Hill.
32. Comroe, J.H., *Physiology of Respiration*. 2 ed. 1977, Chicago: Year Book Medical Publishers. 316.
33. Cottrell, G.P., *Cardiopulmonary Anatomy and Physiology for Respiratory Care Practitioners*. 2001, Philadelphia: F. A. Davis Company. 389.
34. Des Jardins, T., *Cardiopulmonary Anatomy Physiology*. 4 ed. 2002, Albany: Delmar. 550.
35. Jensen, D., *The Principles of Physiology*. 2 ed. 1980, New York: Appleton-Century-Crofts. 1068.
36. *Reliever inhalers linked to risk of asthma deaths*, in *The New Zealand Herald*. 2002: Auckland.
37. Beasley, R. and M. Masoli, *Editorial: Asthma in New Zealand - time to get control*. The New Zealand Medical Journal, 2003. **116**(1174).

38. Johnston, M., *Asthma groups at odds over new drug*, in *The New Zealand Herald*. 2002: Auckland.
39. Marieb, E.N., *Human anatomy & physiology*. 4th ed. 1998, Menlo Park, Calif: Benjamin/Cummings.
40. Feinberg, B.N., *Applied Clinical Engineering*. 1986, Egnlewood Cliffs: Prentice-Hall.
41. Cameron, J.R. and J.G. Skofronick, *Medical Physics*. 1978, New York: Wiley. 615.
42. Weibel, E.R., *Morphometry of the Human Lung*. 1963, New York: Academic Press.
43. Weibel, E.R., *The Pathway for Oxygen*. 1984, Cambridge, MA: Harvard Univ. Press. 425.
44. Weibel, E.R., *Fractal geometry: a design principle for living organisms*. Am J Physiol Lung Cell Mol Physiol, 1991. **261**(6): p. L361-369.
45. Horsfield, K. and G. Cumming, *Morphology of the bronchial tree in man*. J Appl Physiol, 1968. **24**: p. 373-383.
46. Au, P. and A. Al-Jumaily, *Asthma Relief and Airway Mechanics "A Literature Review"*. to appear in Transworld Research Network, Advances in Vibration, 2002. **TRN/SV/3**.
47. Horsfield, K., *Diameters, generations, and orders of branches in the bronchial tree*. J Appl Physiol, 1990. **68**(2): p. 457-461.
48. Kamm, R.D., *Airway Wall Mechanics*. Annu. Rev. Biomed. Eng., 1999. **1**: p. 47-72.
49. Salvi, S.S., K. Suresh Babu, and S.T. Holgate, *Is Asthma Really Due to a Polarized T Cell Response Toward a Helper T Cell Type 2 Phenotype?* Am. J. Respir. Crit. Care Med., 2001. **164**(8): p. 1343-1346.
50. Wiggs, B.R., et al., *A model of the mechanics of airway narrowing*. Journal of Applied Physiology, 1990. **69**(3): p. 849 - 860.
51. Marieb, E.N., *Essentials of human anatomy and physiology*. 7 ed. 2003, San Francisco: Benjamin Cummings. 588.
52. Al-Jumaily, A.M. and Y. Al-Fakhri, *Occlusion Identification in Respiratory System Using Asymmetric Model*. Accepted for publication in the International Journal of Nonlinear Science and Application, 2002. **7**(1).
53. Al-Jumaily, A.M. and Y. Du, *Obstruction Identification in a Compliant Tube with Application to Airway Passages*. Accepted for publication in the Journal of Vibration and Control.
54. Al-Jumaily, A.M. and P. Mithrarathne, *Simulation of respiratory system for identifying airway occlusion*. Journal of Nonlinear Sciences and Numerical Simulations, 2000. **2**(1): p. 21-28.
55. Elad, D., R.D. Kamm, and A.H. Shapiro, *Tube law for the intrapulmonary airway*. American Physiological Society, 1988: p. 7-13.
56. Freezer, N.J., C.J. Lanteri, and P.D. Sly, *Effect of pulmonary blood flow on measurements of respiratory mechanics using the interrupter technique*. J Appl Physiol, 1993. **74**(3): p. 1083-1088.

57. Gibson, G.J., *Lung Volumes and Elasticity*, in *LUNG FUNCTION TESTS: Physiological Principles and Clinical Applications*, J.M.B. HUGES and N.B. PRIDE, Editors. 1999, W B Saunders: London. p. 314.
58. Ishizaka, K., M. Matsudaira, and T. Kaneka, *Input Acoustic Impedance Measurement of the Subglottal System*. Journal of Acoustical Society of America, 1976. **60**(1): p. 190-197.
59. Jaffrin, M.Y. and P. Kesic, *Airway resistance: a fluid mechanics approach*. Journal of Applied Physiology, 1974. **36**(3): p. 354 - 361.
60. Lambert, R.K., P.D. Pare, and M. Okazawa, *Stiffness of peripheral airway folding membrane in rabbits*. J Appl Physiol, 2001. **90**(6): p. 2041-1266.
61. Pedersen, O.F., et al., *Wave-speed-determined flow limitation at peak flow in normal and asthmatic subjects*. Journal of Applied Physiology, 1997. **83**(5): p. 1721 - 1732.
62. Suki, B., R.H. Habib, and A.C. Jackson, *Wave propagation, input impedance, and wall mechanics of the calf trachea from 16 to 1,600 Hz*. J Appl Physiol, 1993. **75**(6): p. 2755-2766.
63. Rohrer, F., *Der Stromungswiderstand in den menschlichen Atemwegen*. Pflugers Arch. ges. Physiol., 1915. **162**: p. 255 - 259.
64. Pedley, T.J., R.C. Schroter, and M.F. Sudlow, *The prediction of pressure drop and variation of resistance within the human bronchial airways*. Respiration Physiology, 1970. **9**: p. 387 - 405.
65. Von Neergaard, K. and K. Wirz, *Die Messung der Stromungswiderstande in der Atemwege des Menschen*. insbesondere beim Asthma und Emphysema. Z. Klin. Med., 1927. **195**: p. 51 - 82.
66. Jackson, A.C., H.T.J. Hmilhorn, and N.J. R, *A reevaluation of the interrupter techniques for airway resistance measurement*. Journal of Applied Physiology, 1974. **36**(2): p. 264-282.
67. Lombardi, E., et al., *Reference Values of interrupter respiratory resistance in healthy preschool white children*. Thorax, 2001. **56**: p. 691-695.
68. Oostveen, E., et al., *The forced oscillation technique in clinical practice: methodology, recommendations and future developments*. European Respiratory Journal, 2003. **22**(6): p. 1026-1041.
69. Dubois, A.B., S.Y. Botelho, and J.H.J. Comroe, *A New Method for Measuring Airway Resistance in Man Using a Body Plethysmograph: Values in Normal Subjects and in Patients with Respiratory Disease*. J Clin Invest, 1956. **35**: p. 327.
70. Delacourt, C., et al., *Comparison of the Forced Oscillation Technique and the Interrupter Technique for Assessing Airway Obstruction and Its Reversibility in Children*. Am. J. Respir. Crit. Care Med., 2001. **164**(6): p. 965-972.
71. Dubois, A.B., et al., *Oscillation mechanics of lungs and chest in man*. J Appl Physiol, 1956. **8**: p. 587-594.
72. Fisher, A.B., A.B. Dubois, and R.W. Hyde, *Evaluation of the Forced Oscillation Technique for the Determination of Resistance to Breathing*. The Journal of Clinical Investigation, 1968. **47**: p. 2045-2057.

73. Frey, U., et al., *High-frequency Respiratory Impedance Measured by Forced-Oscillation Technique in Infants*. Am. J. Respir. Crit. Care Med., 1998. **158**(2): p. 363-370.
74. Hayden, M.J., et al., *Using Low-frequency Oscillation to Detect Bronchodilator Responsiveness in Infants*. Am. J. Respir. Crit. Care Med., 1998. **157**(2): p. 574-1391.
75. Dekker, E., *The transition between laminar and turbulent flow in the trachea*. J Appl Physiol, 1961. **16**: p. 1060-1064.
76. James, A.L., P.D. Pare, and J.C. Hogg, *The mechanics of airway narrowing in asthma*. American Journal of Respiratory and Critical Care Medicine, 1989. **139**: p. 246 - 246.
77. Fredberg, J.J., et al., *Friction in airway smooth muscle: mechanism, latch, and implications in asthma*. J Appl Physiol, 1996. **81**(6): p. 2703-.
78. Lambert, R.K., et al., *A computational model for expiratory flow*. J Appl Physiol, 1982. **52**: p. 44-56.
79. Lambert, R.K. and P.D. Pare, *Lung parenchymal shear modulus, airway wall remodeling, and bronchial hyperresponsiveness*. J Appl Physiol, 1997. **83**(1): p. 140-714.
80. Fredberg, J.J., et al., *Canine pulmonary input-impedance measured by transient forced oscillations*. Journal of Biomedical Engineering, 1978. **100**: p. 67 - 71.
81. Kinsler, L.E. and A.E. Frey, *Fundamental of Acoustics*. 1962, New York: Wiley.
82. Schmid-Schoenbein, G.W., and Y.C. Fung, *Force perturbation of respiratory system : (B) A continuum mechanics analysis*. Journal of Applied Physiology, 1978. **63**: p. 367 - 398.
83. Fredberg, J.J., *A modal perspective of lung response*. Journal of Acoustic Society of America, 1978. **63**: p. 962 - 966.
84. Fredberg, J.J. and A. Hoenig, *Mechanical response of the lungs at high frequencies*. J Biomed Eng, 1978. **100**: p. 57-66.
85. Al-Jumaily, A.M. and A.M. Al-Saffar, *Dynamic Response Characteristics of Upper Respiratory System*. Journal of the Acoustical Society of America, 1999. **106**(4 : 2): p. 2127.
86. Carr, J.J. and J.M. Brown, *Introduction to Biomedical Equipment Technology*. Third ed. 1998, Upper Saddle River.: Prentice-Hall.
87. Avanzolini, G. and P. Barbini, *A Comparative Evaluation of the Three On-line Identification Methods for a Respiratory Mechanical Model*. IEEE Transactions of Biomedical Engineering, 1985. **BME-32**(11).
88. Officer, T.M., R. Pellegrino, and V.B.J.R., *Rodarte, Measurements of pulmonary resistance and dynamic compliance with airway obstruction*. Journal of Applied Physiology, 1998. **85**(3): p. 1982 - 1988.
89. Kaczka, D.W., et al., *Airway and Lung Tissue Mechanics in Asthma . Effects of Albuterol*. Am. J. Respir. Crit. Care Med., 1999. **159**(1): p. 169-91.

90. Soedel, W., *Vibrations of Shells and Plates*. 2nd ed. 1993, New York: Marcel Dekker, Inc. 470.
91. Yu, Y.-Y., *Free Vibrations of Thin Cylindrical Shells Having Finite Lengths with Freely "Supported and Clamped Edges*. J Appl Mech, 1955. **22**: p. 547-552.
92. Leissa, A.W., *Vibration of Shells*. 2 ed. 1993, New York: Acoustical Society of America through the American Institute of Physics.
93. Kraus, H., *Thin Elastic Shells*. 1967, New York: John Wiley & Sons, Inc.
94. Ventsel, E. and T. Krauthammer, *Thin Plates and Shells*. 2001, Basel: Marcel Dekker. 666.
95. Timoshenko, S.P. and Woinowsky-Krieger, *Theory of plates and shells*. 2 ed. 1959, New York: McGraw-Hill. 580.
96. Bankier, A., et al., *Bronchial wall thickness: appropriate window settings for thin-section CT and radiologic-anatomic correlation*. Radiology, 1996. **199**(3): p. 831-836.
97. Parker, H., K. Horsfield, and G. Cumming, *Morphology of distal airways in the human lung*. J Appl Physiol, 1971. **31**(3): p. 386-391.
98. Markus, S., *The Mechanics of Vibrations of Cylindrical Shells*. 1988, New York: Elsevier Science. 159.
99. Fung, Y.C. and E.E. Sechler, eds. *Thin-Shell Structures Theory, Experiment, and Design*. 1974, Prentice-Hall: London.
100. Lord Rayleigh, *Theory of Sound*. 2 ed. 1894, London: Macmillan.
101. Au, P.M. and A.M. Al-Jumaily. *Dynamic Characteristics of Tracheobronchial Walls*. in *The 8th Annual New Zealand Engineering and Technology Postgraduate Conference*. 2001. Hamilton: University of Waikato.
102. Hoff, N.J., *The Accuracy of Donnell's Equations*. Journal of Applied Mechanics, Trans. ASME, 1955. **77**: p. 329-334.
103. Arnold, R.N. and G.B. Warburton, *The Flexural Vibrations of Thin Cylinders*. Proceedings of the Institution of Mechanical Engineers, 1953. **167**: p. 62-74.
104. Naghdi, P.M. and J.G. Ferry, *On the Equations of Motion of Cylindrical Shells*. Journal of Applied Mechanics, Trans. ASME, 1954. **76**: p. 160-166.
105. Koval, L.R. and E.T. Cranch. *On the Free Vibrations of Thin Cylindrical Shells Subjected to an Initial Static Torque*. in *4th US Nat'l Congr Appl Mech*. 1962.
106. Halpern, D. and J.B. Grotberg, *Fluid-elastic instabilities of liquid-lined flexible tubes*. J. Fluid Mech., 1992. **244**: p. 615-632.
107. Halpern, D., B. Hamer, and J.B. Grotherg, *Capillary-Elastic Instabilities of Liquid Lined Flexible Tubes: A Model of Airway Closure*. BED Advances in Bioengineering ASME, 1993. **26**: p. 223-226.
108. Hill, M.J., T.A. Wilson, and R.K. Lambert, *Effects of surface tension and intraluminal fluid on mechanics of small airways*. J Appl Physiol, 1997. **82**(1): p. 233-297.

109. Horsfield, K., et al., *Models of the human bronchial tree*. J Appl Physiol, 1971. **31**(2): p. 207-217.
110. Courant, R., *Variational Method for the Solution of Problems of Equilibrium and Variations*. Bulletin of the American Mathematical Society, 1943. **49**.
111. Lee, S., et al., *Determination of resonance frequency of the respiratory system in respiratory distress syndrome*. Arch Dis Child Fetal Neonatal Ed, 1999. **80**: p. F198-F202.
112. Horsfield, K. and G. Cumming, *Functional consequences of airway morphology*. J Appl Physiol, 1968. **24**(3): p. 384-390.
113. Horsfield, K., et al., *Effect of heart rate and stroke volume on gas mixing in dog lung*. J Appl Physiol, 1982. **53**(6): p. 1603-1607.
114. Horsfield, K., W. Kemp, and S. Phillips, *An asymmetrical model of the airways of the dog lung*. J Appl Physiol, 1982. **52**(1): p. 21-26.
115. Brody, A.W. and A.B. Dubois, *Determination of Tissue, Airway and Total Resistance to Respiration in Cats*. J Appl Physiol, 1956. **9**(2): p. 213-218.
116. Dubois, A.B., et al., *Production and absorption of nitric oxide gas in the nose*. J Appl Physiol, 1998. **84**(4): p. 1217-1338.
117. Dubois, A.B., et al., *Nitric oxide production and absorption in trachea, bronchi, bronchioles, and respiratory bronchioles of humans*. J Appl Physiol, 1999. **86**(1): p. 159-1338.
118. Au, P.M. and A.M. Al-Jumaily. *A Dynamic Investigation of the Airways*. in *The 9th Annual New Zealand Engineering and Technology Postgraduate Conference*. 2002. Auckland: Auckland University of Technology.
119. Dossing, O., *Structural Testing Part 1-Mechanical Mobility Measurements*. 1988, Bruel & Kjaer http://www.bksv.com/pdf/Structural_Testing_1.pdf.
120. Dossing, O., *Structural Testing Part 2-Modal Analysis and Simulation*. 1988, Bruel & Kjaer http://www.bksv.com/pdf/Structural_Testing_2.pdf.
121. Avitabile, P., *Experimental Modal Analysis - A Simple Non-Mathematical Presentation*. Sound and Vibration, 2001. **January 2001**: p. 1-11.
122. Inman, D.J., *Engineering Vibration*. 2 ed. 2001, New Jersey: Prentice Hall. 621.
123. He, J. and Z.-F. Fu, *Modal Analysis*. 2001, Oxford: Butterworth-Heinemann. 291.
124. Lai-Fook, S.J., *Lung Tissue Mechanics*, in *Respiratory Biomechanics: Engineering Analysis of Structure and Function*, M.A.E. FARRELL and J.R. LIGAS, Editors. 1990, Springer-Verlag: New York. p. 39-43.
125. Lai-Fook, S.J. and R.E. Hyatt, *Effects of age on elastic moduli of human lungs*. J Appl Physiol, 2000. **89**(1): p. 163-168.
126. Hermawan, V., *Experimental Techniques to Determine the Young's Modulus of the Trachea*, in *Mechanical and Production Engineering*. 2004, Auckland University of Technology: Auckland. p. 110.
127. Russell, D.A., *Measuring the Vibrational Behavior of a Baseball/Softball Bat*, <http://www.kettering.edu/~drussell/bats-new/modal.html>. 2003.

128. Brauer, J.R., ed. *Finite Element Analysis. What Every Engineer Should Know About*, ed. W.H. MIDDENDORF. Vol. 23. 1988, Marcel Dekker: New York. 219.